ISSN (Print) 2616-7263
ISSN (Online) 2663-1261

Л.Н. Гумилев атындағы Еуразия ұлттық университетінің

ХАБАРШЫСЫ
BULLETIN
ВЕСТНИК

of L.N. Gumilyov
Eurasian National University

Евразийского национального
университета имени Л.Н. Гумилева

ТЕХНИКАЛЫҚ ҒЫЛЫМДАР ЖӘНЕ ТЕХНОЛОГИЯЛАР сериясы

TECHNICAL SCIENCES AND TECHNOLOGY Series

Серия ТЕХНИЧЕСКИЕ НАУКИ И ТЕХНОЛОГИИ

№ 2(135)/2021

1995 жылдан бастап шығады

Founded in 1995

Издается с 1995 года

Жылына 4 рет шығады

Published 4 times a year

Выходит 4 раза в год

Нұр-Сұлтан, 2021

Nur-Sultan, 2021

Нур-Султан, 2021

Редакцияның мекенжайы: 010008, Қазақстан, Нұр-Сұлтан қ., Сәтбаев к-сі, 2, Л.Н. Гумилев атындағы Еуразия ұлттық университеті, 402 б.
Тел: +7 (7172) 709-500 (ішкі 31-428). E-mail: *vest_techsi@enu.kz*

Жауапты хатшы, компьютерде беттеген: А. Бекбаева

Л.Н. Гумилев атындағы Еуразия ұлттық университетінің Хабаршысы.
ТЕХНИКАЛЫҚ ҒЫЛЫМДАР ЖӘНЕ ТЕХНОЛОГИЯЛАР сериясы
Меншіктенуші: КеАҚ "Л.Н. Гумилев атындағы Еуразия ұлттық университеті"
Мерзімділігі: жылына 4 рет
Қазақстан Республикасының Ақпарат және коммуникациялар министрлігімен тіркелген 19.04.2021ж. № KZ31VPY00034682 қайта есепке қою туралы куәлігі
Типографияның мекенжайы: 010008, Қазақстан, Нұр-Сұлтан қ., Қажымұқан к-сі 13/1
Л.Н. Гумилев атындағы Еуразия ұлттық университеті
Тел: +7 (7172)709-500 (ішкі 31-428). Сайт: http://bultech.enu.kz

Editorial address: 2, Satpayev str., of. 402, L.N. Gumilyov Eurasian National University,
Nur-Sultan, Kazakhstan, 010008
Tel.: +7 (7172) 709-500 (ext. 31-428), E-mail: *vest_techsi@enu.kz*

Responsible secretary, computer layout: Aliya Bekbayeva

Bulletin of L.N. Gumilyov Eurasian National University.
TECHNICAL SCIENCS and TECHNOLOGY Series
Owner: Non-profit joint-stock company «L.N. Gumilyov EurasianNational University»
Periodicity: 4 times a year
Registered by the Ministry of Information and Communication of the Republic of Kazakhstan
Rediscount certificate № KZ31VPY00034682 from 19.04.2021
Address of Printing Office: 13/1 Kazhimukan str., L.N. Gumilyov Eurasian National
University, Nur-Sultan, Kazakhstan 010008
Tel: +7 (7172) 709-500 (ext.31-428). Website: http:// bultech.enu.kz

Адрес редакции: 010008, Казахстан, г. Нур-Султан, ул. Сатпаева, 2, Евразийский национальный университет имени Л.Н. Гумилева, каб. 402
Тел: +7(7172) 709-500 (вн. 31-428). E-mail: *vest_techsi@enu.kz*

Ответственный секретарь, компьютерная верстка: А. Бекбаева

Вестник Евразийского национального университета имени Л.Н. Гумилева.
Серия ТЕХНИЧЕСКИЕ НАУКИ И ТЕХНОЛОГИИ
Собственник: НАО «Евразийский национальный университет имени Л.Н. Гумилева»
Периодичность: 4 раза в год
Зарегистрирован Министерством информации и коммуникаций Республики Казахстан
Свидетельство о постановке на переучет № KZ31VPY00034682 от 19.04.2021 г.
Адрес типографии: 010008, Казахстан, г. Нур-Султан, ул. Кажымукана, 13/1,Евразийский национальный университет имени Л.Н. Гумилева
Тел.: +7(7172)709-500 (вн.31-428). Сайт: http:// bultech.enu.kz

Л.Н. ГУМИЛЕВ АТЫНДАҒЫ ЕУРАЗИЯ ҰЛТТЫҚ УНИВЕРСИТЕТІНІҢ ХАБАРШЫСЫ.
ТЕХНИКАЛЫҚ ҒЫЛЫМДАР ЖӘНЕ ТЕХНОЛОГИЯЛАР СЕРИЯСЫ

ВЕСТНИК ЕВРАЗИЙСКОГО НАЦИОНАЛЬНОГО УНИВЕРСИТЕТА
ИМЕНИ Л.Н.ГУМИЛЕВА. СЕРИЯ ТЕХНИЧЕСКИЕ НАУКИ И ТЕХНОЛОГИИ

BULLETIN OF L.N. GUMILYOV EURASIAN NATIONAL UNIVERSITY.
TECHNICAL SCIENCE AND TECHNOLOGY SERIES
№ 2(135)/2021

МАЗМҰНЫ/ CONTENTS/ СОДЕРЖАНИЕ

IRSTI 38.65.15, 38.65.17, 38.65.19

D.M. Frolov

Lomonosov Moscow State University, Moscow, Russia
E-mail:denisfrolovm@mail.ru

Calculation scheme of ground freezing depth in Terskol

Abstract. During the construction of avalanche-retaining geotechnical structures in mountainous areas comes up the problem of fixing and stability of these structures in conditions of seasonal and/or long-term freezing of the ground. This paper evaluates the influence of snow cover and air temperature on the depth of freezing and soil stability based on the developed calculation scheme for the winter seasons 2015/16-2019/20 in the Elbrus region. The calculation scheme was based on the problem of thermal conductivity of a three-layer medium (snow, frozen, and thawed soil) with a phase transition at the boundary. The heat balance equation included the energy of the phase transition, the inflow of heat from the thawed ground and the outflow to the frozen ground, and, in the presence of snow cover, through it to the atmosphere.

Keywords: calculating scheme; air temperature; snow cover; ground freezing; mountain regions; construction stability

DOI: doi.org/10.32523/2616-7263-2021-135-2-7-13

Introduction

One of the factors of soil stability on slopes during the construction of avalanche-retaining geotechnical structures in mountainous areas is the freezing of the underlying soil since in mountainous areas the soil can be frozen for eight or more months. However, the recent changes in air temperature and precipitation (primarily in the form of snow) [**5**] lead to a change in the depth and duration of freezing of the soil and, as a result, a decrease in its stability. A model study of soil freezing in the mountains was carried out in [**6**]. In this paper, based on the developed calculation scheme, the depth of ground freezing for the last five winter seasons is estimated based on data on the thickness of snow cover and air temperature for the weather station Terskol. Weather Station Terskol is located in the valley Azau in Elbrus region at an altitude of 2141 m above sea level. The average temperature in January is -7°C, July - 13.4°C, and the average sum of negative monthly temperatures in the winter period (November-March) is -20°C. During the period of snow accumulation (in November-March), an average of about 280 mm of precipitation falls, causing the accumulation of snow cover up to 70-80 cm thick. Calculations of changes in the depth of ground freezing were performed according to the proposed calculation scheme based on data on the thickness of snow cover and air temperature based on a three-layer model of the medium (thawed soil, frozen soil, snow) and assuming a linear change in temperature in the media and heat flow according to Fourier's law. This simplified calculating scheme is used since it requires only air temperature and snow thickness data and is very easy in conducting calculations using the solution of only one ordinary differential equation at each time step.

Methodology

The article calculates the freezing depth based on data on air temperature and snow cover thickness for weather stations Terskol for the snow-covered soil surface for the winter seasons 2015/16-2019/20 according to the proposed calculation scheme. The calculation scheme was based on the problem of thermal conductivity of a three-layer medium (snow, frozen and thawed soil) with a phase transition at the boundary of frozen and thawed soil. The heat balance equation included the energy of the phase transition, the inflow of heat from the thawed ground and the outflow to the frozen ground and, in the presence of snow cover, through it to the atmosphere. The heat flux was calculated according to Fourier's law, as the product of the thermal conductivity and the temperature gradient. It was assumed that the

temperature in each medium varies linearly (for example, [3]). For snow cover and frozen ground, the formula of thermal conductivity of a two-layer medium was used.

The calculation of ground freezing based on data on air temperature and snow cover thickness and thermal conductivity during the winter period made it possible to estimate the intensity of the freezing front movement during this time period. The dependence of the speed of the freezing front movement was found according to the calculated scheme. The scheme took into account the freezing of the ground from below on the frozen ground mass in winter, based on data on the daily air temperature (and the thickness and thermal conductivity of the snow cover).

The heat balance equation was written as $F_1=cLV+F_2$, or as:

$$dh_{fg}/dt = V = (F_1 - F_2)/cL, \quad (1)$$

where: F_1 – heat outflow through the frozen ground (and snow cover) from the freezing front (W/m^2) to the atmosphere; $c\ L\ V = c\ L\ dh_{fg}/d\tau$– consumption heat at the phase transition, c, moisture content of the soil (1-4 kg/cm*m^2), (last value corresponds to the complete filling of pores with water from a lightweight clay with a density of 2000 kg/m^3 and a porosity 0,617 [1]); L – energy of the phase transition (335 kJ/kg); $V = dh_{fg}/d\tau$ – the speed of the freezing front (cm/s); F_2 – heat exchange in the cooling melt the ground before the freezing front (W/m^2).

The heat flux was expressed according to the Fourier law: $F = -\lambda$ grad T. The heat flow through the frozen ground from the freezing front to the atmosphere in the case of snow cover was expressed in terms of thermal conductivity and heat flow of a combination of two media (snow cover and frozen ground) how to:

$$F_1 = -\lambda \frac{\Delta T}{\Delta x} = -\frac{\Delta T}{\frac{\Delta x_s}{\lambda_s} + \frac{\Delta x_{fg}}{\lambda_{fg}}} = \frac{-T_{air}}{\frac{h_s}{\lambda_s} + \frac{h_{fg}}{\lambda_{fg}}}, \quad (2)$$

Here T_{air} is the air temperature, h_s and h_{fg} are the snow thickness and freezing depth, and λ_s and λ_{fg} are the thermal conductivity of snow and frozen ground.

It was assumed that at a depth of 10 m in the ground there is a point of zero annual temperature fluctuations T_0 with an average annual value of about 7°C. Therefore

$$F_2 = -\lambda_{thg} \frac{\Delta T}{\Delta x} = \lambda_{thg} \frac{T_0}{10 - h_{thg}}, \quad (3)$$

Here λ_{thg} is the thermal conductivity of thawed soil. Calculations were performed in one-day increments. At first, it was assumed that the thickness of the frozen groundh_{fg} was 0.5 cm. At each time step (every day) was calculated (calculated) the freezing rate V and the value of the frozen ground thicknessh_{fg} for the next day (time step). According to [1], the average thermal conductivity of thawed and frozen clay soil could be taken as 1.4 and 1.8 W/m°C. The average thermal conductivity *of* snow λ_c was calculated relative to the density according to the formula of A. V. Pavlov [**2**] and was taken equal to 0.18 W/m°C.

Results and Discussion

In this paper, a difference scheme was constructed for the derived first-order time differential equation for changing the depth of soil freezing by approximating this differential equation by the explicit Euler method:$h_{fg}(t_{n+1}) = h_{fg}(t_n) + \Delta T\ V(t_n)$. According to the obtained difference scheme, for each winter season 2015/16-2019/20, calculations of changes in the depth of soil freezing were made. An example of the calculation results for the winter season 2016/17 is shown in figure 1.

a)

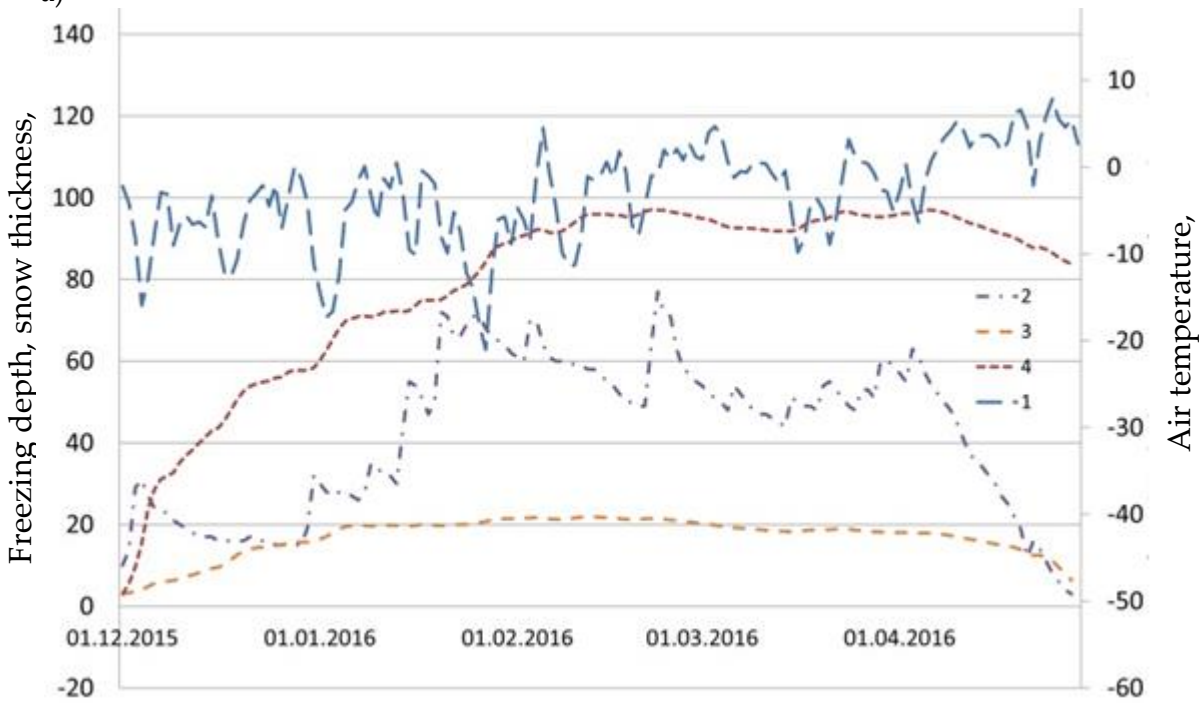
Freezing depth, snow thickness,
Air temperature,
140
120
100
80
60
40
20
0
-20
10
0
-10
-20
-30
-40
-50
-60
01.12.2015
01.01.2016
01.02.2016
01.03.2016
01.04.2016
-2
3
4
-1

b)

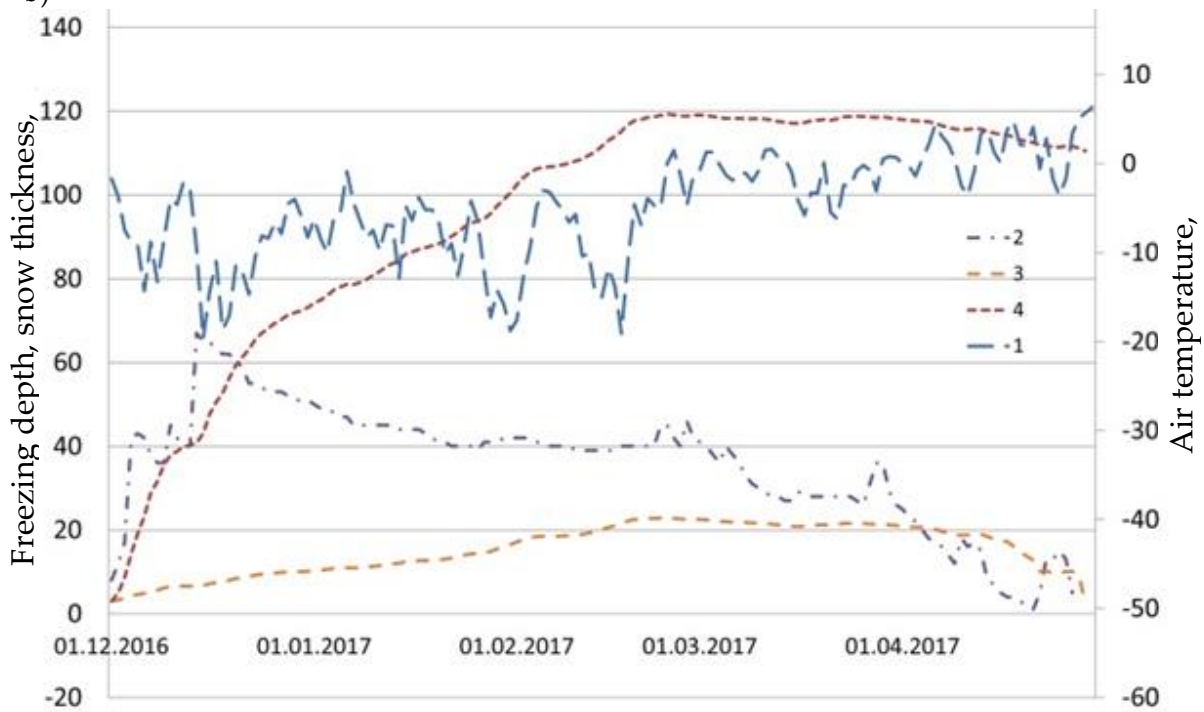
Freezing depth, snow thickness,
Air temperature,
140
120
100
80
60
40
20
0
-20
10
0
-10
-20
-30
-40
-50
-60
01.12.2016
01.01.2017
01.02.2017
01.03.2017
01.04.2017
-2
3
4
-1

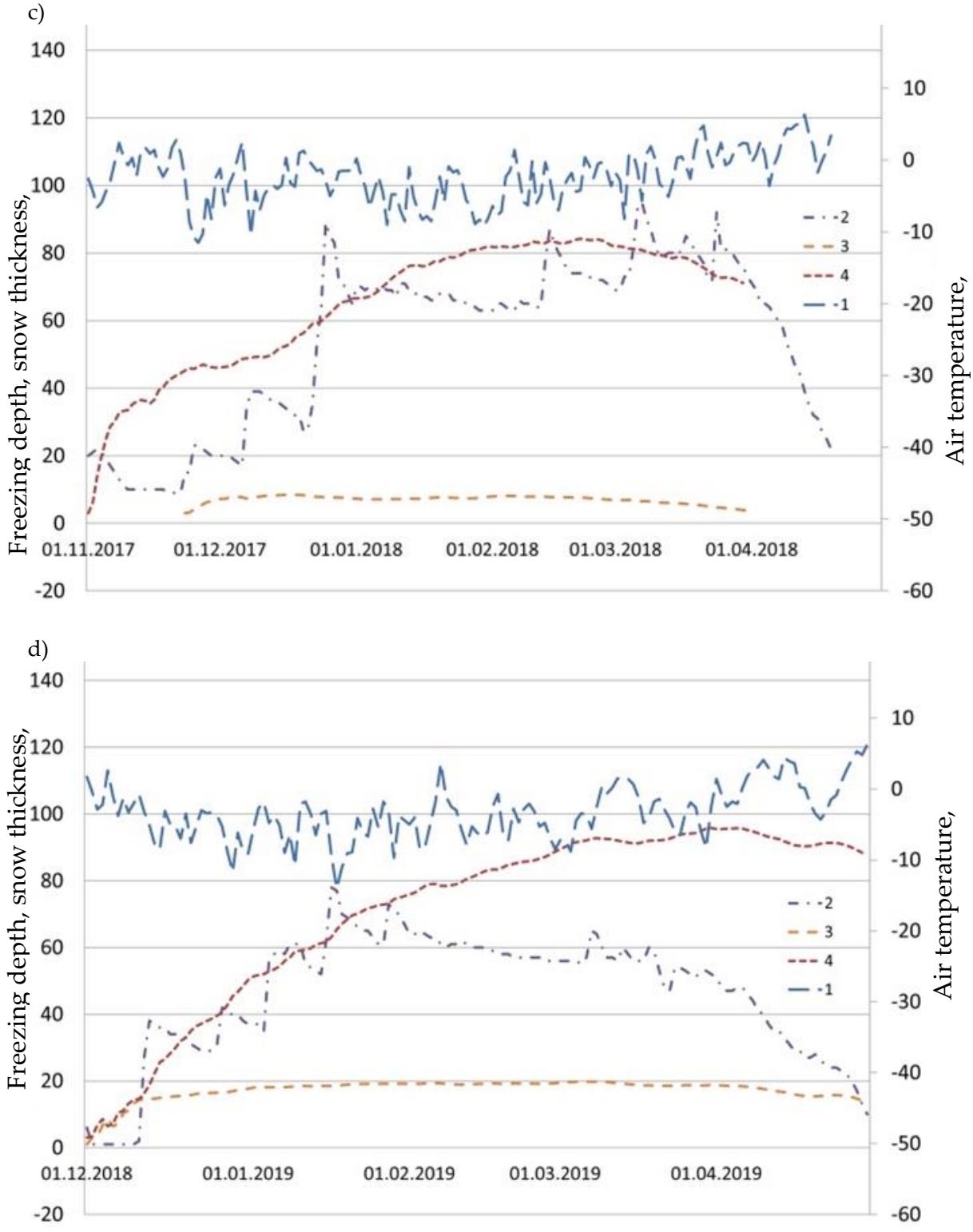

Figure 1. Changes in air temperature and freezing depth based on calculations for snow-covered and exposed ground surfaces for a weather station Terskol for winter periods 2015/16-2018/19 (1 – air temperature, 2 -thickness of snow cover, and 3-estimated depth of freezing of the ground under the snow cover 4-estimated depth of freezing of exposed ground).

The calculation method used is well physically justified. The method solution describes well the process of changing the freezing depth during the winter season. The successful operation of the method needs to set the initial data as accurately as possible. The consistency of the method was proven in the work [4].

Results of calculating the maximum ground freezing depth for a weather station Terskol for the winter periods 2015/16-2019/20 are shown in Table 1.

Table 1

Changes in the maximum ground freezing depth, average snow cover thickness for February, and the sum of negative monthly temperatures for a weather station Terskol for winter periods 2015/16-2019/20

Winterperiod	Sum of negative monthly temperature, °C	Averaged February snow cover thickness, cm	Max. freezing depth of snow-covered ground, cm	Max. freezing depth of exposed ground, cm
2015/16	-18,7	60	21	97
2016/17	-27,7	40	23	119
2017/18	-14,2	70	8	83
2018/19	-19,4	60	20	96
2019/20			20	

Conclusion

The thickness of the accumulated snow cover can reach half a meter or more. At the same time, the ground under the snow-covered surface freezes, according to calculations, by an average of 20 centimeters or more. In the case of partial or complete blowing off of the snow cover, freezing of the ground can occur to a depth of 1 meter or more and last for a longer period. Thus, the proposed method for calculating the dynamics of the depth of soil freezing based on data on air temperature and snow cover thickness allows us to assess the freezing of soil as a factor of soil stability during the construction of avalanche protection structures in mountains. Also it is necessary to take into account that for the forecast, we do not have current values of air temperature and snow cover thickness. It may be necessary to use their long-term values (trends in their change) to check the possibility of using this methodology for forecasting.

The work was carried out on the topic of the State Law "Danger and risk of natural processes and phenomena" (121051300175-4).

Reference

1. Грунтоведение. Под ред. В.Т. Трофимов. - Москва: Изд-во МГУ, Наука, -2005, -1024 с.
2. Павлов А.В. Теплофизика ландшафтов. -Новосибирск: «Наука», -1979, -284 с.
3. DeGaetano, A.T., Cameron M.D., Wilks D.S. Physical simulation of maximum seasonal soil freezing depth in the united states using routine weather observation // Journal of Applied Meteorology, -2001, -40(3), -pp. 546-555.
4. Frolov D. M. Winter regime of temperature and snow accumulation as a factor of ground freezing depth variations // E3S Web of Conferences. -2020. -Vol. 163, no. 01005. -P. 1-5. https://doi.org/10.1051/e3sconf/202016301005.
5. Golubev V.N., Petrushina M.N., Frolov D.M. Winter regime of temperature and precipitation

as a factor of snow-cover distribution and its stratigraphy // Annals of Glaciology, -2008, -49, -pp. 179-186.

6. Haberkorn A., Wever N., Hoelzle M., Phillips M., Kenner R., Bavay M., Lehning M. Distributed snow and rock temperature modeling in steep rock walls using Alpine3D. Cryosphere Discuss. -2016. https://doi.org/10.5194/tc-2016-73.

Д.М. Фролов

Ломоносов атындағы Мәскеу мемлекеттік университеті, Мәскеу, Ресей

Терскөлдегі топырақтың қату тереңдігін есептеу схемасы

Аңдатпа. Қар көшкінін сақтайтын геотехникалық құрылыстарды салу кезінде таулы аудандарда жердің маусымдық және ұзақ мерзімді мұздату жағдайында осы құрылымдарды бекіту және тұрақтылық мәселесі туындайды. Бұл жұмыста Эльбрус аймағында 2015/16-2019/20 қысқы маусымына арналған есептеу схемасы негізінде қар жамылғысы мен ауа температурасының қату тереңдігі мен топырақтың тұрақтылығына әсері бағаланады. Есептеу сызбасы шекарада фазалық ауысуы бар үш қабатты ортаның (қар, мұздатылған және еріген топырақ) жылу өткізгіштік мәселесіне негізделген. Жылу балансының теңдеуіне фазалық ауысудың энергиясы, еріген жерден жылу ағыны, мұздатылған жерге ағу және қар жамылғысы болған жағдайда, қар арқылы атмосфераға өту кірді.

Түйін сөздер: есептеу сызбасы, ауа температурасы, қар жамылғысы, жердің қатуы, таулы аймақтар, құрылыстың тұрақтылығы.

Д.М. Фролов

Московский государственный университет им. М.В. Ломоносова, Москва, Россия

Вычислительная схема для глубины промерзания грунта в Терсколе

Аннотация. При строительстве лавиноудерживающих геотехнических сооружений в горных районах возникает проблема крепления и устойчивости этих сооружений в условиях сезонного и / или длительного промерзания грунта. В данной статье оценивается влияние снежного покрова и температуры воздуха на глубину промерзания и устойчивость почвы на основе разработанной схемы расчета на зимние сезоны 2015/16-2019/20 в районе Эльбруса. В основу расчетной схемы положена задача теплопроводности трехслойной среды (снег, мерзлый и талый грунт) с фазовым переходом на границе. Уравнение теплового баланса включало энергию фазового перехода, приток тепла из талой почвы и отток тепла в мерзлый грунт и, при наличии снежного покрова, отток тепла через снег в атмосферу.

Ключевые слова: расчетная схема, температура воздуха, снежный покров, промерзание грунта, горные районы, устойчивость конструкции.

References

1. Gruntovedenie. Pod red. V.T. Trofimov [Soil science. Edited by V. T. Trofimov].(MSU Publishing House, Nauka Publ., Moscow,2005, 1024 p.) [in Russian].

2. Pavlov A.V. Teplofizika landshaftov [Thermal physics of landscapes]. (Nauka Publ., Novosibirsk, 1979, 284 p.) [in Russian].

3. DeGaetano, A.T., Cameron M.D., Wilks D.S. Physical simulation of maximum seasonal soil freezing depth in the united states using routine weather observation. Journal of Applied Meteorology . 40(3), 546-555 (2001).

4. Frolov D. M. Winter regime of temperature and snow accumulation as a factor of ground freezing depth variations. E3S Web of Conferences. 2020. Vol. 163, no. 01005. P. 1–5. https://doi.org/10.1051/e3sconf/202016301005.

5. Golubev V.N., Petrushina M.N., Frolov D.M. Winter regime of temperature and precipitation as a factor of snow-cover distribution and its stratigraphy. Annals of Glaciology, 2008, 49, pp. 179-186.

6. Haberkorn A., Wever N., Hoelzle M., Phillips M., Kenner R., Bavay M., Lehning M. Distributed snow and rock temperature modeling in steep rock walls using Alpine3D. Cryosphere Discuss. 2016. https://doi.org/10.5194/tc-2016-73.

Information about authors:

Frolov D.M. - Researcher, Lomonosov Moscow State University, Moscow, Russia.

Фролов Д.М. - ғылыми қызметкер, Ломоносов атындағы Мәскеу мемлекеттік университеті, Мәскеу, Ресей.

IRSTI 67.21.19

A. Sarsembayeva*[1], A. Zhusshupbekov[1,2,3], Ph.E.F. Collins[4]

[1]*L.N. Gumilyov Eurasian National University, Nur-Sultan, Kazakhstan*
[2]*Saint-Petersburg State University of Architecture and Civil Engineering, Saint –Petersburg, Russia*
[3]*KGS, LTD, Nur-Sultan, Kazakhstan*
[4]*Brunel University London, London, United Kingdom*
Corresponding author: assel_enu@mail.ru

Evaluation of frost heave in clay soils

Abstract. Frost heaving in clayey soils with a low coefficient of permeability raises a lot of questions regarding the cryosuction, surface tension forces, and accompanying phase transfer of water. The freeze-thaw laboratory test results were considered in this work in terms of temperature and volumetric parameters change, dry density, and water mass transfer. The article presents a model for calculating the mass transfer of water (vapour) in the gas state under the influence of cryogenic forces. Findings include the improved understanding of the heat and mass transfer phenomenon during the unidirectional freezing of soils in an open system. Most of the tests for engineering properties registered a slight reduction in relation to strength, cohesion, and angle of internal friction. However, there was a significant increase in the coefficient of permeability after the freeze-thaw cycles with initially dense compacted soil samples, which was due to loosening and moistening of the soil samples during the heave at sub-zero temperatures. The conceptual model for frost heave in soils was developed based on the vapour mass transfer. There was presented algorithm of vapour flow calculation in unsaturated soils using fundamental thermodynamic equations.

Keywords: frost heave, temperature monitoring, moisture transfer, clayey soils, laboratory testing, vapour transfer.

DOI: doi.org/10.32523/2616-7263-2021-135-2-14-26

Introduction

Clayey soils are well-known as frost susceptible soils, despite they have very low permeability and high surface tension. The surface tension in the ground water is around $63 - 64\ 10^{-7} J\ cm^2$ [1]. The soil structure in the freezing fringe includes the moisture in three phases: the solid part - ice lenses; the liquid phase – hydroscopic and capillary water; and the gas phase – saturated and unsaturated vapour. It should be noted that ground soils are subject to unidirectional freezing, which is usually derived from the top downwards. Ice lenses nucleation starts in the pores and channels with gravimetric water, where the pore water pressure is close to atmospheric level. Withdrawal of the thermal energy during soil freezing induces the following phase transformations: the segregation of water in the liquid phase to ice, accompanied by thermal energy release and condensation of the gas phase to liquid, according to the phase equilibrium. A sharp reduction of the water and gas phases in the freezing pores has been ascribed to the analogy of drying by Henry [2].

Arenson *et al.* [3] has also noted that vertical veins do not grow in thickness as the horizontal lenses do over time. However, Arenson *et al.* did not identify a phase in which moisture is transported. They mentioned some concerns about the suction required to drive the hydraulic conductivity at atmospheric pressure, by determining that the negative pressure should be not less than 900 kPa to draw up the water.

Among all structures, the most vulnerable to frost heaving are highways. Due to the high density and increased thermal conductivity of the pavement and sub–base materials the temperature field in highway subsoils differs only slightly when compared to soils in a natural state [4]. Dynamic traffic load increases the pressure and melts some parts of the ice for a short period of time in highway subsoils [5]. The mechanism of short-term load application to the frozen subsoils can be explained by

a regelation theory, when that part of the ice located closest to the soil particles starts to melt under the pressure. The liquefied water migrates upwards to the cold side as soon as the dynamic load is removed and refreezes in the new place. The dynamic loading here acts as a piston pump.

The study focuses on moisture mass transfer in unsaturated soils, as this is the most likely state of soils under highways in the winter period. The article considers determination of moisture mass transfer implemented with vapour flow.

Research methods

Frost susceptible soils were conducted for 2 freezing-thawing cycles in open system laboratory tests, so the samples were supplied from the base by deionized water (Figure 1). In test 1 nine soil samples of 1 meter length sandy clay soil were compacted artificially to the maximum dry density and placed to the environmental chamber and simultaneously frozen from the top. In test 2 the length of the samples was reduced twice to 50 cm, while column 1 was compacted with the least dry density, increasing in every other column, and reaching the maximum density in column 9. The characteristics of the freeze-thaw cycles are presented in Table 1. The initial parameters of the soil samples are presented in Table 2.

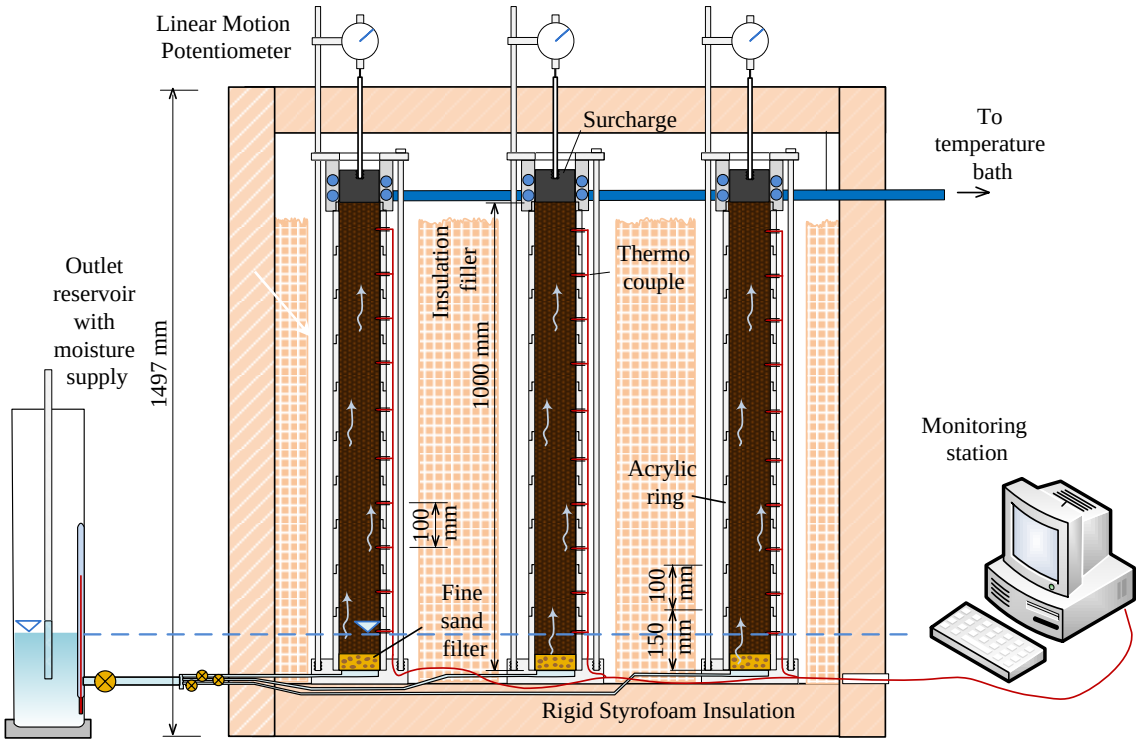

Figure 1. Environmental chamber for freeze-thaw cycles with a capacity of nine 1m length soil columns

Table 1

Freeze-thaw test characteristics

Test no.	Sample length	Base water supply	Dry density of the sample	Sample testing technique
1	100cm	Deionised water	All samples compacted with max dry density: 1.80 Mg/m^3	Three columns removed after the first freeze cycle, three columns after the first thaw and the remained three after the second freeze cycle
2	50cm	Deionised water	Samples compacted with varied dry density: 1.18-1.80 Mg/m^3	Nine columns kept until the end of the second freeze cycle

Table 2

Initial soil samples characteristics

Characteristic	Symbol	Unit	Value	Annotation
Initial moisture content	W	%	17.2	See Figure 3.1 – according to 95% max. dry density – moisture content relationship
Angle of internal friction	φ	°	24.1°	CD direct shear test, moisture content W=17.2%
Cohesion	C	kN/m²	10	
Particle density of sandy clay	ρ_s	Mg/m³	2.615	Soil mixture by mass: 50% sand and 50% kaolinite
Average dry density before freezing cycle	ρ_d	Mg/m³	1.814 ± 0.012	BS Light compaction test operating with 2.5 kg rammer. The mechanical energy applied to the soil is 596 kJ/m³
Initially bulk density at the beginning of the test	ρ	Mg/m³	2.128 ± 0.015	
Uniformity coefficient	Cu	-	2.4	Uniformly-graded sand
Coefficient of curvature	Cc	-	3.65	
Activity of Clays	A	-	0.25	Inactive clays
Liquid limit	w_L	%	37.18	CI – Medium plasticity cone penetrometer test used
Plastic Limit	w_P	%	23.77	Fraction of soil sample passed through 0.425 mm sieve
Average linear shrinkage	L_S	%	5	
Plasticity Index	PI	%	13	

A slow unidirectional freezing technique was used during the freezing to provide enough time for the cryosuction processes [6, 7]. The temperature drop was set by 2 ^{0}C every 24 hours for 12 days and reduced down to -23 °C at the temperature control unit. Temperature sensors were inserted in the center of each sample by every 10 cm of the length. 96 thermocouples continuously recorded the temperature via Pica loggers while frost heave was monitored by vertical linear gauges. The base of the soil samples were kept unfrozen during the entire experiment. By the end of the freeze-thaw cycles the moisture redistribution over the sample length was determined according to standard BS 1377-4:1990 by weight difference of the wet and oven dried sample at 105 °C for 24 hours.

The heat change Q in a mold section over the time t was found as the sum of the cooling heat and the latent heat during the phase transfer:

$$Q \cdot t = Q_1 + Q_2 \quad (1)$$

where, Q_1 – heat energy is used for cooling the vapour mass to the temperature ΔT (equation 5.5); and Q_2 – heat energy used for the phase transfer (eq. 5.7).

$$Q_1 = m_{vapour,}, t_i \cdot C \cdot \Delta T \quad (2)$$

where, $m_{vapour}, t_{1,}$ - mass of vapour at the starting time t_1,g;C – specific heat of vapour passing through the cumulative air voids cross section, $J/kg \cdot ^{o}C$; ΔT – temperature change, ºC; and t – time interval, h.

Density of the vapour is calculated for each period of time, corresponding to the temperature and saturated vapour pressure:

$$\rho_{vapour,t_i} = \frac{m_{vapour,t_i}}{V_{air,t_i}} \quad (3)$$

where, ρ_{vapour,t_i}- vapour density for period of time, g/cm³.

Heat energy for the phase transfer includes the latent heat for the condensation and solidification of the vapour mass difference at the beginning t_1 and end time t_2 of the calculation period.

$$Q_2 = (m_{vapour,1} - m_{vapour,2}) \cdot L \quad (4)$$

where, $m_{vapour,2}$ – mass of the vapour at the end period t_2; L – is a total latent heat $L = L_1 + L_2$, where L_1 - specific latent heat for condensation ($L_1 = 2.3 \cdot 10^6 J/kg$) and L_2 - specific latent heat for solidification ($L_2 = 0.335 \cdot \frac{10^6 J}{kg}$ of 1 kg of water).

The volume of vapour V_{vapour} is equal to the speed of vapour passing through the air voids' cross section A over the time t:

$$V_{vapour} = v \cdot t \cdot A_{air\ voids} \quad (5)$$

where, v – average speed of vapour, cm/h; and $A_{air\ voids}$ – cumulative section cross of the air voids' $A_{air\ voids} = \frac{\pi \cdot {d_a}^2}{4}$, cm², corresponding to the porosity coefficient and moisture content (Figure 2).

Substituting the V_{vapour} in equation (2) the vapour speed was found at the starting time and at the end:

$$v_{vapour} = \frac{Q}{C \cdot \rho \cdot A_{air} \cdot \Delta T \cdot t} \quad (6)$$

The mass of ice built from the vapour passing through the air voids channels in a 10 cm length mould section with correspondent cumulative cross section A_{air} and speed v over time t is calculated:

$$m_{ice} = \rho_{vapour} \cdot V_{air\ voids} = \rho_{vapour} \cdot v \cdot t \cdot A_{air} \quad (7)$$

where, m_{ice} - mass of built ice in grams; ρ_{vapour} – is taken as an average density value of the vapour densities at the start and end time point, g/cm³ .

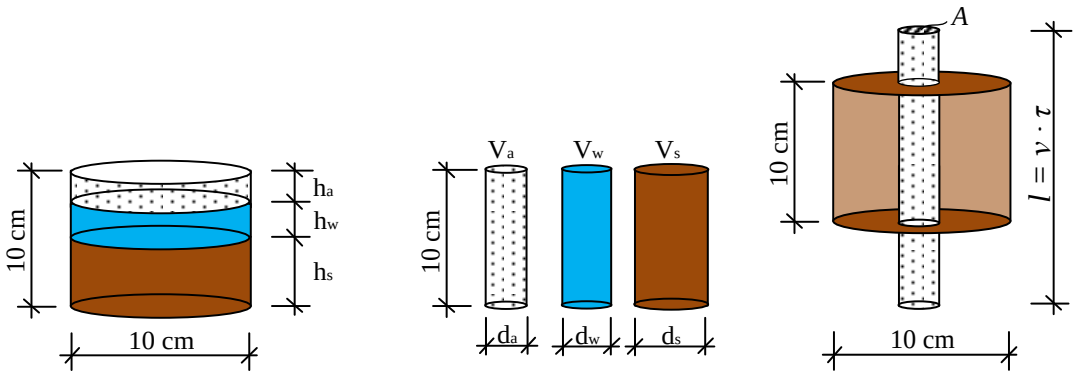

Figure 2. Calculation of the vapour rate passing through the cumulative air voids channel in the mould section over time t

Results and discussion

In Test 1, the temperature drop was less pronounced due to the formation of ice lenses at the top of the soil columns and the resulting latent heat released for the increased amount of water. The top 5 cm of soil in Figure 3a dropped down sub-zero temperatures, while the temperature distribution over the length of the samples stayed in a range of +5 - +10 °C. Ice lens formation was observed at the top of the sample, which appears to act as a heat insulator and prevented the further freezing of the soil. In Test 2 the temperature distribution changed with a range of soil density, although did not obtain a steady pattern of freezing rate in terms of ınıtıal density. This is possible because the freezing rate of 2 °C per day provided sufficient time for temperature distribution across the entire length. Notably, a deceleration of the freezing rate was observed in the second freezing cycle. The temperature field distribution with time in Test 2 was similar to Test 1, where the temperature contours in the second freezing cycle were higher compared to Test 1.

a)

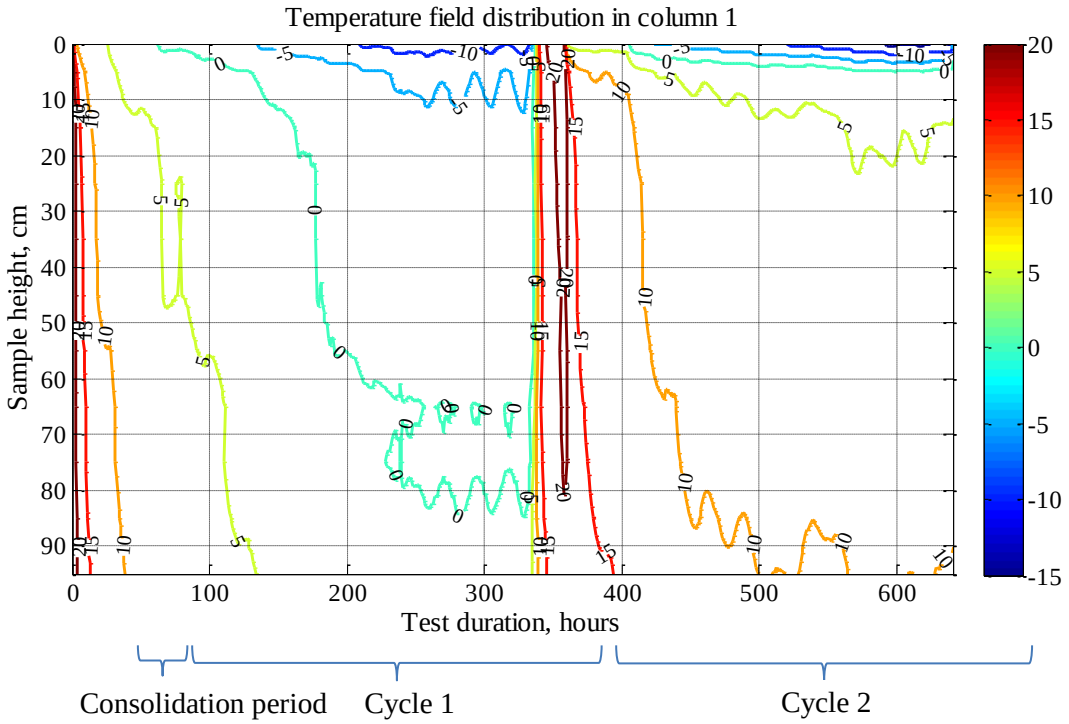

b)

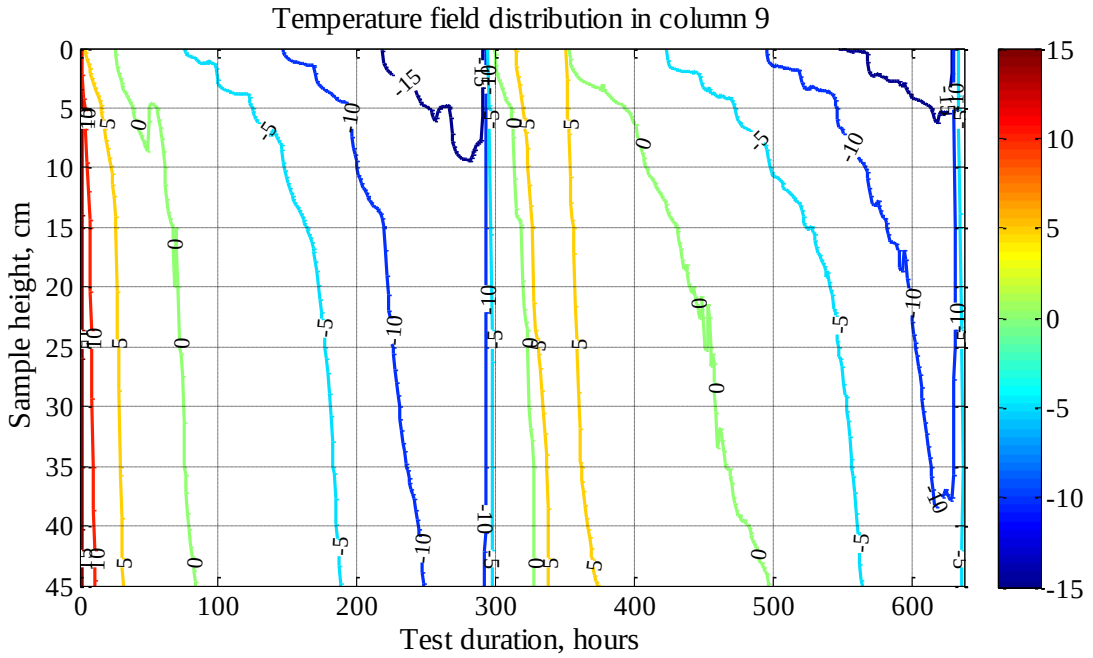

Figure 3. Temperature contours in column 1 in Test 1 and 2, supplied with deionized water from the column base with (a) max and (b) variable soil densities.

The average duration of testing comprised over 600 h. The relationship between the surface temperature and frost heave value over time for the soil samples compacted with maximum dry density is presented in Figure 3. In both tests, the greatest variety of volumetric deformation in the vertical axis was registered by the end of the second freezing cycle. The frost heaving value for test 1 twice exceeds the frost heaving in test 2 correspondently to the length of the sample. In Test 3 with a deionized water supply, the maximum rates of frost heave were achieved in columns 7 and 8, where the dry density was close to the maximum value 1.65-1.79 Mg/m³, while the loose soil samples, with a dry density 1.18-1.47 Mg/m³, registered very weak heaving in the first cycle and consolidation or compression in the second cycle compared to the initial volume.

a)

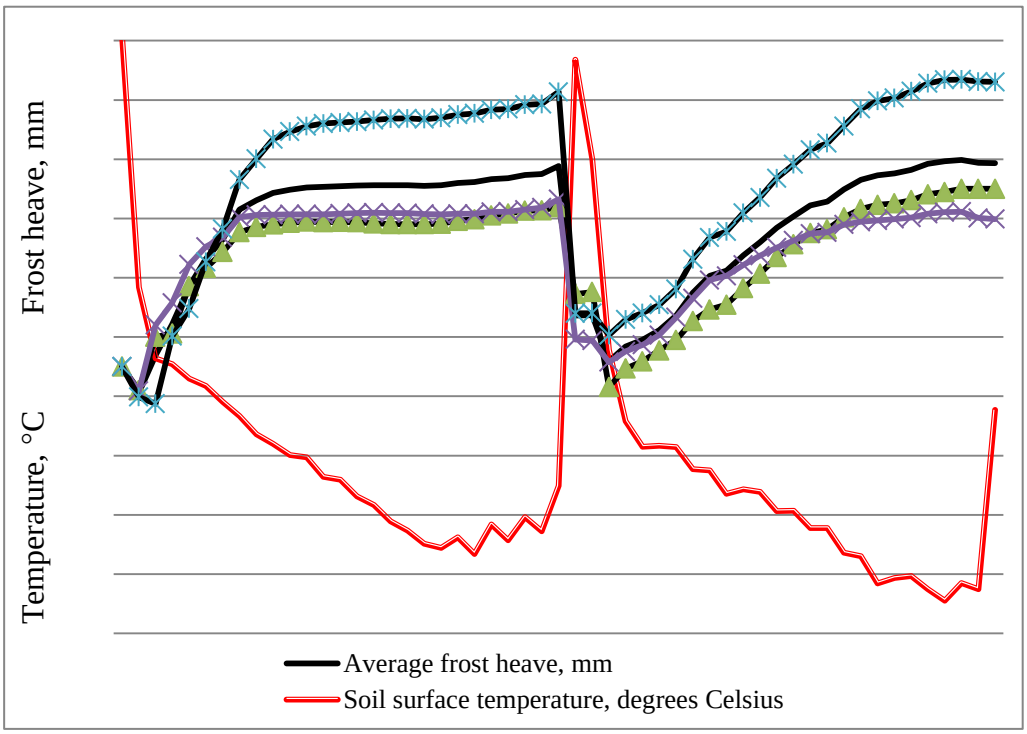

b)

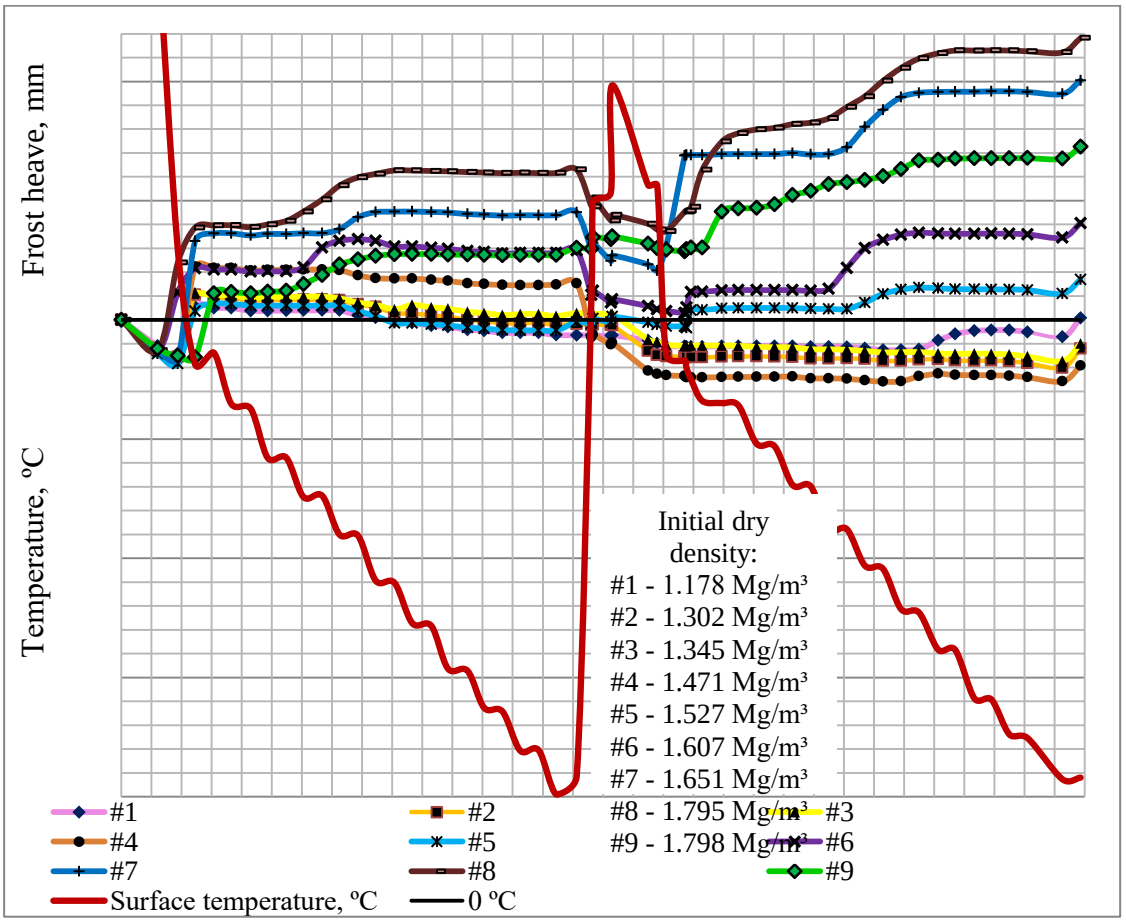

Figure 4. Relationship between surface temperature and frost heave: a - Test 1 b -Test 3

Regarding the moisture intake, there was a significant increase in moisture, reaching 40% in the top 10 cm layer of the soil samples in Test 1, which were draining and moistening the 20 cm under this layer during the thawing period. Although the water was drawn upwards again as the second freezing cycle started. According to the results in Test 2, the moisture content represents advanced water intake in the loose soil, with a dry density range between 1.18-1.65Mg/m³, comparing to dense soils with dry density 1.8 Mg/m³. Except for sample 4, in all the columns the moisture content reached 24.5% or above by the end of the test. The reason for low moisture intakes in sample 4 could have been due to occasional violation of the water supply during the freeze-thaw test.

a)

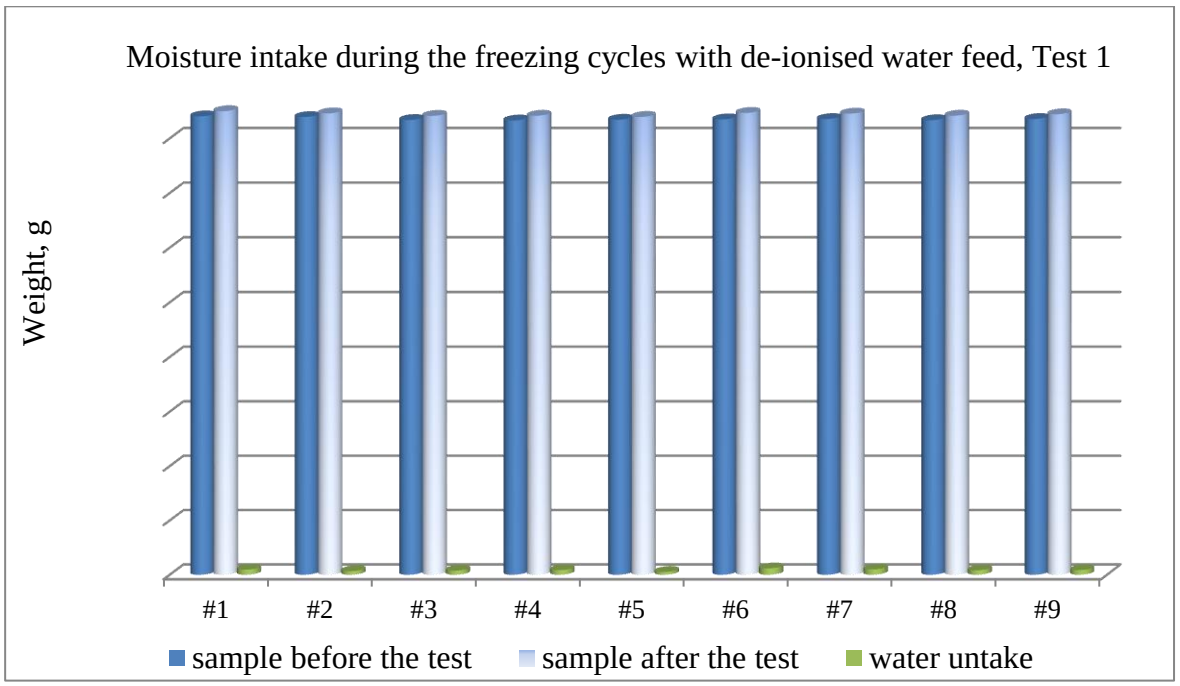

b)

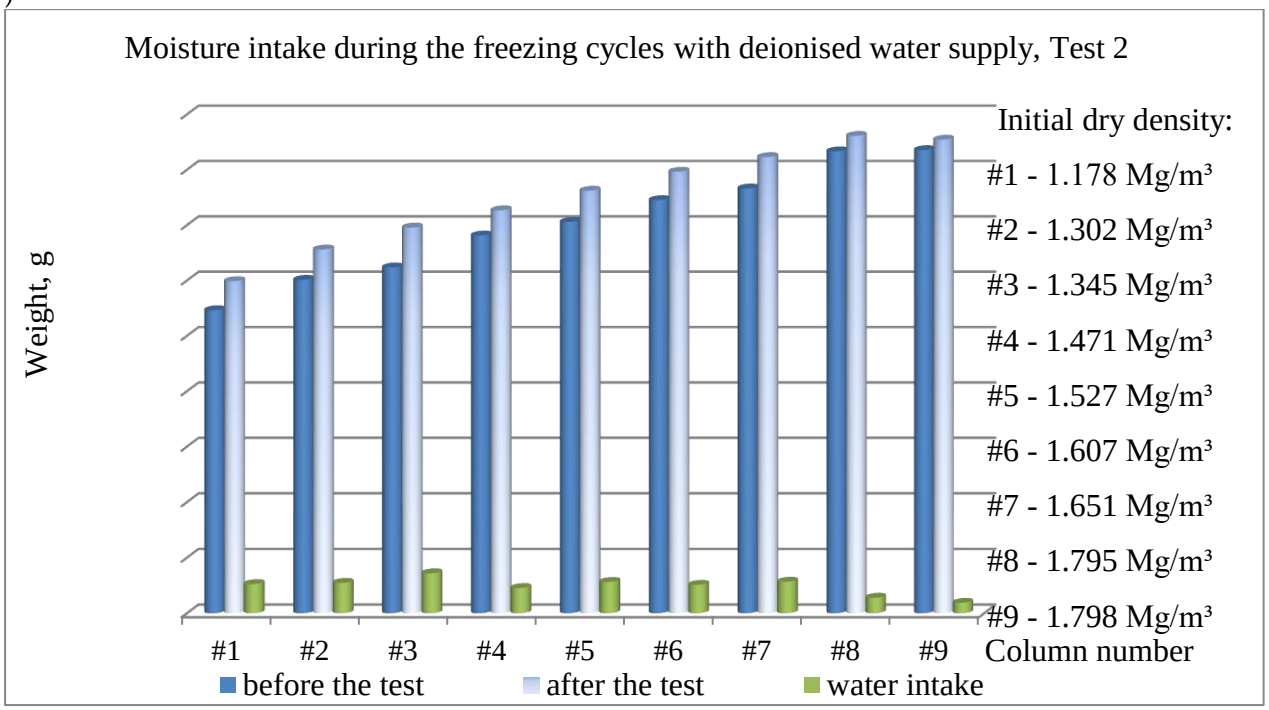

Figure 5. Moisture intake during Test 1 (a) and Test 2 (b) with maximum dry density and 1 m soil sample height

Ice lens formation in the top 10 cm layer caused a highly irregular distribution of moisture, which was confirmed by the centimeter sampling in Figure and also in the soil structure. The moisture intake in Test 2, with a shallow 45 cm depth groundwater supply table was higher than for Test 1, where the water supply was located at 95 cm depth and the soil samples were made with maximum dry density. For this reason, the moisture content between 15 and 45 cm from the soil surface was relatively stable and depended just on the density of the soil samplesa)

a)

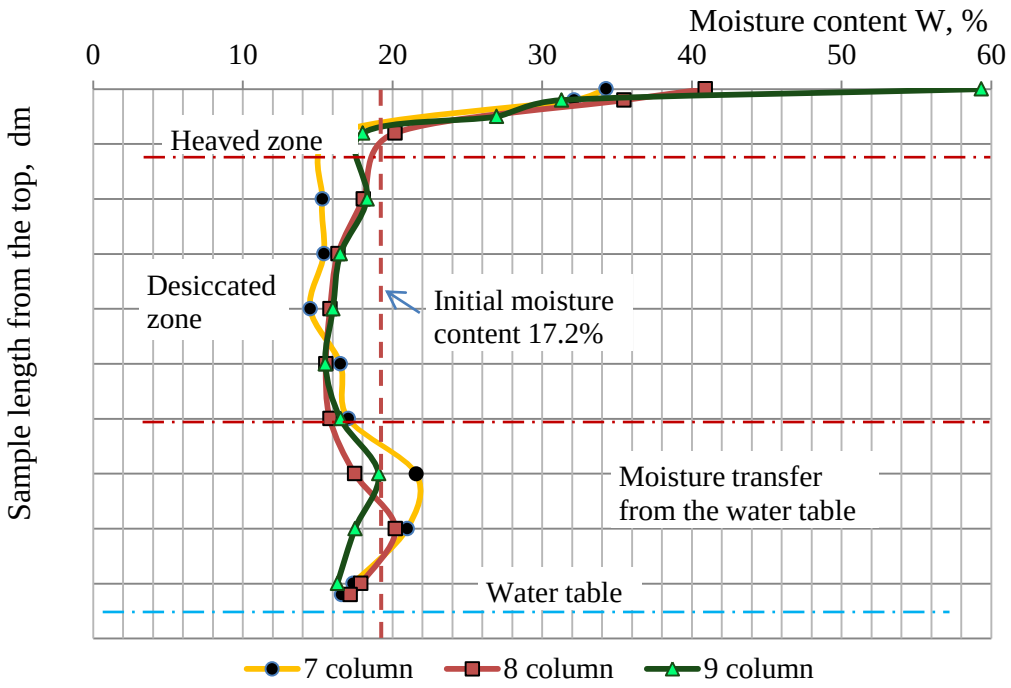

b)

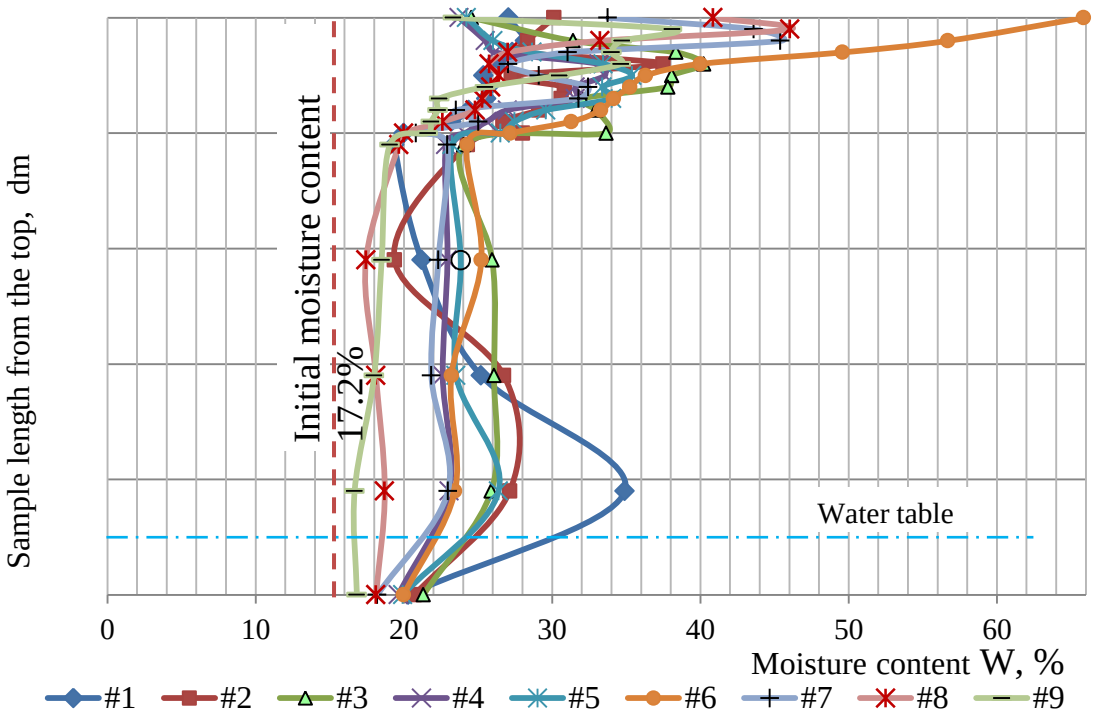

Figure 6. Moisture redistribution by the sample length after two freeze-thaw cycles with a deionized water supply: a –Test 1, b –Test 2

The coefficient of permeability of soil columns in Test 1 varied in the range of *2.9-8.8x10-9* m/s. Here, the moisture transfer was induced by cryosuction forces. The amount of transported moisture is related to the cooling rate and thus to the amount of energy lost, which is distributed to the phase transfer energy and cooling of each soil component, according to its heat conductivity.

Calculations of the vapor mass transfer are presented in Tables 3 and 4 on the example of column 1 in Test 2. The length of the soils sample in Test 3 was 50 cm, which was composed of five assembled mould sections, each 10 cm in length.

Table 3

Initial density characteristic in Column 1, Test 2

Sample section	Volume of solids, cm^3	Volume of voids, cm^3	Voids ratio $e=\varrho_s/\varrho_{dry}-1$	Volume of air , cm^3	Temperature at 590 h	Saturated vapour pressure over ice, P_{si}, Pa	Mass of vapour at 590, g	Density of the saturated vapour at 590h, Mg/m^3
#11	**370.62**	**448.46**	**1.21**	**180.55**	**-10.99**	**237.93**	**$3.55\cdot10^{-4}$**	**$1.97\cdot10^{-6}$**
#12	352.97	432.43	1.23	228.13	-10.30	253.24	$4.76\cdot10^{-4}$	$2.09\cdot10^{-6}$
#13	352.97	432.43	1.23	198.83	-9.49	272.16	$4.45\cdot10^{-4}$	$2.24\cdot10^{-6}$
#14	352.97	432.43	1.23	129.85	-8.36	300.63	$3.19\cdot10^{-4}$	$2.46\cdot10^{-6}$
#15	352.97	432.43	1.23	154.52	-6.46	354.77	$4.45\cdot10^{-4}$	$2.88\cdot10^{-6}$

Table 4

Calculation of the moisture mass transfer in freezing soils on the example of Test 2, column 1

Sample section	Temperature at 614 h, °C	Saturated vapour pressure over ice, P_{si}, Pa	Mass of vapour at 614 h, g	The heat realised in 24 hours $Q\cdot t=m\cdot C\cdot \Delta T$, J	Vapour rate $v=4\cdot N/(C\cdot\rho\cdot\pi\cdot d^2\cdot\Delta T)$, cm per 24 h	Vapour rate, cm/h	Build-up of ice mass between the period 590/614 h, g/hour
#11	**-13.30**	**193.26**	**$2.91\cdot10^{-4}$**	**0.1702**	**9.008**	**0.375**	**$2.67\cdot10^{-6}$**
#12	-12.60	205.98	$3.91\cdot10^{-4}$	0.2269	9.014	0.376	$3.56\cdot10^{-6}$
#13	-11.68	223.81	$3.69\cdot10^{-4}$	0.2016	9.067	0.378	$3.16\cdot10^{-6}$
#14	-10.43	250.35	$2.68\cdot10^{-4}$	0.1363	9.126	0.380	$2.14\cdot10^{-6}$
#15	-8.96	284.98	$3.61\cdot10^{-4}$	0.2237	8.956	0.373	$3.51\cdot10^{-6}$

The average vapour rate was around 0.4 cm/h. The build-up of ice mass between the period in 24-hour period varied in a range of 2.14·10-6 -3.56·10-6 g, depending on the void ratio and temperature change. Here, it is assumed that the porosity coefficient of the sample remains constant during the calculation period. Consequently, the volume of the air voids and the cumulative cross-section of the air voids also remained constant. It should be noted that only heat consumed for the gas phase energy exchange was considered in this problem. The solid and liquid parts have also been cooled down with the heat withdrawn by the cooling machine. However, they are not counted, because all the necessary energy exchange has been done by an automatic set of temperature controls.

Conclusion

There was considered positioning of the soil structure, based on the experimental data of the measured temperature, vertical linear volumetric change registered by testing time, and the obtained moisture-density relation.

Further outcomes have been concluded from the presented material:

1. The obtained results have improved understanding of the heat and mass transfer phenomenon during the unidirectional freezing of soils in an open system.
2. Most of the tests for engineering properties registered a slight reduction in strength, cohesion, and angle of internal friction. However, there was a significant increase in the coefficient of permeability after the freeze-thaw cycles with initially dense compacted soil samples, which was due to loosening and moistening of the soil samples during the heave at sub-zero temperatures.
3. The conceptual model for frost heave in soils was developed based on the vapour mass transfer. The algorithm of vapour flow calculation in unsaturated soils was presented using fundamental thermodynamic equations.
4. The model is suitable for numerical solutions, like finite element analysis or a model like a coupled heat-water transfer, in terms of considering the vapour flow and considering the cryosuction forces. The latent heat for the phase transitions and the dynamic change of the coefficient of porosity and air void volume needs also to be considered.

References

1. Tschapek M., Scoppa C.O. and Wasowski C. The surface tension of soil water / Journal of Soil Science. -1978. -vol. 29, no. 1. -pp. 17-21.

2. Henry K.S. A review of the thermodynamics of frost heave / Henry, K.S. -Hannover, New Hampshire: US Army Corps of Engineers, -2000.

3. Arenson, L.U., Azmatch, T.F. and Sego, D.C. 'A new hypothesis of ice lens formation in frost-susceptible soils'// Ninth International Conference of Permafrost, Fairbanks, Alaska, -2008. -pp. 59-65.

4. Chunpeng H., Yanmin J., Peifeng Ch., Guibo R. and Dongpo H. 'Automatic Measurement of Highway Subgrade Temperature Fields in Cold Areas' / Chunpeng, H. - Intelligent System Design and Engineering Application (ISDEA), 2010 International Conference, -2010. -pp. 409-412.

5. Sarsembayeva A.S., Zhussupbekov A.Zh. Experimental study of deicing chemical redistribution and moisture mass transfer in highway subsoils during the unidirectional freezing // Transportation geotechnics. -2021. -26.

6. Sarsembayeva A, Collins P. A modified freeze-thaw laboratory test for pavement sub soils affected by de-icing chemicals. / Engineering Geology for Society and Territory. Applied Geology for Major Engineering Projects 6. Switzerland: Springer International Publishing. -2015. - p.243.

7. Sarsembayeva A, Collins P. Evaluation of frost Sarsembayeva A, Collins P. Evaluation of frost heave and moisture/chemical migration mechanisms in highway subsoil using a laboratory simulation method // Cold Reg Sci Technology. -2017. -Vol. 133. -Pp. 26-35.

А.С. Сарсембаева[1], А.Ж. Жусупбеков[1,2,3], Ф.Э.Ф. Коллинз[4]
[1]Л.Н. Гумилев атындағы Еуразия ұлттық университеті, Нұр-Сұлтан, Қазақстан
[2]Санкт-Петербург мемлекеттік сәулет-құрылыс университеті, Санкт-Петербург, Ресей
[3]KGS, ЖШС, Нұр-Сұлтан, Қазақстан
[4]Лондондағы Брюнель Университеті, Лондон, Ұлыбритания

Сазды топырақтардың аяздан қатуын анықтау

Аңдатпа. Өткізгіштік коэффициенті төмен сазды топырақта өтетін аяздың қатуы криосакцияға, беттік керілу күштеріне және судың фазалық ауысуына қатысты көптеген сұрақтар туғызады. Бұл жұмыста мұздату-еріту зертханалық зерттеулерінің нәтижелері бойынша температура мен көлемдік параметрлердің өзгеруі, құрғақ топырақтың тығыздығы және су массасының тасымалдануы қарастырылды. Криогендік күштердің әсерінен газ күйіндегі судың (будың) тасымалдануын есептеу моделі келтірілген. Зерттеу нәтижелері ашық жүйедегі топырақты бір бағытты мұздату кезіндегі жылу және масса алмасу құбылысы туралы түсінікті жақсартуды қамтиды. Инженерлік қасиеттерге арналған сынақтардың көпшілігінде үйкеліс күші, беріктігі және ішкі үйкеліс бұрышының шамалы төмендеуі тіркелді. Алайда, бастапқыда тығыздалған топырақ сынамаларымен мұздату-еріту циклдарынан кейін өткізгіштік коэффициентінің едәуір өсуі байқалды. Бұл нөлдік температурада үйінді кезінде топырақ үлгілерінің қопсытуына және ылғалдануына байланысты болды. Буланған массаның тасымалдануына негізделген топырақта аяздан ісінудің тұжырымдамалық моделі жасалған. Сумен қанықпаған топырақтағы бу шығынын есептеу алгоритмі іргелі термодинамикалық теңдеулер көмегімен ұсынылды.

Түйін сөздер: аязды көтеру, температураны бақылау, ылғалдың берілуі, сазды топырақтар, зертханалық сынақ, будың берілуі**.**

А.С. Сарсембаева[1], А.Ж. Жусупбеков[1,2,3], Ф.Э.Ф. Коллинз[4]
[1]Евразийский национальный университет им.Л.Н.Гумилева, Нур-Султан, Казахстан
[2]Санкт-Петербургский государственный архитектурно-строительный университет, Санкт-Петербург, Россия
[3]KGS, ТОО, Нур-Султан, Казахстан
[4]Брюнель Университет Лондона, Лондон, Великобритания

Оценка морозного пучения глинистых грунтов

Аннотация. Морозное пучение в глинистых грунтах с низким коэффициентом проницаемости вызывает множество вопросов, касающихся криогенных сил, поверхностного натяжения и сопутствующего фазового перехода воды. В работе рассмотрены результаты лабораторных испытаний замораживания-оттаивания с точки зрения изменения температурных и объемных параметров, плотности в сухом состоянии и массопереноса воды. Представлена модель для расчета массопереноса воды (пара) в газовом состоянии под действием криогенных сил. Результаты исследований включают улучшенное понимание явления тепломассопереноса при однонаправленном промерзании почв в открытой системе. В большинстве испытаний инженерных свойств было зарегистрировано небольшое снижение соотношения прочности, сцепления и угла внутреннего трения. Однако наблюдалось значительное увеличение коэффициента проницаемости после циклов замораживания-оттаивания с изначально плотными уплотненными образцами грунта, что было связано с разрыхлением и увлажнением образцов

грунта во время вспучивания при отрицательных температурах. На основе паромассопереноса разработана концептуальная модель морозного пучения грунтов. Алгоритм расчета парового потока в ненасыщенных грунтах представлен с использованием фундаментальных уравнений термодинамики.

Ключевые слова: морозное пучение, мониторинг температуры, влагоперенос, глинистые почвы, лабораторные испытания, парообмен.

References

1. Tschapek M., Scoppa C.O. and Wasowski C. The surface tension of soil water. Journal of Soil Science. 29(1), 17-21 (1978).
2. Henry K.S. A review of the thermodynamics of frost heave. Henry, K.S. US Army Corps of Engineers, Hannover, New Hampshire, 2000.
3. Arenson L.U., Azmatch T.F. and Sego D.C. 'A new hypothesis of ice lens formation in frost-susceptible soils'. Ninth International Conference of Permafrost, Fairbanks, Alaska, 2008. pp. 59-65.
4. Chunpeng H., Yanmin J., Peifeng Ch., Guibo R. and Dongpo H. 'Automatic Measurement of Highway Subgrade Temperature Fields in Cold Areas'. Chunpeng, H. - Intelligent System Design and Engineering Application (ISDEA), 2010 International Conference, 2010. 409-412.
5. Sarsembayeva A.S., Zhussupbekov A.Zh. Experimental study of deicing chemical redistribution and moisture mass transfer in highway subsoils during the unidirectional freezing. Transportation geotechnics. 26, (2021).
6. Sarsembayeva A, Collins P. A modified freeze-thaw laboratory test for pavement sub soils affected by de-icing chemicals. Engineering Geology for Society and Territory. Applied Geology for Major Engineering Projects 6. (Springer International Publishing, Switzerland, 2015. p. 243).
7. Sarsembayeva A, Collins P. Evaluation of frost Sarsembayeva A, Collins P. Evaluation of frost heave and moisture/chemical migration mechanisms in highway subsoil using a laboratory simulation method. Cold Reg Sci Technology. 133, 26-35 (2017).

Information about authors:

Assel Sarsembayeva - Civil Engineering, Department of Civil Engineering, L.N. Gumilyov Eurasian National University, Nur-Sultan, Kazakhstan.

Askar Zhussupbekov - Civil Engineering, Department of Geotechnics, Saint-Petersburg State University of Architecture and Civil Engineering, Saint–Petersburg, Russia.

Philip E. F. Collins - Civil Engineering, Department of Civil and Environmental Engineering, Brunel University London, London, United Kingdom.

Асель Сарсембаева - Л.Н. Гумилев атындағы Еуразия ұлттық университетінің құрылыс бөлімі, Нұр-Сұлтан, Қазақстан.

Асқар Жүсіпбеков - Санкт-Петербург мемлекеттік сәулет-құрылыс университетінің геотехника кафедрасының инженерлік-құрылыс факультеті, Санкт-Петербург, Ресей.

Филипп Ф. Коллинз - Брунель университетінің Азаматтық инженерия, Азаматтық және қоршаған орта факультеті, Лондон, Ұлыбритания.

IRSTI 67.11.29

Ph.E.F. Collins

Brunel University, London, England
E-mail: philip.collins@brunel.ac.uk

Ice-affected soil systems under rapid climate warming - insights from the past

Abstract. Current climate warming is expected to lead to ongoing geotechnical change in ice-affected soils. Examining past climate change, particularly cold stage:warm stage transitions can provide an insight into the potential nature of this change and may inform assessments of sites. The evidence is sometimes ambiguous, with periglacial and seismic processes producing similar results. Ice core evidence suggests that cold-warm transitions, such as during the onset of the Greenlandian stage of the Holocene can be high magnitude, but also may feature reversals that add instability to soil systems. Consideration of future geotechnical change in ice-affected soils must therefore take into account potentially complex climate forcing.
Keywords: Periglacial, Greenlandian, deformation, climate change, thaw.

DOI: doi.org/10.32523/2616-7263-2021-135-2-27-36

Introduction

There is scientific consensus that the world is experiencing a period of climatic change, with generally warmer global conditions already becoming apparent (ref). Predictive models suggest the change will continue, with mid- and high-latitude regions being particularly affected. This can be expected to impact on soil systems with distinct threshold conditions, particularly those which are currently characterised by the presence of ice for at least part of the year. The phase change in water in these soils, whether it is in the extent, duration or frequency of freeze-thaw, can be expected to alter their geomechanical properties in the short term and may leave a long term impact.

An understanding of ice-affected soil behaviour during warming episodes is clearly of scientific interest. It is also directly relevant to engineering design which needs to identify and address all the actions and influences that may affect a site (cf. Eurocode: BSI 2002).

Although there is a growing body of research detailing recent change in ice-affected soil systems and associated features in response to warming, the time span of these studies is only just beginning to reveal what may happen as the warming trend continues. There is also an understandable bias towards what might be considered the most sensitive contexts, particularly regions where permafrost is already at the thaw threshold and mountainous sites where steep slopes accentuate change (e.g. Harris et al. 2009; Gao et al. 2021).

These studies are very important, of course, but might not provide a close analogue to what could happen in lower latitude areas affected by higher insolation or by seasonal freezing, or in the coldest high latitude regions. Understanding the potential for geomechanical changes in soils in these areas is important as they are extensive and also home to significant human populations. In such areas, change might be expected to often take place less rapidly and is likely to vary from place to place, reflecting locally different conditions. However, these assumptions need to be tested.

One way to evaluate how ground systems might change is to examine what has happened in the past. In this paper, the influence on soils of the warming event that marked the last glacial-interglacial transitionsexamined for areas that were under periglacial conditions, with a focus on the mid-latitudes, using selected sites. The implications for future changes to fundamental geotechnical parameters are considered.

Cold-stage:warm-stage transitions in the past

The current geological period, the Quaternary, has been marked by multiple climatic shifts. In

mid-high latitudes, these are typically characterised as alternating Ice Ages and interglacials, with cycles occuring over tens of thousands of years, or longer. The reality is that the climatic shifts have often been much shorter, with sometimes abrupt transitions (Taylor et al. 1993).

Unfortunately, issues with preservation and dating mean that it is not always possible to assess whether an identified change in ground conditions occurred at a climate transition or was due to a temporary thaw. There are also issues with interpretation which often reflect the investigator's training – the most obvious being the similarity between features associated with changes in soil ice conditions and those induced by seismicity (van Vliet-Lanoe et al. 2004).In some locations, where regional deglaciation caused glacio-tectonic adjustments, both freeze-thaw and seismicity may have affected soil strength and behaviour. An example of where compressive loading and liquefaction may have happened at around the same time is shown in Figure 1.

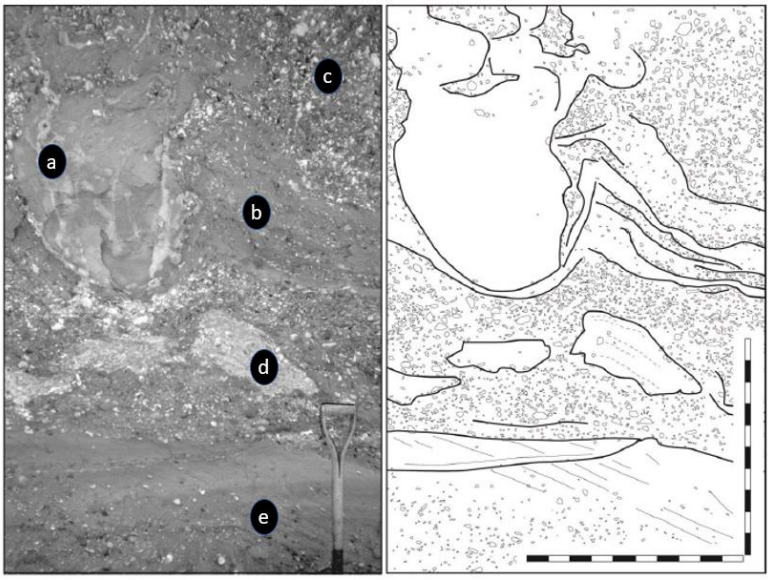

Figure 1. Deformed Middle Quaternary fluvially-derived soils from a site in south-central England. a) sand-silt load cast; b) 'kink' structure indicating lateral compression; c) unstructured sand-clay-gravel, with occasional vertically-oriented clasts; d) boudinage-like structure where a depositional unit has been deformed and broke, with possible rounding of some edges suggesting movement in a liquefied mass; e) undisturbed fluvial sandy gravel.

A selection of different types of feature that could be interpreted either way are presented in Table 1 (modified from Collins 2014).

Table 1

Selected soft sediment deformation structures that might indicate warming or seismicity. Processes most likely to be linked to ice collapse/thaw are marked with an *. Sources provided in Collins 2014.

Periglacial		***Seismic***	
Form	Process and key features	*Form*	Process and key features
Vertically oriented clasts	1. Differential freeze-thaw heave between a clast and the soil/sediment matrix leading to vertical movement and alignment. May occur at a uniform depth across a unit/site	*Aligned clasts*	Clasts aligned to flow of liquefied material. Localised.

	2. Rapid thaw leading to liquefaction and clast alignment*		
Fissure fill / Sediment wedge	Gravity driven (i.e. downwards) infilling of thermal contraction or mass movement-induced fissure. Typically wider at top. May show stratification.*	*Dyke – Neptunian (formed under water) / Fissure fill (sub-aerial)*	Gravity driven (i.e. downwards) infilling of seismically-induced fissure. Typically wider at top. May show stratification.
		Dyke - injection	Pore fluid pressure driven infilling of fissure (principally upwards). Typically narrower at top. Particles may be graded (fining up).
		Sill - injection	Pore fluid pressure driven infilling of fissure (principally lateral).
Ice wedge cast	1. 2. Cyclic thermal contraction/expansion of permafrost producing surficial crack that progressively infills and widens. Often in a polygon. 3. Thaw of ice wedge producing "draw-down" of overlying and adjacent soil/sediment along a line. *	*Thixotropic wedge*	Subsurface movement (and consolidation?) resulting in "draw-down" of overlying and adjacent soil/sediment in a limited area (cm^2?) or along a line.
Mud boil	Surface accumulation fed from injection pipe or larger fissure that reaches the surface.*	*Sand volcano, sand boil*	Surface accumulation fed from typically linear injection dyke that reaches the surface.
Thermokarst depression	Surface depression formed by thaw of ground ice resulting in "draw-down" of overlying soil/sediment in a broad area (m^2 to km^2). May subsequently be infilled.*	*Thixotropic bowl*	Surface depression formed by subsurface movement (and consolidation?) resulting in "draw-down" of overlying soil/sediment in a broad area (m^2?). May subsequently be infilled.

		Floating breccia	Fragments of a previously intact unit, broken by intense lateral cyclic shear and suspended within a matrix of liquefied sediment/soil. Individual fragments might themselves exhibit internal deformation. May be at a ± uniform elevation and may show evidence of horizontal attenuation (pseudo-boudinage structure).
Flame structures	1. Plastic upwards deformation under cyclic freeze-thaw stress* 2. Liquid limit exceeded and spatially variable loading causing injection into overlying soils*	*Diapiric structures*	Plastic upward deformation under seismic load stress. Grades into injection dykes if soil/sediment becomes fully liquefied. Reflects deeper unit having a lower dynamic viscosity than overlying soil/sediment. Margins may feature micro-faults, with upwards displacement. Adjacent areas may show evidence of subsidence.
Load cast, pillow structures	Isolated mass of sediment that has sunk into an underlying unit that has experienced freeze-thaw induced plastic deformation, liquefaction and/or localised consolidation producing density changes.*	*Load cast, pillow structures*	Isolated mass of sediment that has sunk into an underlying unit that has experienced hydro-plastic deformation, liquefaction and/or localised consolidation due to cyclic shear density changes. Range of sizes (<cm to >m).
		Dish/Pocket-and-pillar structures	Modification of existing structures due to shock-induced dewatering.
Involutions	Plastic deformations resulting from ice growth and decay. May also result from rapid thaw settlement and liquefaction.*	*Sismoslump / Involutions*	Convoluted sedimentary structures reflecting in situ deformation due to cyclic lateral seismic loading. Under- and overlying strata may be intact or show grading (increasing deformation towards surface). Structures may show no sign of compression due to subsequent burial.
Wavy structures	Plastic deformations resulting from ice growth and decay.	*Wavy structure / anticline-syncline*	± uniformly folded unit reflecting in situ deformation due to cyclic lateral seismic loading. Under- and overlying strata may be intact or show grading (increasing deformation towards surface). Structures may show no sign of compression due to subsequent burial.

Impact of the last glacial-interglacial transition on terrestrial ground systems

The most precisely defined of the major Quaternary climate transitions is the Late Pleistocene to Holocene. The end of the last major glacial period (Marine Oxygen Isotope stage 2) was marked by significant climatic change. After a glacial maximum at approximately 20,000 years before present (20 kaBP), many geological sites around the world record a warming episode peaking at about 13kaBP, before a return to cold conditions that ended at around 11.65 kaBP i.e. the start of the Greenlandian stage of the Holocene interglacial (Walker et al. 2018).

Characteristics of the Greenlandian

Ice core and other evidence indicates that the transition into the Greenlandianat about 11.65 kaBPwas marked by a significant warming in the northern Hemisphere over a short period – perhaps less than 100 years (Figure 2). The Greenlandian itself, at least in North Atlantic and adjacent areas, was marked by some ongoing climatic instability, reflectingchanges in the relative significance of warm oceanic waters moving north and pulses of meltwater from the North American, Greenland and north European ice sheets (van der Bilt et al. 2019). This instability appears to be shown in ice core data where the rate of change in the climate proxy$d^{18}O$ fluctuates during and after the transition.

Terrestrial impact of the Younger Dryas-Greenlandian transition

It is logical to presume that the impact of this climate change on terrestrial ground environments was substantial and rapid. Direct and unambiguous evidence of how these conditions changed is, however, limited. This is partly due to subsequent erosion, and partly due to lack of dating control. Many features attributeto freeze-thaw and other ice-related processes during the Younger Dryas or earlier date to this transition period.

The scale of the change that affected at least the geotechnical properties of at least the upper parts of soil units can be inferred from fluvial deposits. River sediment sequences in the UK record a sudden change from snow-melt flow regimes represented by coarse sediments to much lower energy conditions represented by significant volumes of sand, silt and clay. In an earlier study of a chalk and clay catchment in south-central England (Collins et al. 1996, 2006), this change was found to have occurred in a timespan less than the probability error for a radiocarbon date, as shown in the example in figure 3.

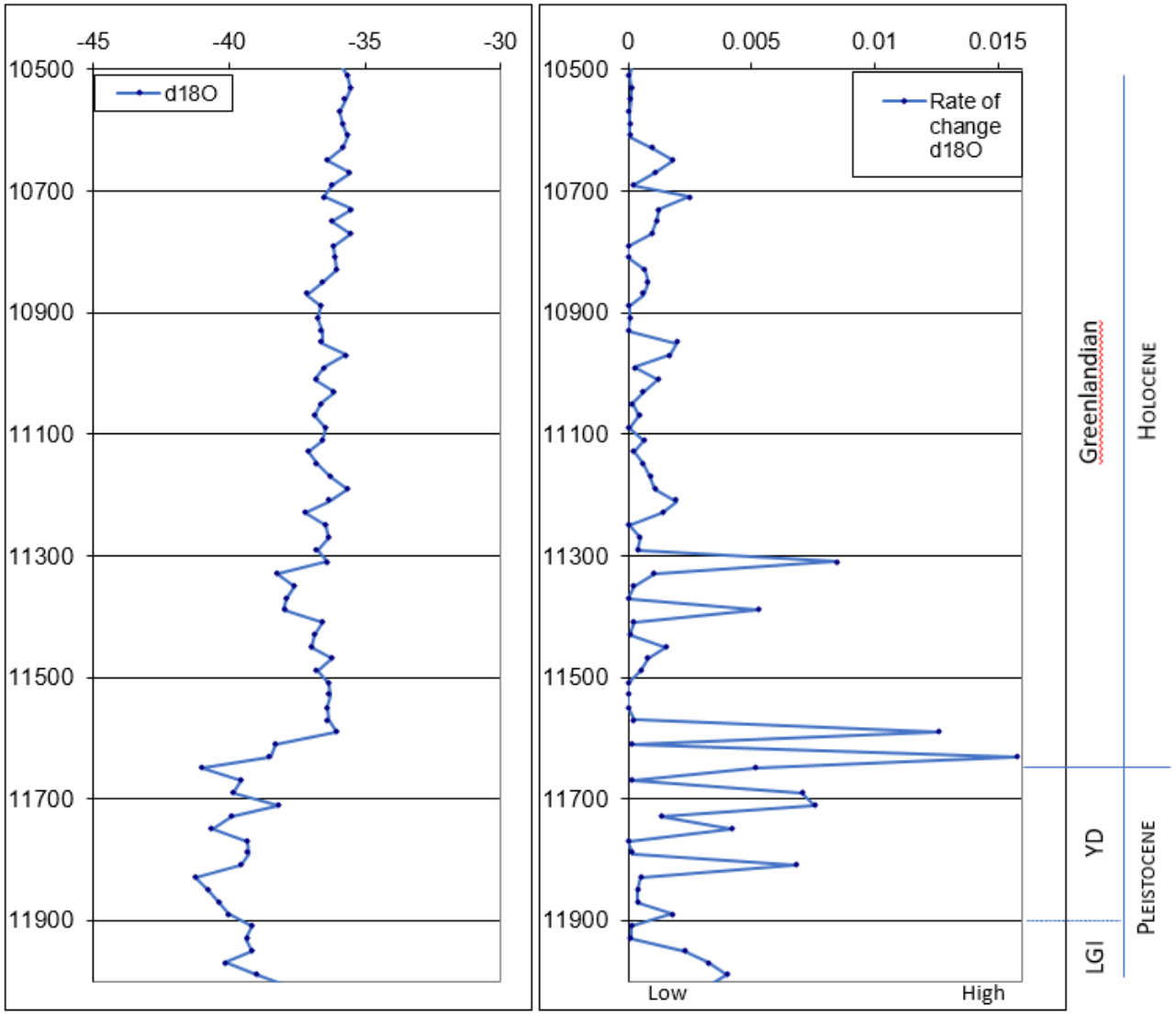

Figure 2. Oxygen isotope record from the GISP2 Greenland ice core stratotype (data source: NOAA-NCEI undated). Left:$d^{18}O$ record for the transition from the Late Pleistocene to the Holocene Greenlandian stage. Right: Rate of change per year for the $d^{18}O$ record, transformed by x^2. Terminology note: Greenlandian, Pleistocene and Holocene are formal chronostratigraphic terms, as defined by the International Commission on Stratigraphy - see Gibbard (2018) and Walker *et al.* (2018); OD = "The oldest Dryas", LGI = Lateglacial Interstadial, YD = Younger Dryas (GS-1), broadly following Lowe and Walker (2014) (usage of terms for this period varies geographically).

The scale of the change that affected at least the geotechnical properties of at least the upper parts of soil units can be inferred from fluvial deposits. River sediment sequences in the UK record a sudden change from snow-melt flow regimes represented by coarse sediments to much lower energy conditions represented by significant volumes of sand, silt, and clay. In an earlier study of chalk and clay catchment in south-central England (Collins et al. 1996, 2006), this change was found to have occurred in a period less than the probability error for a radiocarbon date, as shown in the example in figure 3.

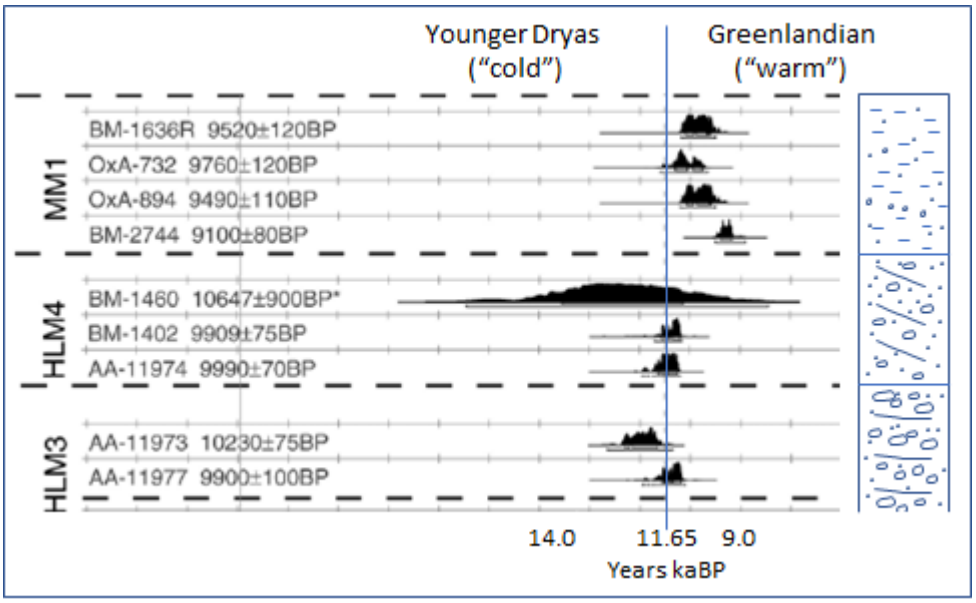

Figure 3. ^{14}C age estimation probability plots for the Late Pleistocene (Younger Dryas stage) to Holocene (Greenlandian stage) transition in the Kennet Valley, UK. After Collins et al. 2006.

The implication of the changed supply of fine-grained sediment into the fluvial systems is that a significant weakening of soils in the catchment occurred. This weakening would have included porewater driven reductions in cohesion, associated reductions in shear strength and, where local conditions permitted, liquefaction. Supporting evidence for this may come from dry valley deposits in the Thames Valley where classic cold climate solifluction deposits are overlain by clast rich soils interpreted as being the result of debris flows (Espejo et al. 1992). It remains uncertain, however, exactly when this sort of mass movement occurred due to the difficulty of dating the transported soil. An example of this is a late stage silt deposit in Poland that has a luminescence date range that overlaps into the Greenlandian stage (Waroszewski et al. 2020).

In other settings, ground ice mounds developed during the Younger Dryas, either as pingos or lithalsas (Pissart 2002). Modern analogs indicate this would have caused significant alterations to soil fabric, with segregated ice creating the potential for high water volumes and void space, and low inter-particle contacts. At Walton Common, where remnant ramparts and adjacent hollows are preserved, Clay (2015) found evidence of rampart collapse through mass wasting, though suggested a simple change from the slumping of coarse-grained soils to the settling out of chalky silt in standing water. Earlier unpublished work by Verasamy and Collins examined early Greenlandian-age soils (dated by pollen stratigraphy) from the same site. They found evidence of an early stabilization of the rampart slopes and hollows that was disrupted by a possibly short interval of instability which fits with the van de Bilt et al. (2019) model of a progressive change interrupted by short-lived reversals.

Conclusion

The geological evidence from past warming episodes indicates that the predominant impact on soils with an ice content is, unsurprisingly, a phase change affecting the degree of saturation. With this is an increased likelihood of soil structural collapse. However, there is some evidence that warming phases can be complex, and short-term cooling can occur. As a result, any consideration of the impact of current climate change on the geotechnical properties of soils and the associated risk to structures should consider the possibility of short-term refreezing.

References

1. BSI 2002. BS EN 1990:2002. Eurocode: Basis of Structural Design. British Standards Institution, London.

2. Clay P. 2015. The origin of relic cryogenic mounds at East Walton and Thompson Common, Norfolk, England. Proceedings of the Geologists' Association -126, -522-535 p. https://doi.org/10.1016/j.pgeola.2015.06.006.

3. Collins P.E.F. 2014. Active tectonic risk assessment - Problems with soil and soft sediment deformation structures. In Lollino, G; Giordan, D; Thuro, K; et al. (editors) IAEG-XII Proceedings. September 2014. DOI: 10.13140/2.1.5047.0407.

4. Collins P.E.F. 1996. Fenwick I.M., Keith-Lucas D.M. and Worsley P. 1996. Late Devensian river and floodplain dynamics and related environmental change in northwest Europe, with particular reference to a site at Woolhampton, Berkshire, United Kingdom. Journal of Quaternary Science 11, 357-375 p.

5. Collins P.E.F., Worsley P., Keith-Lucas D.M. and Fenwick I.M. 2006. Floodplain environmental change during the Younger Dryas and Holocene: evidence from the lower Kennet Valley, south central England. Palaeogeography, Palaeoclimatology, Palaeoecology 233, 113-133 p.

6. BS EN 1990:2002. Eurocode: Basis of Structural Design. British Standards Institution,London.

7. Espejo J.M.R., Catt J.A. and Mackney D. 1992. The origin of very flinty dry-valley deposits in the Marlow area, Buckinghamshire, England. Journal of Quaternary Science 7, -P. 227-234.

8. Gao T., Zhang Y., Kang S., Abbott B.W., Wang X., Zhang T., Yi S. and Gustafsson O. (2021) Accelerating permafrost collapse on the eastern Tibetan Plateau. Environmental Research Letters 16, https://doi.org/10.1088/1748-9326/abf7f0.

9. Harris C, Arenson L.U., Christiansen H.H. et al. 2009. Permafrost and climate in Europe: Monitoring and modelling thermal, geomorphological and geotechnical responses. Earth Science Reviews 92, -P. 117-171. DOI: 10.1016/j.earscirev.2008.12.002.

10. Lowe J. and Walker M.J.C. 2014 Reconstructing Quatyernary Environments. 3rd Edition. Routledge.

11. Pissart A. 2002. Palsas, lithalsas and remnants of these periglacial mounds. A progress report. Progress in Physical Geography 26,605–621.https://doi.org/10.1191/0309133302pp354ra.

12. Taylor K.C, Lamorey G.W. Doyle G.A. et al.. 1993. The flickering switch of Late Pleistocene climate change. Nature 361, -P. 432-436.

13. van der Bilt, W.G.M., D'Adrea W.J., Werner J.P. and Bakke J. 2019. Early Holocene Temperature Oscillations Exceed Amplitude of Observed and Projected Warming in Svalbard Lakes. Geophysical Research Letters 46, -P. 14732-14741. https://doi.org/10.1029/2019GL084384.

14. Van Vliet-Lanoe B., Magyari A and Meilliez F. 2004. Distinguishing between tectonic and periglacial deformations of quaternary continental deposits in Europe. Global and Planetary Change 43, -P. 103-127.

15. Walker, Mike; Head, Martin J.; Berkelhammer, M. et al. (2018). Formal ratification of the subdivision of the Holocene Series/ Epoch (Quaternary System/Period): two new Global Boundary Stratotype Sections and Points (GSSPs) and three new stages/subseries. Episodes. Subcommission on Quaternary Stratigraphy (SQS). 41 (4), -P. 213-223. doi:10.18814/epiiugs/2018/018016.

16. Waroszeski J., Sprafke T., Kabala C. et al. 2020. Chronostratigraphy of silt-dominated Pleistocene periglacial slope deposits on Mt. Sleza (SW, Poland): Palaeoenvironmental and pedogenic significance. Catena 190, DOI: 10.1016/j.catena.2020.104549.

Филип Э.Ф. Коллинз
Азаматтық және экологиялық инженерия кафедрасы, Брунель университеті Лондон, Аксбридж, UB8 3PH, Ұлыбритания

Климаттың тез жылынуы жағдайында мұздатылған топырақ жүйелерінің жағдайы - өткенге түсінік

Аңдатпа. Қазіргі климаттың жылынуы мұздатылған топырақтың үздіксіз геотехникалық өзгеруіне әкеледі деп күтілуде. Өткен климаттың өзгеруін, әсіресе суық кезеңді қарастыру: жылы ауысулар осы өзгерістің ықтимал табиғаты туралы түсінік бере алады және ондай жердің жағдайы бойынша түсінік беруі мүмкін. Анықталған ақпарат кейде екіұшты болып келеді. Периглазиялық және сейсмикалық процестер кейде ұқсас нәтижелерді береді. Мұздатылған топырақтардың негізгі көрсеткіштері суық-жылы ауысулар, мысалы, голоценнің Гренландия кезеңінің басталуы кезінде үлкен магнитуда болуы мүмкін. Сонымен қатар, топырақ жүйелеріне тұрақсыздық қосатын кері ауысулар болуы мүмкін. Мұз әсер ететін топырақтардың болашақтағы геотехникалық өзгеруін қарастыру үшін күрделі климаттық өзгеруді ескеру қажет.

Түйін сөздер: перигласиялық топырақтар, Гренландия, деформациялар, климаттың өзгеруі, еру.

Филип Э.Ф. Коллинз
Департамент гражданской и экологической инженерии, Лондонский университет Брунеля, Аксбридж, UB8 3PH, Соединенное Королевство

Мерзлые почвенные системы в условиях быстрого потепления климата: выводы из прошлого

Аннотация. Ожидается, что текущее потепление климата приведет к постоянным геотехническим изменениям в почвах многолетней криолитозоны. Изучение прошлых изменений климата, особенно переход холодной стадии в теплую, может дать представление о потенциальной природе этого изменения, а также информацию для оценивания таких участков. Получаемые данные исследования не всегда однозначны: перигляциальные и сейсмические процессы дают схожие результаты. Данные о ледяных кернах свидетельствуют, что переходы от холода к теплу, например, в начале гренландского этапа голоцена, могут иметь большие масштабы, но также могут иметь инверсии, которые добавляют нестабильность почвенным системам. Поэтому при рассмотрении будущих геотехнических изменений в почвах многолетней криолитозоны необходимо учитывать потенциально сложные климатические воздействия.

Ключевые слова: перигляциальный грунт, Гренландия, деформации, изменение климата, оттепель.

References

1. BSI 2002. BS EN 1990:2002. Eurocode: Basis of Structural Design. British Standards Institution, London.

2. Clay P. 2015. The origin of relic cryogenic mounds at East Walton and Thompson Common, Norfolk, England. Proceedings of the Geologists' Association 126, 522-535. https://doi.org/10.1016/j.pgeola.2015.06.006.

3. Collins P.E.F. 2014. Active tectonic risk assessment - Problems with soil and soft sediment deformation structures. In Lollino, G; Giordan, D; Thuro, K; et al. (editors) *IAEG-XII Proceedings*. September 2014. DOI: 10.13140/2.1.5047.0407.

4. Collins P.E.F. 1996. Fenwick I.M., Keith-Lucas D.M. and Worsley P. 1996. Late Devensian river and floodplain dynamics and related environmental change in northwest Europe, with particular reference to a site at Woolhampton, Berkshire, United Kingdom. Journal of Quaternary Science 11, 357-375.

5. Collins P.E.F., Worsley P., Keith-Lucas D.M. and Fenwick I.M. 2006. Floodplain environmental change during the Younger Dryas and Holocene: evidence from the lower Kennet Valley, south central England. Palaeogeography, Palaeoclimatology, Palaeoecology 233, 113-133.

6. BS EN 1990:2002. Eurocode: Basis of Structural Design. British Standards Institution, London.

7. Espejo J.M.R., Catt J.A. and Mackney D. 1992. The origin of very flinty dry-valley deposits in the Marlow area, Buckinghamshire, England. Journal of Quaternary Science 7, 227-234.

8. Gao T., Zhang Y., Kang S., Abbott B.W., Wang X., Zhang T., Yi S. and Gustafsson O. (2021) Accelerating permafrost collapse on the eastern Tibetan Plateau. Environmental Research Letters 16, https://doi.org/10.1088/1748-9326/abf7f0.

9. Harris C, Arenson L.U., Christiansen H.H. et al. 2009. Permafrost and climate in Europe: Monitoring and modelling thermal, geomorphological and geotechnical responses. Earth Science Reviews 92, 117-171. DOI: 10.1016/j.earscirev.2008.12.002.

10. Lowe J. and Walker M.J.C. 2014 Reconstructing Quatyernary Environments. 3rd Edition. Routledge.

11. Pissart A. 2002. Palsas, lithalsas and remnants of these periglacial mounds. A progress report. Progress in Physical Geography 26,605–621.https://doi.org/10.1191/0309133302pp354ra.

12. Taylor K.C, Lamorey G.W. Doyle G.A. et al.. 1993. The flickering switch of Late Pleistocene climate change. Nature 361, 432-436.

13. van der Bilt, W.G.M., D'Adrea W.J., Werner J.P. and Bakke J. 2019. Early Holocene Temperature Oscillations Exceed Amplitude of Observed and Projected Warming in Svalbard Lakes. Geophysical Research Letters 46, 14732-14741. https://doi.org/10.1029/2019GL084384.

14. Van Vliet-Lanoe B., Magyari A and Meilliez F. 2004. Distinguishing between tectonic and periglacial deformations of quaternary continental deposits in Europe. Global and Planetary Change 43, 103-127.

15. Walker, Mike; Head, Martin J.; Berkelhammer, M. et al. (2018). Formal ratification of the subdivision of the Holocene Series/ Epoch (Quaternary System/Period): two new Global Boundary Stratotype Sections and Points (GSSPs) and three new stages/subseries. Episodes. Subcommission on Quaternary Stratigraphy (SQS). 41 (4): 213-223. doi:10.18814/epiiugs/2018/018016.

16. Waroszeski J., Sprafke T., Kabala C. et al. 2020. Chronostratigraphy of silt-dominated Pleistocene periglacial slope deposits on Mt. Sleza (SW, Poland): Palaeoenvironmental and pedogenic significance. Catena 190, DOI: 10.1016/j.catena.2020.104549.

Information about the author:

Philip E.F. Collins - Reader in Geology & Geotechnical Engineering, Brunel University London, United Kingdom.

Филип Э.Ф. Коллинз - Лондондағы Брунель университетінің геология және геотехникалық инженерия бөлімінің оқытушысы.

IRSTI 67.11.29

G. Tleulenova*, A. Zhussupbekov, Zh. Shakhmov, A. Omarov

L.N.Gumilyov Eurasian National University, Nur-Sultan, Kazakhstan
Corresponding author:gulshattleulenova23@mail.ru

Numerical analysis of pile foundations in seasonally freezing soil ground

Abstract. The article presents the results of numerical analysis for pile foundation in seasonally freezing soil ground. This project uses the static tests of soil by piles at the construction site of Cargo off-loading facilities (Prorva, Atyrau region, Kazakhstan). The project area is located along the east coast of the Caspian Sea, both onshore and offshore, near the Prorva oilfield, Kazakhstan. At present, the North Caspian Sea has a limited water depth (max 8 m). According to the test results have been made design changes in the pile foundation. Static tests (SCLT) were carried out on the piles with 16m in length and precast concrete joint pile foundations with a total length of 22m to 27m. This research is important for an understanding of the interaction mechanism of precast composite joint piles with seasonally freezing soil ground of the Caspian Sea coastal area of the site.

Keywords: pile, numerical analysis, Load-Settlement, PIT.

DOI: doi.org/10.32523/2616-7263-2021-135-2-37-48

Introduction

Seasonal freezing of soils is a problem soil. In the production of winter conditions, engineers are faced with the problem of assessing frost-prone soils and making the right decisions to ensure the strength, reliability, durability, and stability of buildings. The frost hazard of soils in construction is understood as their ability to influence the stability of structures in the process of freezing-thawing when interacting with piles. According to the construction standards, the choice of the method of construction of the foundations should be determined based on engineering and geological studies. To make technological decisions, additional data are needed to characterize the cryogenic properties of soils in the process of freezing and thawing of soils.

Engineering and geological structure of site "Prorva"

Table 1 describes the engineering and geological conditions of the construction site. According to the physical and mechanical properties of the soil and the results of laboratory tests in the geological section, three engineering-geological elements (IGE) were identified. The standard values of the physical and mechanical properties of soils are given based on the results of testing samples of all wells.

The table 1 presents a geotechnical structure of the site.

Table1

Geological and lithological conditions of the construction site

EGE	Layer Description	C	φ, deg.	$\gamma_{natural}$ *), kN/m^3	Su, kPa	E*oed. ref*
EGE-2	Clay silt.	0.7	29,4	19.3	15	2.750
EGE-3	The sand is medium-dense, dense	2.7	31.5	19.0	-	30.000
EGE-7	The clay is light, dusty	20.8	24.7	19.1	80	2.000
EGE-8	The sandisdense	2.4	31.8	20.0	-	40.000
EGE-9	Clay	22.7	23.8	20.6	150	4.000
EGE-10	Clay	25	24.7	20.2	150	2.000

Pile Integrity Test (PIT) research

Mainly to ensure the safety of the head of a solid reinforced concrete composite pile, since most of the destruction is observed in its head part, even though 1.5 - 2.0 times higher than in the middle part. This phenomenon is explained by the fact that during immersion, the strength of the pile in the head part decreases due to the formation of microcracks, and then, as the number of impacts increases, the destruction of the head part of the pile occurs, while the strength of the pile trunk remains unchanged [1-5].

The quality of the pile is often determined by a low-stress continuity test, which is performed immediately after driving. The tests allow you to find out which piles should undergo additional inspection. The measurement is carried out by hitting the pile head with a hand hammer and evaluating the reaction of the head using an accelerometer [9]. For continuous control, non-destructive methods are used. To determine the actual pile lengths, locate defects (cracks, weak sections), and evaluate the mechanical characteristics of concrete piles, seismic-acoustic (sound) and ultrasonic control methods are used.

Working with seismoacoustic and ultrasonic devices is divided into two stages: testing piles on the construction site and interpreting the information obtained using special software.

To ensure the registration of the second wave in the piles, it is carried out with the help of special equipment, followed by leveling the surface of the head and mounting sensors (accelerometers) in accordance with Figures 1, 2.

The accuracy of determining the pile length depends on the accuracy of the stress wave velocity. When the pile length is known, the wave propagation velocity can be matched to the known length.

The solution to the issue of guaranteed safety of the reinforced concrete pile structure during its immersion in the ground is one of the main tasks of the developed problem.

The tests were carried out in seasonally freezing soils, the graphs show the integrity of the pile foundations in Figure 3.

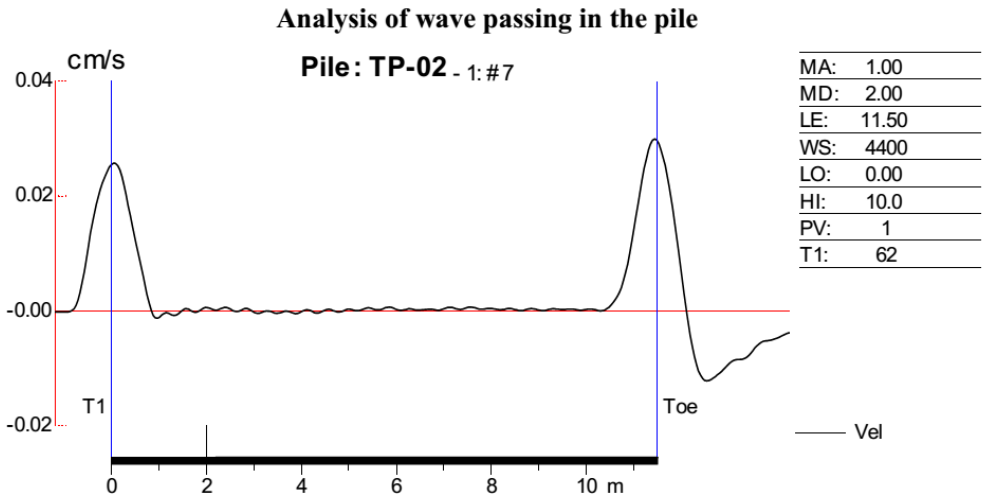

Figure1.Test results of piles TP-02by the method of PIT

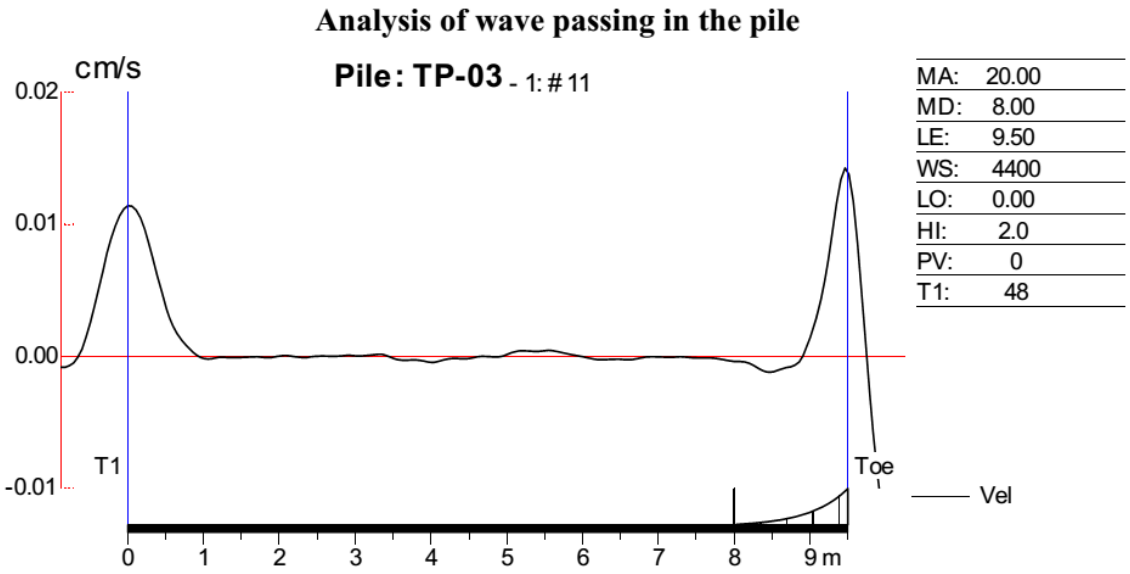

Figure 2. Test results of piles TP-03 by the method of PIT

The peculiarity of modern technology is the presence of docking units, which must retain their strength and shape after clogging each section. Thus, for the conditions of modern technology, it is necessary to introduce another condition, where the total number of blows of the pile-breaking equipment (or vibrations of the vibration loader) (N), capable of loading the pile at a given mark or before reaching its value of the effective load perceived by one pile, should be less than the impact resistance of the butt joint (Ncr), which is in the worst conditions (1) [1-4]:

$$N<N_{cr} \quad (1)$$

Fugure3. PIT pile testing

Numerical simulation by the finite element method in the Plaxis 2D

Currently, numerical calculation methods are used to quantify the VAT (stress-strain state) of inhomogeneous ground masses interacting with underground structures of buildings and structures, including FEM (finite element methods) [10]. The basis of these methods is the joint solution of a system of differential equations of equilibrium, continuity, and physical equations. The latter determine the dependence of the soil deformation on the stress state. Currently, there are different methods for describing physical equations, depending on the need to consider the linear, nonlinear, and rheological properties of soils.

The Plaxis 2D program has the advantages of relative simplicity and ease of use, as well as the availability of a soil model that is optimal for the task of this dissertation research [10].

The geometric dimensions of the composite pile model with a width of 0.4 m and various lengths from 22 to 27 meters were used in the calculation.

On the contact surface of the pile with the ground, interface elements were used to consider the displacement of the places of contact of the soil with the pile model.

The current version of PLAXIS 2D allows you to use only a linear color scale. In this regard, due to the large difference between the minimum and maximum shear deformations, it turned out that it was impossible to display them simultaneously in the same drawing.

Since the pile foundation is symmetrical to the vertical axis, only half of the area of the soil mass and the pile foundation were considered in the calculation scheme. The calculation scheme was automatically divided into triangular finite elements. The number of considered types of elements (layers) is 6 (the sequence of layers of the soil mass is shown in Figure 4).

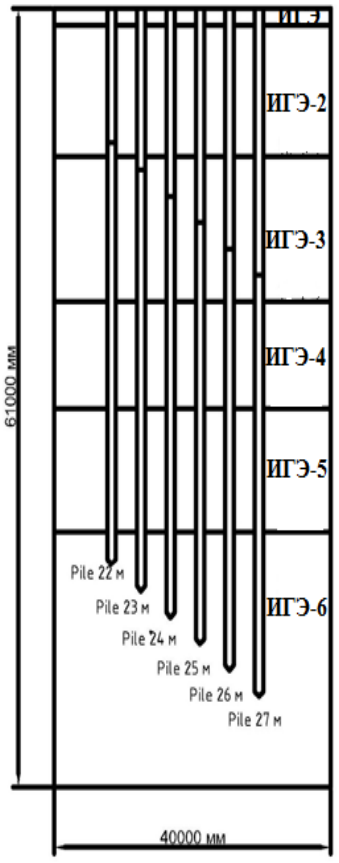

Figure 4. Diagram of the arrangement of the sequence of layers of the soil mass and the pile foundation

Piles of different lengths from 22 to 27 meters were tested using various simulations (Figure 4):

a) Pile 22m-the total length of the composite piles is 22 meters, the length of the first section is 16 meters, the length of the second section is 6 meters;

b) Pile 23m-the total length of the composite piles is 23 meters, the length of the first section is 16 meters, the length of the second section is 7 meters;

c) Pale 24m-the total length of the composite piles is 24 meters, the length of the first section is 16 meters, the length of the second section is 8 meters;

d) Pile 25 m-the total length of the composite piles is 25 meters, the length of the first section is 16 meters, the length of the second section is 9 meters;

e) Pile 26m-the total length of the composite piles is 26 meters, the length of the first section is 16 meters, the length of the second section is 10 meters;

e) Pile 27m-the total length of the composite piles is 27 meters, the length of the first section is 16 meters, the length of the second section is 11 meters.

Numerical simulation of testing of composite piles with a length of 22 to 27 meters

This section discusses the calculation of the pile foundation draft. The general methods of creating a geometric model, constructing a finite element grid, performing calculations using the finite element method, and evaluating the results obtained are considered in detail.

The load-bearing capacity of the piles was determined based on the results of numerical simulation of each pile operation in the PLAXIS 2D software package. The stress-strain state of the base was calculated using the Mora-Coulomb elastic-plastic model. The calculations were carried out in an axisymmetric setting.

Step-by-step pile loading was modeled by increasing the applied load on the pile, and the maximum vertical load was 3,278 kN. The main parameters tracked for the results are the amount of applied load and the pile draft. As a result of the calculation, the "load-draft" graphs were constructed.

Geometric models of numerical simulation of composite driving piles with a length of 22 meters to 27 meters (Pile 22 m-Pile27 m) are shown in Figure 5.

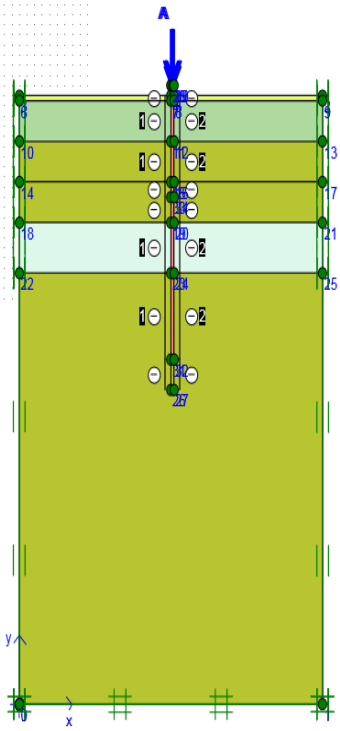

Figure 5. Geometric model of a composite pile with a length of 27 m

The finite element meshes generated automatically by the Plaxis 2D program for composite piles with a length of 22 meters to 27 meters (Pile 22 m - Pile27 m) are shown in Figure 6.

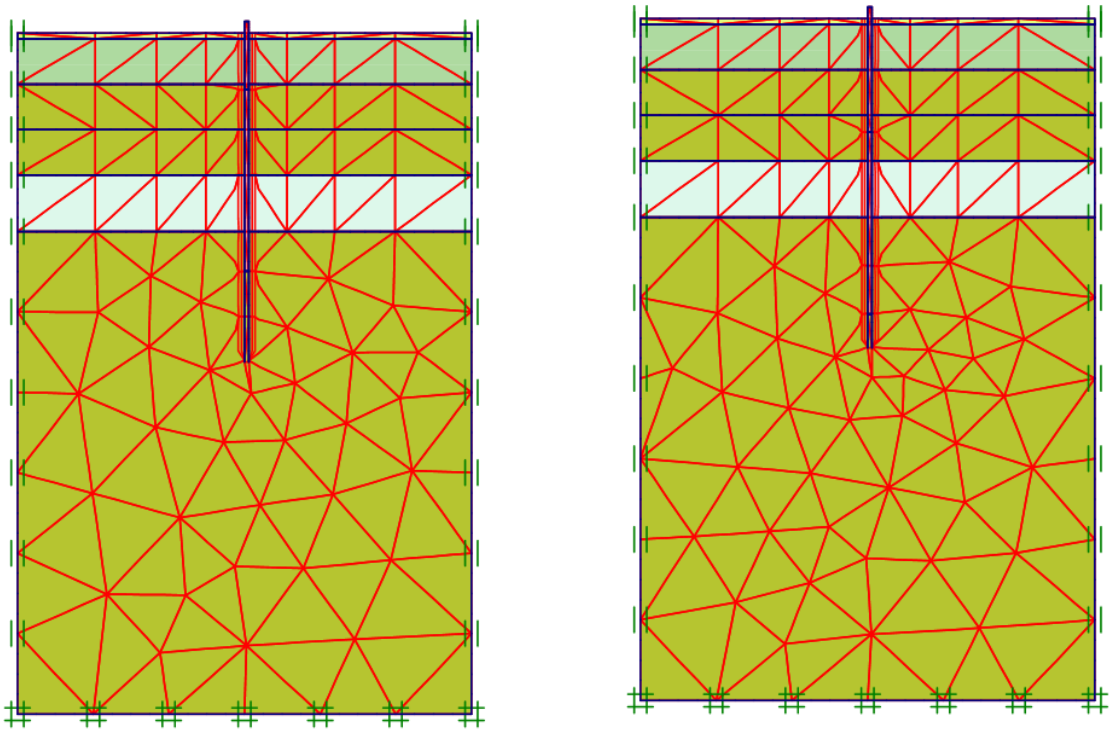

Fugure 6. Finite element grid (Pile 22, 27m)

Isolines of total ground movements under vertically static loads for composite piles with a length of 22 meters to 27 meters (Pile 22 m – Pile27 m) are shown in the figure 7.

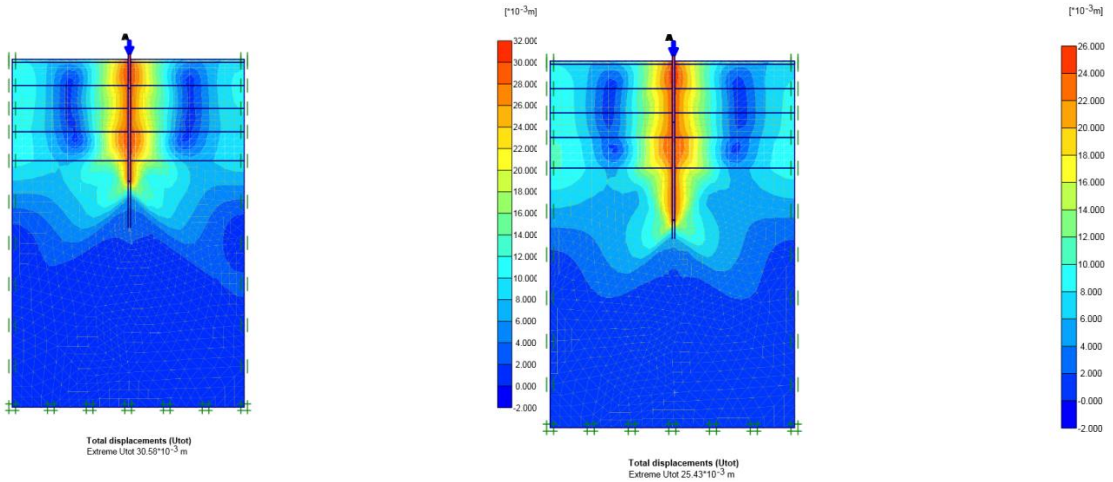

Fugure 7. Full displacement (Pile 22, 27 m)

Vertical movement isolines for composite piles with a length of 22 meters to 27 meters (Pile 22 m – Pile27 m) are shown in the figure 8.

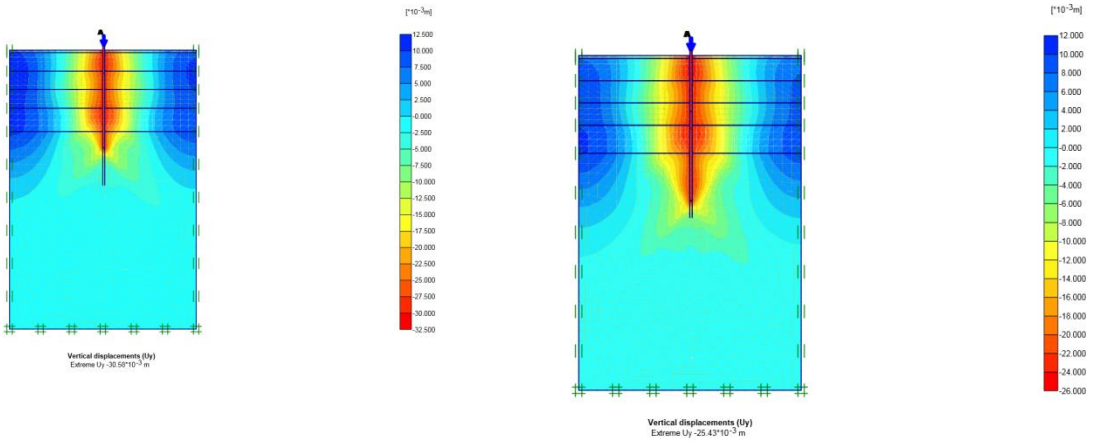

Figure 8. Vertical movement (Pile 22, 27m)

Isolines of horizontal ground movements under vertically static loads for composite piles with a length of 22 meters to 27 meters (Pile 22 m-Pile 27 m) are shown in the figure 9.

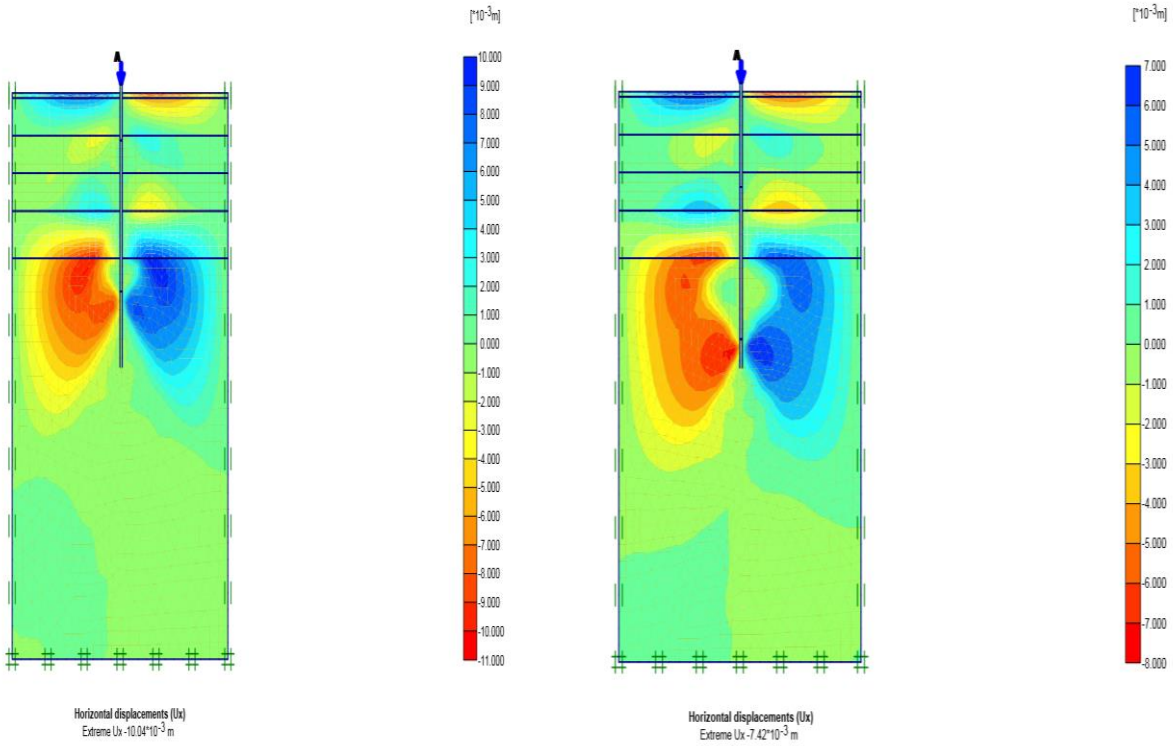

Figure 9. Horizontal movement (Pile 22, 27 m)

Comparison of numerical simulation results

Figure 10shows a comparison of the test results the "Load-Settlement" curve obtained by the SLT method, the length of the composite piles is from 22 meters to 27 meters [1, 4-9].

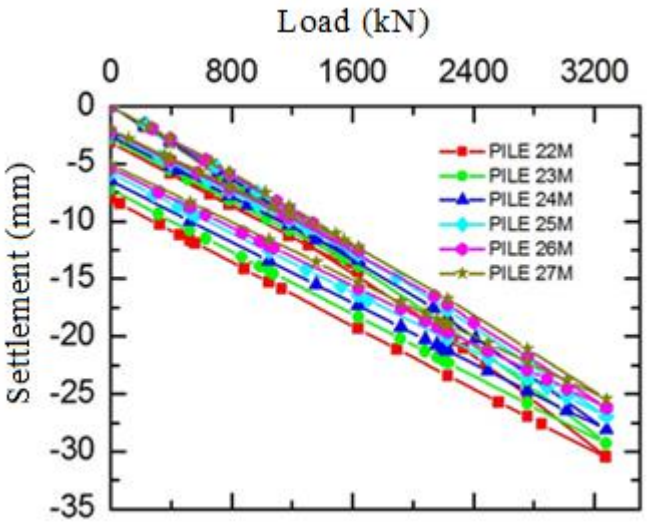

Figure 10.Load-Settlement graph based on Plaxis 2D results

The superposition of the curves showed that the convergence of the graphs is observed only at the initial stage of loading, then there is a change in the trajectory of the curve depending on the length of the pile. For a pile with a length of 22 meters, the draft was 30.58 mm, and for a maximum length of a composite pile of 27 meters, the draft was 25.43 mm.

For the partial value of the maximum resistance of the pile to the indentation load Fu, it is necessary to take the load under the influence of which the tested pile will receive a draft equal to S and determined by the formula 2 [10]:

$$S = \zeta S_{u,mt} = 0{,}2 \cdot 8 = 16\text{мм} \quad (2)$$

$S_{u,mt}$ =8см-the limit value of the average foundation draft of the projected building, set according to the instructions of the SNiP 5.01-01-2002 [6-8];

where: ζ is the transition coefficient from the limit value of the average foundation sediment of a building or structure Su, mtk to the pile sediment obtained during static tests with conditional sediment stabilization, according to the requirements of the SNIP 5.01-101-2003 the value of the coefficient should be taken as ζ=0.2.

The results on the maximum resistance of the piles to the indentation load under the influence, in which the tested pile received 16 mm of precipitation from the dependence of the length of the pile, can be seen in Table 2.

Table 2

Determination of the load-bearing capacity of piles at a fixed settlement

№	Pile number	The load-bearing capacity of the pile at a fixed draft of 16 mm
1.	№ pile 22m	1727 kN
2.	№ pile 23m	1815 kN
3.	№ pile 24m	1883 kN
4.	№ pile 25m	1975 kN
5.	№ pile 26m	2139 kN
6.	№ pile 27m	2229 kN

Conclusion

The estimated load-bearing capacity of the driving pile with a cross-section of 40x40 cm and a length of 25 m was 2400 kN, which confirms the sufficient load-bearing capacity of the foundation soils for piles of this depth of immersion.

The section has developed geometric models of composite driving piles with a length of 22 meters to 27 meters (Pile 22 m – Pile27) musing numerical simulation in the Plaxis 2D environment. The calculation of the stress-strain state of the base is based on the elastic-plastic Mohr-Coulomb model in an axisymmetric formulation. The piles were gradually loaded by increasing the applied load on the pile, resulting in a maximum vertical load of 3,278 kN.

Vertical displacements for composite piles with a length of 22 meters to 27 meters (Pile 22 m – Pile27 m) after the calculation stage in the Plaxis 2D environment ranged from 25 mm to 30 mm, this is consistent with the results of field tests.

The load-bearing capacity of the piles was compared at a fixed draft of 16 mm and the change in load-bearing capacity per one linear meter of the depth of immersion of the pile was calculated.

The method of testing composite piles by the SCLT method is performed in accordance with the ASTM standard. According to the results of field tests of composite piles by the SCLT method, the load-bearing capacity of the piles was 2067 kN, 2042 kN and 2333 kN, respectively, for pile lengths from 23 m to 26.75 m, and these values do not exceed the values of the maximum load-bearing capacity according to the Davisson limit method.

On the basis of conducting a series of field tests of composite piles in the conditions of complex multi-layered soils of Western Kazakhstan, it is recommended to use non-destructive methods for controlling the continuity of composite piles. The low-stress continuity test (PIT method) identifies pile defects that may reduce load-bearing capacity.

Geometric models of composite driving piles with a length from 22 meters to 27 meters (Pile 22 m – Pile 27 m) were developed using numerical modeling in the Plaxis 2D environment and the stress-strain state of the base was calculated using the elastic-plastic Mohr-Coulomb model in an axisymmetric formulation. As a result, vertical displacements were determined for composite piles with a length of 22 meters to 27 meters (Pile 22 m-Pile27 m) from 25 mm to 30 mm, which is confirmed by the results of field tests, and the load-bearing capacity of piles with a fixed settlement of 16 mm was compared.

Based on the results of numerical simulation of construction sites Prorvain seasonally freezing soil ground bearing capacity of pile foundations have a slight deviation of the pile settlement.

References

1. Zhussupbekov A.Zh. ,Omarov A., Moldazhanova A., Tulebekova A.S., Borgekova K., Tleulenova G. The investigations of the interaction of joint piles with problematical soil ground in Kazakhstan // Seventh International Conference on Geotechnique, Construction Materials and Environment - GEOMATE2017. - Japan,2017.-P.138-145.

2. Zhussupbekov A.Zh., Omarov A.R. Modern advances in the field geotechnical testing investigations of pile foundations. // The 15th Word Conference of Associated Research Centers for the Urban Underground Space. - Saint-Petersburg, Russia: - 2016, - P. p. 531-535.

3. Zhussupbekov A.Zh., Omarov A.R., Zhukenova G.A. The experience in applying of static load and O-cell pile testing geotechnologies in problematical soil conditions of Astana. // International Mini symposium Chubu (IMS-CHUBU). -Nagoya, Japan. - 2016. - P. 44.

4. Zhussupbekov A.Zh., Lukpanov R.E., Omarov A.R. The application of the static load methods of pile foundations in construction of site Expo-2017. // Scientific journal Soil Mechanics and Foundation Engineering (Impact Factor-2015=0.221). ISSN 0038-0741. New-York, USA.-2016.- Vol.: Issue 4. -P. 251-256.

5. Ashkey, E. "Interaction of CFA bored piles with soil condition in Astana". Adissertation submitted for the PhD degree, - Astana, Kazakhstan, - 2008. -P. 50-52.

6. Zhussupbekov A.Zh., Omarov A.R. Modern advances in the field geotechnical testing investigations of pile foundations. The 15th Word Conference of Associated Research Centers for the Urban Underground Space. - Saint-Petersburg, Russia. - 2016. - p. 531-535.

7. K. Beckhaus, H. Heinzelmann. Ultrasonic Integrity Testing for Bored Piles - A Challenge. // International Symposium Non-Destructive Testing in Civil Engineering (NDTCE 2015), - 2015.

8. ASTM D5882-16, Standard Test Method for Low Strain Impact Integrity Testing of Deep Foundations, ASTM International, West Conshohocken, PA, 2016.

9. Tleulenova G.T., Tulebekova A.S. Integrity Test (PIT) pile tests in winter on sites. VestnikL.N.Gymilyov ENU. Technical science series.-2017. - №4(119). - P. 345-348.

10. Zhussupbekov A.Zh., Tleulenova G.T., Omarov A.R., Tanyrbergenova G.K. Numerical simulation of foundations of freezing soil. VestnikKBTU.-2020. - Vol.1 (52),-P. 137-142.

Г.Т. Тлеуленова, А.Ж. Жусупбеков, Ж.А. Шахмов, А.Р. Омаров

Л.Н. Гумилев атындағы Еуразия ұлттық университеті, Нұр-Сұлтан, Қазақстан

Топырақтың маусымдық қатуы кезіндегі қадалық іргетастарды сандық талдау

Аңдатпа.Мақаладатопырақтыңмаусымдыққатужағдайындағықадалыіргетастыңнәтижелерікелтірілген. Бұлжобадақайтатиеуқұрылыстарының (Прорва, Атырауоблысы, Қазақстан) құрылысалаңындақадаларментопырақтыңстатикалықсынауларыпайдаланылады. Жоба ауданы Каспий теңізінің солтүстік-шығыс жағалауының бойында, Прорва, Қазақстан мұнай кен орнына жақын жерде орналасқан. Қазіргі уақытта Солтүстік Каспийдің тереңдігі шектеулі (максимум 8 м). Сынақ нәтижелері бойынша қадалық іргетасқа конструктивті өзгерістер енгізілді. Статикалық сынақтар жалпы ұзындығы 27 метрге дейін 16 метрлік қадалар мен құрастырмалы темірбетон байланыстырғыш қадаларда жүргізілді. Бұл зерттеулер құрама қадалардың Каспий теңізі учаскесінің жағалау аймағының проблемалы топырағымен өзара әрекеттесу механизмін түсіну үшін маңызды.

Түйін сөздер:қадалар, сандық сынақтар, жүктеме-отыру, PIT.

Г.Т. Тлеуленова, А.Ж. Жусупбеков, Ж.А. Шахмов, А.Р. Омаров

Евразийский национальный университет им. Л.Н. Гумилева, Нур-Султан, Казахстан

Численный анализ свайных фундаментов в условиях сезонного промерзания грунта

Аннотация. В статье представлены результаты работы свайного фундамента в условиях сезонного промерзания грунта. В данном проекте используются статические испытания грунта сваями на строительной площадке перегрузочных сооружений (Прорва, Атырауская область, Казахстан). Район проекта расположен вдоль восточного побережья Северо-Восточного Каспийского моря, как на суше, так и на шельфе, недалеко от нефтяного месторождения Прорва (Казахстан). В настоящее время Северный Каспий имеет ограниченную глубину (максимум 8 м). По результатам испытаний были внесены конструктивные изменения в свайный фундамент. Статические испытания проводились на 16-метровых сваях и сборных железобетонных

соединительных сваях общей длиной до 27 м. Эти исследования важны для понимания механизма взаимодействия сборных составных свай с проблемным грунтом прибрежной зоны участка Каспийского моря.

Ключевые слова: свая, численный анализ, нагрузка-осадка, PIT.

References

1. Zhussupbekov A.Zh., Omarov A., Moldazhanova A., Tulebekova A.S., Borgekova K., Tleulenova G. The investigations of the interaction of joint piles with problematical soil ground in Kazakhstan. Seventh International Conference on Geotechnique, Construction Materials and Environment. GEOMATE2017. Japan, 2017. P.138-145.

2. Zhussupbekov A.Zh., Omarov A.R. Modern advances in the field geotechnical testing investigations of pile foundations. The 15th Word Conference of Associated Research Centers for the Urban Underground Space. Saint-Petersburg, Russia, 2016.p. 531-535.

3. Zhussupbekov A.Zh., Omarov A.R., Zhukenova G.A. The experience in applying of static load and O-cell pile testing geotechnologies in problematical soil conditions of Astana. International Mini symposium Chubu (IMS-CHUBU). Nagoya, Japan. 2016. P. 44.

4. Zhussupbekov A.Zh., Lukpanov R.E., Omarov A.R. The application of the static load methods of pile foundations in construction of site Expo-2017. Scientific journal Soil Mechanics and Foundation Engineering (Impact Factor-2015=0.221). ISSN 0038-0741. New-York, USA.4, 251-256(2016).

5. Ashkey, E. "Interaction of CFA bored piles with soil condition in Astana". A dissertation submitted for the PhD degree. Astana, Kazakhstan, 2008. P. 50-52.

6. Zhussupbekov A.Zh., Omarov A.R. Modern advances in the field geotechnical testing investigations of pile foundations. The 15th Word Conference of Associated Research Centers for the Urban Underground Space. Saint-Petersburg, Russia, 2016. p.531-535.

7. K. Beckhaus, H. Heinzelmann. Ultrasonic Integrity Testing for Bored Piles - A Challenge. International Symposium Non-Destructive Testing in Civil Engineering (NDTCE 2015), 2015.

8. ASTM D5882-16, Standard Test Method for Low Strain Impact Integrity Testing of Deep Foundations, ASTM International, West Conshohocken, PA, 2016.

9. Tleulenova G.T., Tulebekova A.S. Integrity Test (PIT) pile tests in winter on sites. Vestnik L.N. Gymilyov ENU. Technical science series. 4(119), 345-348(2017).

10. Zhussupbekov A.Zh., Tleulenova G.T., Omarov A.R., Tanyrbergenova G.K. Numerical simulation of foundations of freezing soil. VestnikKBTU.1(52),137-142(2020).

Information about authors:

G.T. Tleulenova - Ph.D., Senior lecturer in Department of Civil Engineering, L.N. Gumilyov Eurasian National University, Nur-Sultan, Kazakhstan.

A.Zh. Zhussupbekov - Doctor of Technical Sciences, Professorin Department of Civil Engineering, L.N. Gumilyov Eurasian National University, Nur-Sultan, Kazakhstan.

Zh.A. Shakhmov - Ph.D., Associate Professor in Department of Civil Engineering, L.N. Gumilyov Eurasian National University, Nur-Sultan, Kazakhstan.

A.R. Omarov - Ph.D., Associate Professor in Department of Civil Engineering, L.N. Gumilyov Eurasian National University, Nur-Sultan, Kazakhstan.

Г.Т. Тлеуленова - корреспонденция үшін автор, «Ғимараттар және ғимараттарды жобалау» кафедрасының аға оқытушы, Ph.D., Л. Н. Гумилев атындағы Еуразия ұлттық университеті, Нұр-Сұлтан, Қазақстан.

А.Ж. Жусупбеков - «Ғимараттар және ғимараттарды жобалау» кафедрасының профессоры, техника ғылымдарының докторы, *Л.* Н. Гумилев атындағы Еуразия ұлттық университеті, Нұр-Сұлтан, Қазақстан.

Ж.А. Шахмов - PhD., «Ғимараттар және ғимараттарды жобалау» кафедрасының доценті, *Л.* Н. Гумилев атындағы Еуразия ұлттық университеті, Нұр-Сұлтан, Қазақстан.

А.Р. Омаров - PhD., «Ғимараттар және ғимараттарды жобалау» кафедрасының м.а. доценті, *Л.* Н. Гумилев атындағы Еуразия ұлттық университеті, Нұр-Сұлтан, Қазақстан.

IRSTI 67.21.29

T. Ono

Hokkai-GakuenUniversity,Sapporo, Japan
E-mail: tono@hgu.jp

A Proposal of Standard Test Method for Frost Susceptibility of Soil

Abstract. A recommendation of a standard test method for frost susceptibility of soil is proposed. The recommendation is required in order to have a design technique of common and equivalent quality not only in domestic but international practice. This topic is one of the essential and current objectives of Technical Committee 216 (ISSMGE) and has been discussing to the present. The purpose of the proposed recommendation test method is defined, different methods from several countries are compared, necessary and common articles are selected and some items are specified to discuss. It is expected that this proposal would take a role to be a draft suggestion to promote discussion and achieve a final recommendation.
Keywords: Frost susceptibility of soil, Test method, TC216.

DOI: doi.org/10.32523/2616-7263-2021-135-2-49-57

Attempt for standardization of frost heave test

In 1989, there was held an International Symposium on Frost Geotechnical Engineering organized by ISSMFE Technical Committee TC-8 on Frost (the present TC216), Finnish Geotechnical Society (SGY), and Technical Research Center of Finland (VTT) in Finland. The reference testing procedures for the use of laboratory frost heave tests in the determination of frost susceptibility of soil were published in the Work report 1985-1989[1)] by TC-8.

In 1995, comparative laboratory frost heave tests were carried out with common soil material planned by TC-8. Twelve laboratories had reported test results, but a final summary report was not published. A comparison report of the test results by nine Japanese institutes is available[2)].

Definitions of Terms

The terms are defined as follows for one dimensional freezing test with cylindrical cell.

Frost susceptibility -The propensity for a soil to accumulate ice and to heave during freezing

Frost heave - Upward displacement due to volume increase of soil with growing ice layers (ice lens) parallel to 0°C isothermal when soil freezes with water supply.

Amount of frost heave - Change of specimen height during freezing.

Frost heave ratio - Ratio of volume increase to initial volume of the specimen.

Frost heave rate - Increase of frost heave divided by length of time.

Freezing rate - Speed of advancement of freezing line into the unfrozen soil.

Existing Test Methods

Figures 1 to 4 show test devices which are publicized in literature or currently available by the author. Tables 1 to 3 summarize their dimension and procedure. The classification by frost susceptibility index used in those methods are shown in Tables 4 to 6. These devices and procedures have been set up and used for different purpose of freezing test.

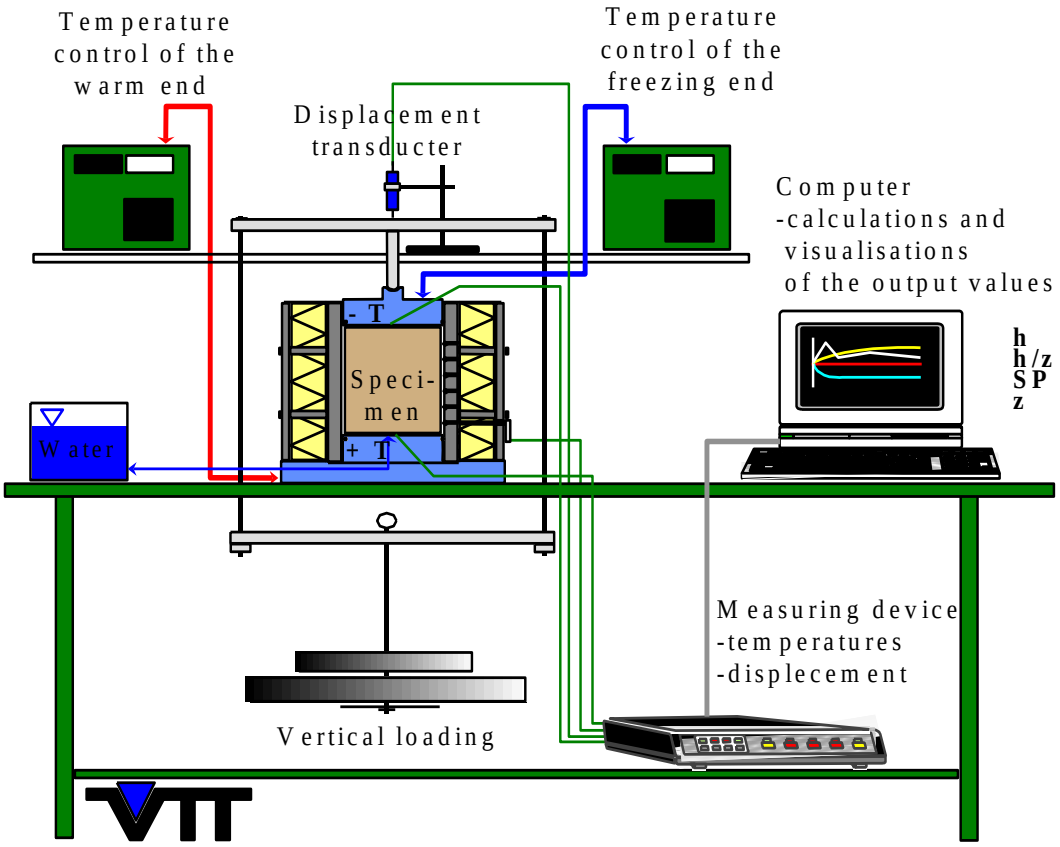

Figure 1. Test device used in Sweden

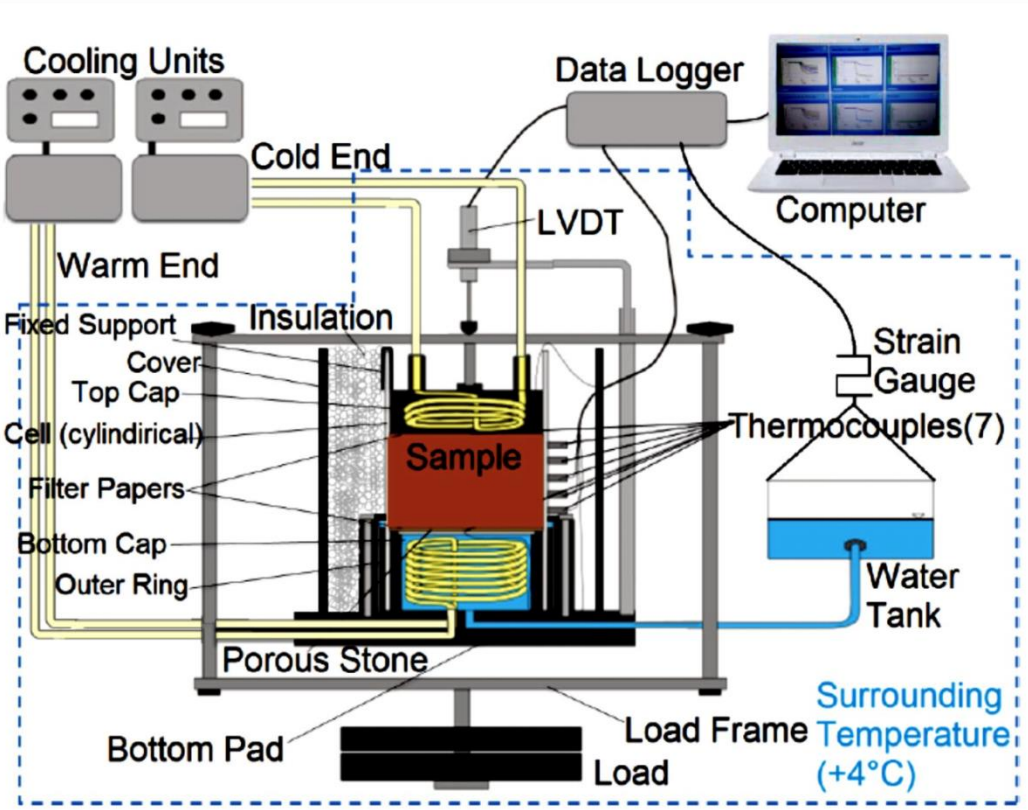

Figure 2. Test device used in Finland[3)]

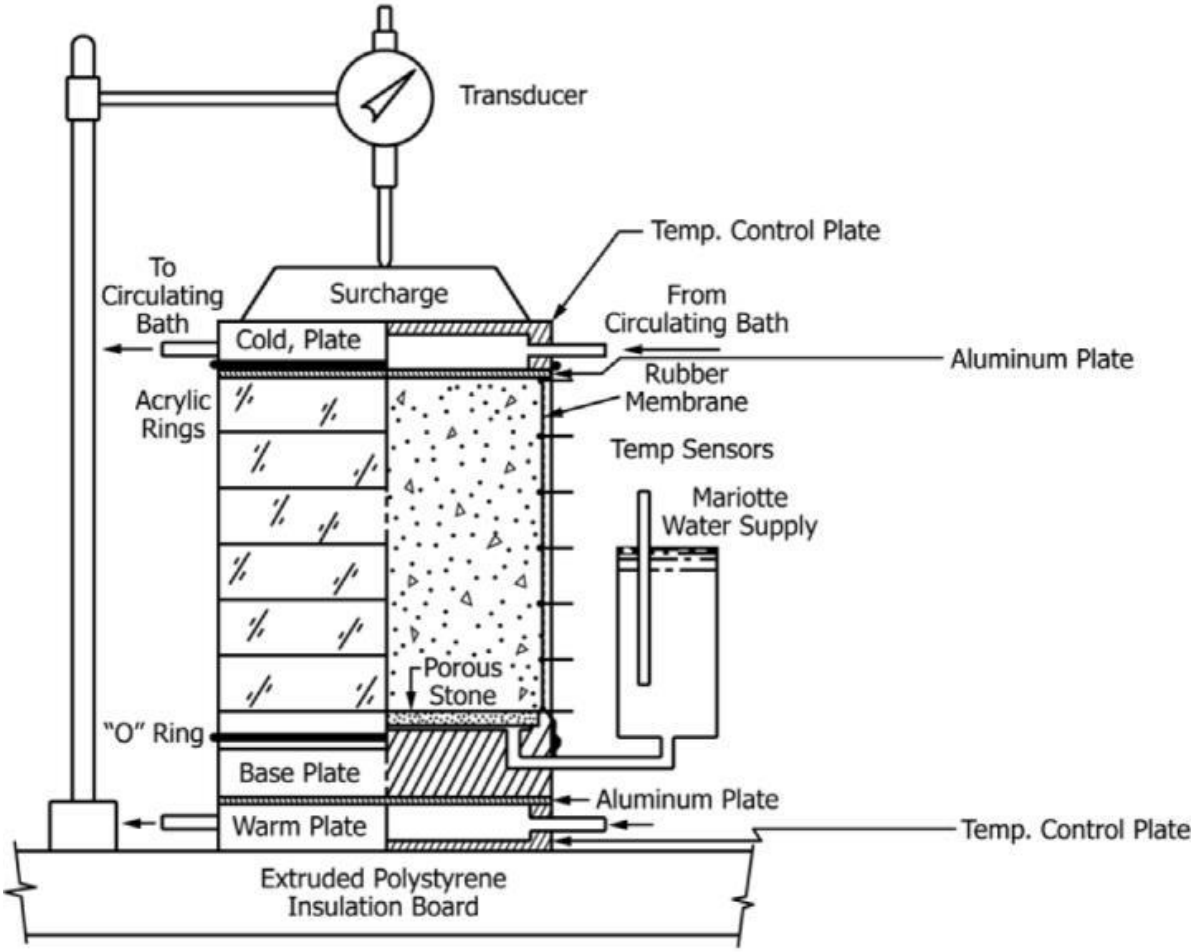

Figure 3. Test device written in ASTM (USA)[4] US

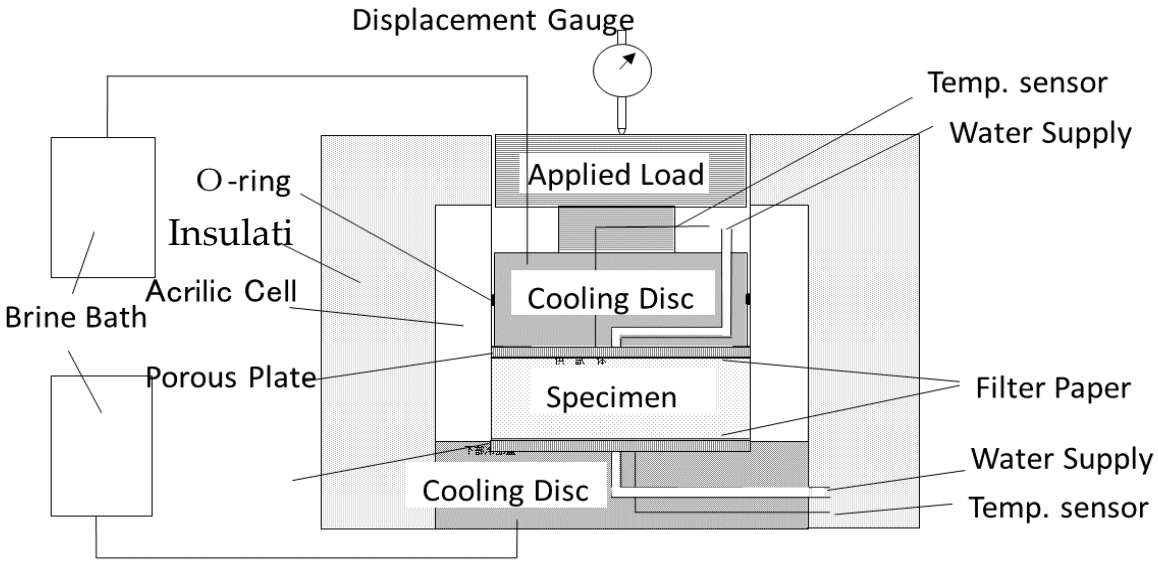

Figure 4. Test device used in Japan[5] US

Table 1

Dimension and Procedure

	Sweden	Finland
Purpose	frost heave	frost heave, thaw compression, frost susceptibility
Parameters obtained	segregational heave, heat extraction rate	frost heave ratio, SP
Specimen	compacted	undisturbed/compacted
Applied loads	-	2,20,40 kPa
Water supply	bottom	bottom
Temp. of top/bottom	cold / warm fixed	-3 ^{o}C / +1 ^{o}C fixed
Temp. sensors	7 thermocouples	8 thermistors
Freezing direction	top to bottom	top to bottom
Test duration	4 days	24 hours
Friction control	-	rubber membrane
Specimen size D/H	100/100 mm	80-150/70-200
Freezing and thawing	can be performed	two cycles
Chamber/Insulation	+4 ^{o}C/70 mm	0±1 ^{o}C/split barrel

Table 2

Dimension and Procedure

	USA(ASTM-D5918)	Japan (JGS-0171)
Purpose	frost susceptibility, thaw weakening	frost susceptibility
Parameters obtained	heave rate, bearing ratio	heave rate
Specimen	compacted	compacted/undisturbed
Applied loads	3.5 kPa	10 kPa
Penetration rate	3.6 mm/hour	1-2 mm/hour
Water supply	from bottom	from top

Temp. of top/bottom	cold / warm fixed	+0 °C / -0.1 °C/hour
Temp. sensors	7 thermocouples	2 pt100 sensors(top and bottom)
Freezing direction	top to bottom	bottom to top
Test duration	5 days	until penetrated top
Friction control	rubber membrane, multi-ring cell	slight space, greased wall, freezing direction
Specimen size D/H	150/150	100/50
Freezing and thawing	two cycles and CBR	no thawing process
Classification	average frost heave rate	maximum heave rate

Table 3

Dimension and Procedure (for artificial freezing)[6)]

	JAPAN(JGS-0172)
Purpose	frost heave for artificial freezing
Parameters obtained	frost heave ratio, thaw settlement ratio and design parameters
Specimen	undisturbed
Applied loads	field over burden stress
Water supply	from top
Temp. of top/bottom	+0 °C / cooling rate required to obtain parameters
Temp. sensors	2 pt100 sensors(top and bottom)
Freezing direction	from bottom to top
Test duration	until penetrated top
Friction control	slight space, greased wall

Specimen size D/H	60/20-40
Freezing and thawing	one cycle
Model	$\xi = \xi 0 + (\sigma 0/\sigma)(1+ (U0/U)^{1/2})$, ξ : frost heave rate, U: penetration rate, σ : confining stress

Table 4

Classification by Frost Susceptibility Index, SP[7)]

	Segregation Potential SP mm^2/Kh
Negligible	< 0.5
Low	0.5 – 1.5
Medium	1.5 – 3.0
Strong	>3.0

Table 5

Classification by Frost Susceptibility Index, ASTM(USA)[8)]

	Symbol	8-H Heave Rate *mm/day*
Negligible	NFS	<1
Very low	VL	1 to 2
Low	L	2 to4
Medium	M	4 to8
High	H	8 to16
Very high	VH	>16

Table 6

Classification by Frost Susceptibility Index, JGS(Japan)[5)]

	Frost Heave Rate U_h *mm/h*, Freezing Rate 1-2 *mm/h*
Low	< 0.1
Medium	0.1– 0.3
High	≧ 0.3

Recommendation of Test Method for Frost Susceptibility of Soil

First of all, it is proposed that the index of frost susceptibility of soil is categorized in the physical property of soil such as Atterberg index, because most of engineering purposes to carry out frost susceptibility test would be to investigate not to obtain "how much it heaves", but to know "it is frost susceptible or not as a material" for the initial judgement of necessary frost protection in the field. A proper frost heave test, as a model test with field conditions, will be then selected to obtain required data for the detailed practical design.

Frost susceptibility test of soil as a physical index test should have clear output to show the susceptibility and classification of soil making use of certain reliable parameter obtained from the test. However, it is not a practical idea to indicate single parameter index as a common recommendation method as we know several index parameters already working in different countries or areas shown above. Our task is to show a practical guideline which works well for the engineering purpose with an acceptable concept.

Followings are basically referred to the Work report 1985-1989 by TC-8[1)], and modified by considering the existing methods for proposal of essential testing elements to obtain a frost susceptibility index and classify the frost susceptibility of material.

This recommendation does not restrict any optional procedure and dimension as far as the frost susceptibility index is practically reliable and works well, and the method provides value which is not relying on material and tester.

Test device

Test device consists of cylindrical test cell, temperature and displacement measurement sensors, measurement system for supplied water volume, loading device, temperature control unit and data acquisition equipment. The cell should be constructed of a material with low thermal conductivity and insulated with proper insulation material to keep a horizontal freezing front line in the sample during test. The friction between the sample and the cell wall should be minimized with appropriate manner. Temperatures should be controlled with the precision of 0.1 degree at least.

Sample preparation

Saturated compacted sample with appropriate density is used to ensure a stable physical test results as possible.

Test and Test results

Temperatures, displacement and supplied water volume should be recorded during freezing with suitable intervals for the purpose.

It is recommended to confirm to start freezing without delay of frost heave by means of avoiding the super cooling of sample surface at the beginning of freezing process, and to check the amount of frost heave coinciding with the calculated value from the supplied water volume.

Test results should give an index parameter to determine and classify the frost susceptibility of the material.

Determination of frost susceptibility

The index parameter to determine and classify the frost susceptibility should have good corresponding relation with the field observation to ensure its certainty.

Discussion

Test Device

The insulation around the cell and the precision of temperature sensors are shown as essential items especially for a testing under low temperature to obtain proper data, but other details for device are not indicated because several testing devices with different dimensions and styles are already used and working now.

Test

The recommendation of avoiding supercooling and checking frost heave by water volume is one of the reasonable methods to increase the accuracy of test results. Typical techniques to break supercooling are "tapping" and "thermal shock".

Frost Susceptibility Index

Frost susceptibility index should have a basis which is connected well to field observation as a practical physical index. It is expected to clarify correlation between the index and the field data in the explanation of test method.

References

1. ISSMFE Technical Committee on Frost, TC-8The use of laboratory frost heave tests in the determination of frost susceptibility: International Symposium on Frost Geotechnical Engineering, VTT Symposium 94. Saariselkä, Finland, 1989. -P. 37-42.

2. Ono T., Fukuda M. and Mitachi T. Comparative Frost Heave Test Results in Japan: Proceeding of Ninth International Conference on Cold Regions Engineering, ASCE. Duluth, USA,-1998. -P. 624-635.

3. VTT Method Description Frost heave test Thaw compression test, TPPT-R07, -1999.

4. ASTM Standard Test Methods for Frost Heave and Thaw Weakening Susceptibility of Soils, ASTM D 5918- 96, -P. 3, -1996.

5. JGS (Japanese Geotechnical Society) Test method for frost susceptibility of soils, JGS 0172, -2009.

6. JGS (Japanese Geotechnical Society) Test method for frost heave prediction of soils, JGS 0171, -2009.

7. ISSMFE Technical Committee on Frost, TC-8Work Report 1985-1989: International Symposium on Frost Geotechnical Engineering, VTT Symposium 94, Saariselkä , Finland, -1989, -P. 21.

8. ASTM Standard Test Methods for Frost Heave and Thaw Weakening Susceptibility of Soils, ASTM D 5918- 96, -P. 8, -1996.

Т. Оно

Хоккай-Гакуен университеті, Саппоро, Жапония

Топырақтың аязға төзімділігін сынау әдісінің стандарт ретінде ұсынысы

Аңдатпа. Топырақтың аязға бейімділігі бойынша стандартты сынау әдісі ұсынылады. Ұсыныс тек отандық қана емес, халықаралық тәжірибеде де ортақ және баламалы сапаны жобалау техникасына ие болу үшін қажет. Бұл тақырып 216 Техникалық Комитетінің (ISSMGE) маңызды әрі ағымдағы мақсаттарының бірі болып табылады. Осы уақытқа дейін талқыланып келеді. Ұсынылатын тестілеу әдісінің мақсаты айқындалды, бірнеше елдердің әртүрлі әдістері салыстырылды, қажет әрі жалпы мақалалар таңдалды, кейбір тармақтар талқылауға ұсынылды. Бұл ұсыныс талқылауға ықпал етіп, соңғы ұсынысқа қол жеткізу үшін ұсыныстың жобасы бола алады деп күтілуде.

Түйін сөздер: топырақтың аязға бейімділігі, тест әдісі, TC216.

T.Оно

Университет Хоккай-Гакуэн, Саппоро, Япония

Проект метода определения морозостойкости грунтов в качестве общепринятого стандарта

Аннотация. Предложена рекомендация по стандартному методу испытаний на морозостойкость грунтов, которая необходима для того, чтобы методика проектирования общего и равноценного качества была не только в отечественной, но и в международной практике. Данная тема является одной из основных и текущих задач Технического комитета 216 (ISSMGE) и обсуждается до сих пор. Определяется цель предлагаемого рекомендательного метода тестирования, сравниваются различные методы из нескольких стран, выбираются необходимые и общие статьи, а также указываются некоторые вопросы для обсуждения. Ожидается, что это предложение сыграет роль проекта предложения, способствующего обсуждению и выработке окончательной рекомендации.

Ключевые слова: морозостойкость почвы, метод испытания, ТС216.

References

1. ISSMFE Technical Committee on Frost, TC-8The use of laboratory frost heave tests in the determination of frost susceptibility: International Symposium on Frost Geotechnical Engineering, VTT Symposium 94. Saariselkä, Finland, 1989. P. 37-42.

2. Ono T., Fukuda M. and Mitachi T. Comparative Frost Heave Test Results in Japan: Proceeding of Ninth International Conference on Cold Regions Engineering, ASCE. Duluth, USA, 1998. P. 624-635.

3. VTT Method Description Frost heave test Thaw compression test, TPPT-R07, 1999.

4. ASTM Standard Test Methods for Frost Heave and Thaw Weakening Susceptibility of Soils, ASTM D. 5918 – 96, P. 3, 1996.

5. JGS (Japanese Geotechnical Society) Test method for frost susceptibility of soils, JGS 0172, 2009.

6. JGS (Japanese Geotechnical Society) Test method for frost heave prediction of soils, JGS 0171, 2009.

7. ISSMFE Technical Committee on Frost, TC-8Work Report 1985-1989: International Symposium on Frost Geotechnical Engineering, VTT Symposium 94, Saariselkä , Finland, 1989, P. 21.

8. ASTM Standard Test Methods for Frost Heave and Thaw Weakening Susceptibility of Soils, ASTM D 5918- 96, P. 8, 1996.

Information about author:

T. Ono - ТС21 төрағасы, Хоккай - Гакуену ниверситеті, Саппоро, Жапония.

T. Ono - Chair of TC21, Hokkai - Gakuen University, Sapporo, Japan.

IRSTI 67.21.17

Y.J. Ji, X. Li*

Key Laboratory of Urban Underground Engineering of Ministry of Education, Beijing Jiaotong University, Beijing, China
Corresponding author: ceXuLi2012@163.com

The equilibrium time and deformation characteristic of sulfate saline soil in 1D saline expansion test

Abstract. The salt expansion disease is serious for the soil containing sodium sulfate in cold regions. This paper carried out one-dimensional swelling tests of saline soil, and numerical cooling tests of soil to explore the stability time of salt swelling deformation and determine the standard procedure of the salt swelling test method. The test results demonstrate that: (A) the temperature equilibrium and crystallization process are almost completed simultaneously in the one-dimensional (1D) salt expansion test; (B) Referring to the standard of consolidation test, a standard that the expansion rate is less than 0.02mm/h can be used in the salt expansion test; (C) The required time for temperature equilibrium of soil is quadratic to sample size and is much faster with liquid bath condition comparing to gas bath condition. Because the deformation and temperature are synchronized, the deformation stabilization time of different size samples in different cooling media is recommended.This can provide a reference for the deformation equilibrium time of the salt swelling test.
Keywords: Sulfate, Saline soil, Salt expansion, Cooling test, Stabilize time.

DOI: doi.org/10.32523/2616-7263-2021-135-2-58-63

Introduction

When the soil's soluble salt content is greater than or equal to 0.3%, and the sagged salt expansion, or corrosion occurs, the soil is referred toas saline soil [1]. Saline soil is widely distributed in Northwest China [2]. When the environmental temperature decreases, the salt crystallizes in sulfate saline soil and salt swelling happens.The salt will crystallize and dissolve driven by the temperature difference between day and night, and it is easy to cause engineering diseases in the continuous salt swelling-collapse process. To more clearly understand the effect of temperature on the salt expansion process, Wan et al. [3-6] conducted salt expansion experiments with different cooling rates. However, in a closed system, the salt expansion is driven by temperature, and how much crystallization is completed when the temperature is stable, and whether the salt expansion is synchronized with the soil temperature is unclear. Given the cooling conditions and sample size, what is the temperature stabilization time of the sample, the temperature stability of the sample, and the stability standard of deformation, there is no specific specification. The main purpose of this article is: (a) Determining whether the deformation stabilization time and the temperature stabilization time of saline soil are synchronized. (b) Determining the deformation stabilization time of the salt expansion test.

Methods

2.1 1D salt expansion test of big size samples

Test device andTest procedure:

The test equipment is the salt expansion test barrel, DT85, PT100 temperature sensor, and the digital dial indicator.

The soil sample is compacted in six layers, and two PT100 sensors are embedded in the center of the sample, and the temperature of the center point of the soil is collected every 1 minute through DT85. A digital dial indicator is installed on the top of the sample and set to collect data every 1 minute. The test box can realize the automatic constant temperature function. The test takes 25 ℃→12 ℃→8 ℃→

4℃ as the cooling gradient, the cooling rate of the incubator is 1 ℃/min, and the sample is cured at 25 ℃ for 12 h, and then cooled to 12 ℃, after the constant temperature for 24 h, decrease to the next level of temperature at the same cooling rate and so on.

2.2 1D salt expansion test of small size samples

Test device andTest procedure:

Test equipment is the cutting ring with a diameter of 6.18 cm and a height of 4cm, the Vernier caliper, and the C4-600 programmable thermostat.

The test chamber can automatically adjust thetemperature change according to the set cooling program. The test uses 25 ℃→12 ℃→8 ℃→4 ℃→1 ℃ as the cooling gradient, the cooling rate of the incubator cooling stage is set according to the test plan, the sample is cured at 25 ℃ for 24 h, and the temperature is reduced to 12 ℃ at the set cooling rate, after a constant temperature of 24 h, it will also drop to the next level of temperature at the set cooling rate and so on. At each level of constant temperature, it will be measured by Vernier calipers every certain time (usually 2-4 h).

2.3 Numerical simulation method

According to the soil type, dry density, and moisture content of the salt expansion test sample, refer to relevant literature[7], determine the parameters of the model, and determine the heat transfer coefficient based on the cooling method. The dry density is 1700 kg/m^3.The sample's moisture content is 15.50%.The thermal Conductivity and the Specific heat capacity are 0.8 W/(m·K) and 1600 J/(kg·K). In the air bath conditions, the Heat transfer coefficient is 5 W/cm^2·K. In the liquid bath conditions, the Heat transfer coefficient is 200 W/cm^2·K.The numerical simulation cooling process is consistent with the actual soil sample cooling process.

Results and Discussion

The test results of the 1D salt expansion test are shown in Figure 1 and Figure 2.

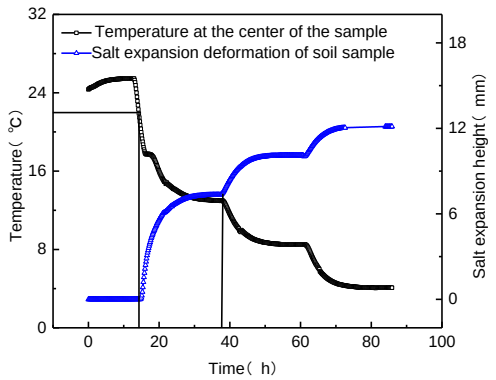

Figure 1. Variation of temperature at sample time center and sample height (big size sample)

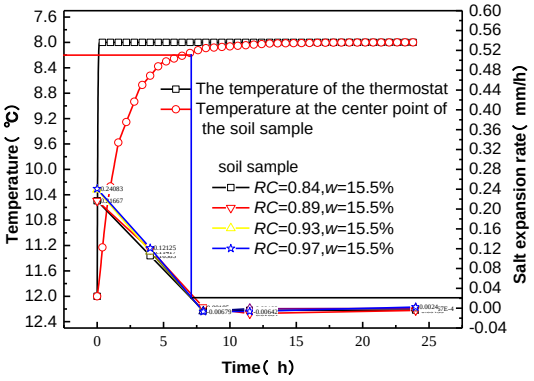

Figure 2. Curve of soil sample swelling rate versus at 8℃ (small size sample)

The test results in Figure 1 demonstrate that the salt expansion and temperature equilibrium are occurring co-transcriptionally.

Because the salt swell test is similar to the consolidation test, the deformation stability standard of the salt swell test can be formulated by analogy with the consolidation test. Therefore, the stability standard of the salt expansion test is: the deformation per hour at each temperature is not more than 0.02 mm or the temperature is stable for 24 hours. Figures 2 shows that the soil sample is deformed and stabilized at 12 °C and then cooled to 8 °C. Taking the temperature completion rate of 95% (ie 8.2 °C) as the temperature stability standard, and taking the salt expansion rate less than 0.02 (mm/h) as the deformation stability standard, the temperature curve, and the salt expansion rate curve under this stable standard can be obtained. At one point, this time point is the salt swelling and deformation

stability time. The time when the temperature completion rate reaches 95% is the same as the deformation stability standard.

When the cooling conditions are the same and the sample size is different, the temperature gradient inside the sample is different, and the temperature equilibrium time is also different. The effective radius r_s characterize different sizes, and its expression is:

$$r_s = 3V / S \quad (1)$$

where V is the sample volume; S is the sample surface area.

The temperature completion rate of 95% is taken as the sample temperature's stability standard comprehensively considering the test efficiency and the test accuracy. As the temperature stabilization time is minimal when the temperature difference differs, the average value of the temperature stabilization time at all levels is taken as the temperature stabilization time of the sample. The relationship between the sample's temperature stabilization time and the effective radius is shown in Figure 3.

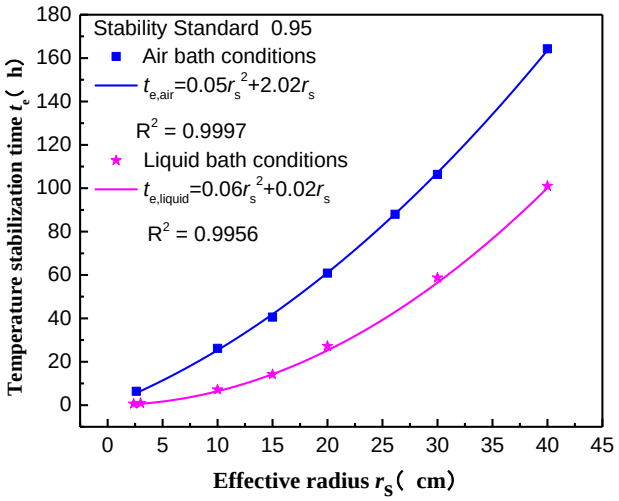

Figure 3. The relationship between the temperature stabilization time of the sample and the effective radius of the sample

The list of deformation stability time of samples under different sizes and different cooling methods are shown in Table 1.

Table 1

List of deformation stability Time

Experiment type	Sample size(D,H)	Equivalent radius (cm)	Cooling method	Balance time (h)
Confined 1D salt expansion test	6.18 cm, 4 cm	2.61	Gas bath	7
	17.9 cm,11.59 cm	7.59		20
	61.8 cm, 40 cm	26.1		88
3D salt expansion test	3.91 cm, 8 cm	2.37	Liquid bath	0.5
	5 cm, 10 cm	3		0.7
	50 cm, 80 cm	28.56		46

Conclusion

Through the laboratory and numerical tests, the following conclusions are obtained:

1. In the sulfate saline soil, the salt crystallization, salt expansion, and temperature equilibrium are occurring co-transcriptionally.

2. The salt expansion and deformation stability standard can be used as that the expansion rate is less than 0.02 mm/h, and the temperature stability standard can be used as that the temperature completion rate reaches 95%.

3. The temperature stabilization time of the sample has a parabolic relationship with the effective radius of the sample.

4. Comparing to an air bath, the liquid bath can greatly reduce the equilibrium time.

Reference

1. Jia Y.B. Construction Technology of Roadbed in Swelling Soil Area. Tunnel Construction, 2006.(in Chinese).

2. Dong C.H., Dong X.M., Tests on the Dissolve Settlement Characteristics of Sulphate Saline Soil. Applied Mechanics and Materials.Conf., Jinan, China, -2013.361-363:1071-1074.DOI:10.4028/www.scientific.net/AMM.361-363.1071.

3. Lai Y.M., Wan X.S., Zhang M.Y. An experimental study on the influence of cooling rates on salt expansion in sodium sulfate soils. Cold Regions Science and Technology. -2016.-Vol.124, p. 67-76. DOI:10.1016/j.coldregions.2015.12.014.

4. Wan, X.S., You Z.M., Wen H.Y., Crossley W., 2017. An experimental study of salt expansion in sodium saline soils under transient conditions. Journal of Arid Land. -2017. -Vol. 9(6), -p. 865-878. DOI:10.1007/s40333-017-0029-z.

5. Wan X.S., Hu Q.J., Liao M.K. Salt crystallization in cold sulfate saline soil. Cold Regions Science and Technology. -2017. -Vol.137, -p.36-47. DOI: 10.1016/j.coldregions.2017.02.007.

6. Wan X.S., Liu E.L., Qiu E.X., et al., Study on phase changes of ice and salt in saline soils. Cold Regions Science and Technology. -2020.172:102988. DOI:10.1016/j.coldregions.2020.102988.

7. Wang T.X., Liu Z.C., Lu J.Experimental study on coefficient of thermal conductivity and specific volumeheat of loess. Rock and Soil Mechanics. -2007. -Vol.28(4), -p. 655-658. DOI:10.1182/blood-2005-08-3320.(in Chinese).

Y.J. Ji, X. Li

Білім министрлігінің қалалық жерасты инженериясының негізгі зертханасы, Бейжің Цзяотун университеті, Пекин, Қытай

1D тұздан ісіну сынағындағы сульфатты-тұзды топырақтың тепе-теңдік уақыты мен деформациясы

Аңдатпа.Тұздан ісіну мәселесі натрий сульфаты бар топырақ үшін салқын аймақтарда ауыр болып келеді. Бұл жұмыста тұзды топырақтың бір өлшемді ісінуі, қаныққан натрий сульфаты ерітіндісінің кристалдану сынағы және топырақтың сандық салқындату сынақтары жүргізіліп, тұздан ісіну деформациясының тұрақтылық уақытын зерттеп, тұздан ісінуді сынау әдісінің стандартты тәртібі анықталды. Өткізген сынақ нәтижелері: (A) температураның тепе-теңдігі және кристалдану процесі бір бағыттағы тұздан ісіну сынағында бір мезгілде аяқталады; (B) консолидация сынағының стандартына сілтеме жасай отырып, ісіну жылдамдығы 0,02мм/сағ-тан аз болатын тұздан ісіну стандартты сынағында қолдануға болады; (C) топырақтың

температуралық тепе-теңдігінің талап етілетін уақыты квадраттық өлшемге сәйкес келеді және сұйық орта жағдайымен газ ортасының күйімен салыстырғанда әлдеқайда жылдам болады. Деформация мен температура синхрондалғандықтан, әр түрлі салқындатқыш ортадағы әр түрлі өлшемді үлгілердің деформацияны тұрақтандыру уақыты ұсынылады. Осы тұжырымдардың негізінде бір өлшемді тұздан ісіну сынау әдісінің стандартты процедурасы ұсынылады, онда сынақ жабдықтары, сынақ процесі, тұздан ісінудің деформациясын тұрақтандыру уақыты және мәліметтерді өңдеу әдісі келтірілген.

Түйін сөздер: сульфат, тұзды топырақ, тұзды ісіну, уақытты тұрақтандыру, тәжірибе әдісі.

Яньцзе Цзи, Ксу Ли

Ключевая лаборатория городского подземного строительства Министерства образования, Пекинский университет Цзяотун, Пекин, Китай

Продолжительность равновесия и деформационные характеристики сульфатно-засоленного грунта: набухание при одномерном испытании

Аннотация. Проблема солевой экспансии является очень серьезной для грунтов, содержащих сульфат натрия в холодных регионах. В статье представлены результаты, связанные с испытаниями на одномерное набухание засоленной почвы, испытанием на кристаллизацию насыщенного раствора сульфата натрия и численными испытаниями на охлаждение почвы для изучения времени стабильности деформации набухания солевых грунтов и определения стандартной процедуры метода испытания на набухание солевых грунтов. Результаты испытаний показали: (A) процесс температурного равновесия и кристаллизации почти завершаются одновременно при одномерном испытании на солевое расширение; (B) стандарт испытания на уплотнение, согласно которому скорость расширения составляет менее 0,02 мм/ч, может использоваться при испытании на солевое расширение; (C) требуемое время для температурного равновесия почвы квадратично по отношению к размеру образца и намного быстрее в условиях жидкой среды по сравнению с условиями в газовой среде. Поскольку деформация и температура синхронизированы, рекомендуется время стабилизации деформации образцов разного размера в разных охлаждающих средах. На основе этих результатов предлагается стандартная процедура метода одномерного испытания на солевое расширение, в котором приводятся испытательное оборудование, процесс испытания, время стабилизации, деформации солевого расширения и метод обработки данных.

Ключевые слова: сульфат, засоленный грунт, солевое расширение, время стабилизации, экспериментальный метод.

Reference

1. Jia Y.B. Construction Technology of Roadbed in Swelling Soil Area. Tunnel Construction, 2006.(in Chinese).

2. Dong C.H., Dong X.M., Tests on the Dissolve Settlement Characteristics of Sulphate Saline Soil. Applied Mechanics and Materials.Conf., Jinan, China, 2013.361-363:1071-1074.DOI:10.4028/www.scientific.net/AMM.361-363.1071.

3. Lai Y.M., Wan X.S., Zhang M.Y. An experimental study on the influence of cooling rates on salt expansion in sodium sulfate soils. Cold Regions Science and Technology. 124, 67-76(2016). DOI:10.1016/j.coldregions.2015.12.014.

4. Wan, X.S., You Z.M., Wen H.Y., Crossley W. An experimental study of salt expansion in sodium saline soils under transient conditions. Journal of Arid Land. 9(6), 865-878(2017).

5. Wan X.S., Hu Q.J., Liao M.K. Salt crystallization in cold sulfate saline soil. Cold Regions Science and Technology. 137, 36-47(2017).DOI: 10.1016/j.coldregions.2017.02.007.

6. Wan X.S., Liu E.L., Qiu E.X., et al., Study on phase changes of ice and salt in saline soils. Cold Regions Science and Technology. 172:102988(2020).DOI:10.1016/j.coldregions.2020.102988

7. Wang T.X., Liu Z.C., Lu J.Experimental study on coefficient of thermal conductivity and specific volumeheat of loess. Rock and Soil Mechanics. 28(4), 655-658(2007).DOI:10.1182/blood-2005-08-3320.(in Chinese)

Information about authors:

Яньцзе Цзи, - Бейжің Цзяотун университетінің құрылыс бөлімі, Пекин, Қытай.
Ксу Ли - Бейжің Цзяотун университетінің құрылыс бөлімі, Бейжің, Қытай.
Yanjie Ji - Department of Civil Engineering, Beijing Jiaotong University, Beijing, China.
Xu Li - Department of Civil Engineering, Beijing Jiaotong University, Beijing, China.

IRSTI 90.27.31

B.U. Baikhozhayeva*, A.K. Zhumagali, A.E. Moldakhmetova

L.N.Gumilyov Eurasian National University, Nur-Sultan, Kazakhstan
Corresponding author: bajxozhaeva63@enu.kz

Comparison of the results of pH measurements in a buffer solution

Abstract. As a result of the increasing need to study the choice of the assigned value during the inter-laboratory comparisons is becoming more and more relevant. Since the assigned value is a reference point when comparing the results of the participants of the qualification test. Frequently, qualification verification providers face a number of problems when choosing the assigned value. An incomplete analysis of the results of interlaboratory comparisons will lead to an inaccurate assessment of the competence of the laboratory, which contributes to the revocation of the certification of the accreditation of the laboratory participant.

This article attempts to provide a complete statistical analysis of the results of interlaboratory comparisons from the beginning to the end of the tour with the content of all statistical analyses recommended in GOST ISO/IEC 17043-2013.

The results of interlaboratory comparisons conducted in testing laboratories of Kazakhstan aimed at ensuring metrological traceability of pH measurements in a buffer solution are presented. The reference values of the buffer solution are determined in the state scientific metrological center.

Keywords: Traceability; reference laboratory; metrology; testing laboratory; interlaboratory comparison.

DOI: doi.org/10.32523/2616-7263-2021-135-2-64-70

Introduction

The relevance of the article. Participation in interlaboratory comparisons is one of the mandatory conditions for confirming the technical competence of the laboratory in accordance with GOST ISO/IEC 17025-2019, one of the forms of quality management of measurement results in laboratories (clause 7.7 of GOST ISO/IEC 17025-2019). [1]

Interlaboratory comparisons are a necessary and effective tool for ensuring the uniformity of measurements in the country and the quality of measurements in laboratories. Interlaboratory comparisons - organization, execution and evaluation of measurements or tests of the same or several similar samples by two or more laboratories in accordance with pre-established conditions. [2]

Research methods: alternative experimental methods and robust statistical methods.

The main part. The interlaboratory comparisons considered in this article were carried out according to the MLS schedule for 2020. [3]

The purpose of the work was to check the competence of the laboratory by means of interlaboratory comparisons. The subject of verification is the technological, informational and methodological support of the traceability of measurements in testing laboratories (IL).

The test was aimed at assessing the comparability of the results of laboratory measurements in sludge when determining the pH in a buffer solution.

10 IL were taken in interlaboratory comparisons.

The measurement results obtained during interlaboratory comparisons can be further used by laboratories for internal control of their performance indicators.

The article presents the specific results of the participants with a detailed statistical analysis in accordance with GOST ISO/IEC 17043-2013 and ST RK ISO 13528-2010.

The coordinator of the comparisons was RSE "KazInMetr". Certificate of accreditation no. KZ. C. 01. 1512 is valid for"05" August 2024. [4]

The comparison program "Determination of pH in buffer solution" involved 10 laboratories with different pH measurement technologies. It shows the level of acids and alkalis in the water, determining

what effect this can have on plants and fish. This indicator is an important indicator that affects a person's well-being. The deviation of this value from the norm indicates problems in the water supply, which should be paid attention to.

Description of samples for qualification testing

The sample of the qualification verification program was the state standard sample (GSO) pH of the reference buffer solution of the 2nd category of EBR2 7.41 pH, which is an aqueous solution of potassium dihydrophosphate and sodium monohydrophosphate. Extended uncertainty of the assigned value (k=2, P=95%) ±0.01 pH. The assigned value of the sample was established by an experimental calculation method according to the procedure for preparing GSO.

Traceability of the assigned value is ensured by using a standard sample of the 2nd category, an aqueous solution of sodium tetraborate 10-water; traceability to the standards of units of mass and volume is ensured by using verified scales, measuring flasks in accordance with State verification schemes for measuring mass and volume.

The samples were labeled, divided into portions with the indication of the sample code. In order to maintain confidentiality, the correspondence of the cipher of the sample and the participant of the comparisons was available only to one of the comparison coordinators.

The delivery of all samples was carried out simultaneously. All samples were tested for stability and uniformity before delivery. The results of uniformity and stability are presented in Tables 1, 2.

Table 1

Data for checking uniformity

Bottle number	Serving 1	Serving 2
3	7,413	7,416
8	7,417	7,415
6	7,409	7,416
11	7,416	7,413
14	7,407	7,404
20	7,41	7,414
27	7,408	7,411
26	7,412	7,409
38	7,406	7,412
41	7,408	7,404
General average		7,41100
SKO (S_x), standard deviation		0,00357
S_w, sample standard deviation for all samples		0,00288
S_s, standard deviation between samples		0,00293

Table 2

Data for checking stability

Bottle number	Serving 1	Serving 2
74	7,413	7,416
94	7,412	7,413
General average		7,4135
Deviation		0,0025

Table 3

Participants ' results

Laboratory code	pH value	Extended uncertainty, pH
Laboratory 1	7,36	0,06
Laboratory 2	7,15	0,1
Laboratory 3	7,5	0,2
Laboratory 4	7,42	0,04
Laboratory 5	7,4	0,1
Laboratory 6	7,4	0,08
Laboratory 7	7,43	0,1
Laboratory 8	7,42	0,06
Laboratory 9	7,38	0,08
Laboratory 10	7,32	0,1

Comparison of the assigned value with the robust average

In accordance with ST RK ISO 13528: if a standard sample is used as a sample for checking qualifications, then after the participants have made measurements, the robust average value of x*, estimated from the results of the participants ' measurements, should be compared with the assigned value of X. In this case, the inequality must be fulfilled:

$$|x^*\text{-}X| < 2\sqrt{\frac{(1{,}25s^*)^2}{p} + u_x^2}$$

x* - robust average value;

s* - robust standard deviation;

p – number of participants;

u_x- standard uncertainty of the assigned value X. [5]

The robust mean value and robust standard deviation are determined in accordance with the Annex to the ST RK ISO 13528-2010. The robust mean value is 7.40 pH, the robust standard deviation is 0.05 pH. [6]

The results of checking the inequality: the deviation from the assigned value with the uncertainty of the difference is 0,01<0,04.

The choice of statistics for evaluating the characteristics of functioning

In accordance with GOST ISO/IEC 17043 and ST RK ISO 13528, the performance characteristics of the participants are evaluated using the quantitative indicator z. The use of the z indicator is valid only if the conditions for limiting the uncertainty of the assigned value are met. If

$$u_x \leq 0{,}3\overline{\sigma}$$

then the uncertainty of the assigned value of $u_x$is insignificant, and there is no need to take it into account when interpreting the results of the qualification check. If the condition is not met, then the uncertainty of the assigned value should be taken into account when interpreting the test results using appropriate quantitative indicators.

The results of checking the condition for limiting the uncertainty of the assigned value are 0,005≤0,014. This means that the z indicator will be used to evaluate the functioning characteristics of the listed measured values, which does not take into account the amount of uncertainty of the assigned value.

The standard deviation for the qualification assessment was determined from the data obtained from the cycle of the qualification verification project, calculated using the robust analysis of Algorithm A in Appendix C given by ST RK ISO/IEC 13528-2010.

Table 4

Robust analysis

Laboratory code	Measuredvalue, pH	1-processing	2-processing
		δ =0,025 x*- δ=7,34 x*+ δ=7,46	δ =0,025 x*- δ=7,34 x*+ δ=7,46
Laboratory 1	7,36	7,36	7,36
Laboratory 2	7,15	7,34	7,34
Laboratory 3	7,5	7,46	7,46
Laboratory 4	7,42	7,42	7,42
Laboratory 5	7,4	7,4	7,4
Laboratory 6	7,4	7,4	7,4
Laboratory 7	7,43	7,43	7,43
Laboratory 8	7,42	7,42	7,42
Laboratory 9	7,38	7,38	7,38
Laboratory 10	7,32	7,34	7,34
Robust average value, x*	7,4	7,4	7,4
Robust standard deviation, s*	0,037	0,05	0,05

Evaluation of the functioning characteristics

Table 5

Evaluation of a quantitative indicator

Laboratory code	Meaning pH	Extended uncertainty, pH	z
Laboratory 1	7,36	0,06	-1,11
Laboratory 2	7,15	0,1	-5,76
Laboratory 3	7,5	0,2	1,99
Laboratory 4	7,42	0,04	0,22
Laboratory 5	7,4	0,1	-0,22
Laboratory 6	7,4	0,08	-0,22
Laboratory 7	7,43	0,1	0,44
Laboratory 8	7,42	0,06	0,22
Laboratory 9	7,38	0,08	-0,66
Laboratory 10	7,32	0,1	-1,99

The evaluation of the characteristics of the functioning of the laboratory was carried out according to the quantitative indicator z according to the formula:

$$z=(x-X)/\overline{\sigma}$$

x – measurement result of the participating laboratory,

X – assigned value.

$\overline{\sigma}$ – standard deviation for the qualification assessment.

The performance characteristic is evaluated as follows:

at $|z| \leq 2$ -the quality of the test results is recognized as satisfactory;

at $2 < |z| \leq 3$ -the quality of the test results is considered doubtful and subject to additional verification;

at $|z| > 3$-the quality of the test results is considered unsatisfactory.

Conclusion

The analysis of the measurement results presented by the laboratories participating in the comparisons showed that the majority of the participants in the comparisons successfully coped with the task of measuring the controlled indicators.

The conducted interlaboratory comparison to ensure the reliability of measurements can be considered as a metrological certification of a standard sample. Such a model will allow laboratories to participate in interlaboratory comparisons without a certified standard sample, which significantly affects the absence of a standard sample in medical laboratories.

The values of the z indicators except for Laboratory 2 did not exceed the limits of the permissible values ($|z| \leq 2$), which corresponds to satisfactory performance of the work, and Laboratory 2 exceeded the limits of the permissible values ($|z| > 3$), which corresponds to unsatisfactory performance of the work in the field of pH determination.

References

1. ГОСТ ISO/IEC 17025-2019 «Общие требования к компетентности испытательных и калибровочных лабораторий» [Электорон. ресурс]. -2019. -URL: https://docs.cntd.ru/document/1200166732 (дата обращения: 24.11.2020).

2. ГОСТ ISO/IEC 17043-2013 «Оценка соответствия. Основные требования к проведению проверки квалификации» [Электорон. ресурс]. -2013. -URL:https://docs.cntd.ru/document/1200108187 (дата обращения: 24.11.2020).

3. График проведения межлабораторных сличений [Электорон. ресурс]. -2020.-URL: https://kazinmetr.kz/upload/services/10_graph_2020.pdf(дата обращения: 08.12.2020).

4. Аттестат аккредитации проверки квалификации [Электорон. ресурс]. -2020.-URL: https://kazinmetr.kz/upload/services/%D0%9F%D1%80%D0%BE%D0%B2%D0%B0%D0%B9%D0%B4%D0%B5%D1%80%20%E2%84%96KZ.%D0%A1.01.1512_05.08.2019_%D1%80%D1%83%D1%81.jpg (дата обращения: 08.12.2020)

5. СТ РК ISO13528-2010 «Статистические методы, применяемые при проверке квалификации лабораторий посредством межлабораторных сличений». [Электорон. ресурс]. -2010. -URL: https://www.egfntd.kz/rus/tv/343634.html?sw_gr=-1&sw_str=&sw_sec=24 (дата обращения: 25.11.2020).

6. Д.А. Паляничко, В.И. Згуря, Р.Г. Папуша Применение робастных методов анализа данных при ограниченном числе наблюдений: Электрические и компьютерные системы. [Электорон. ресурс]. -2012. -URL: https://elibrary.ru/item.asp?id=17782085 (дата обращения 14.11.2020)

Б.У. Байхожаева, А.Қ. Жұмағали., А.Е. Молдахметова
Л.Н.Гумилев атындағы Еуразия ұлттық университеті
Нұр-Сұлтан қ., Қазақстан Республикасы

Буферлік ерітіндідегі pH өлшеу нәтижелерін салыстыру

Аңдатпа. Қажеттіліктің өсуінің нәтижесінде зертханааралық салыстыру өткізу кезінде тірек мәнін таңдауды зерделеу маңызы бар және одан да астам өзекті болып келеді. Берілген мән біліктілікті тексеруге қатысушылардың нәтижелерін салыстыру кезінде тірек нүктесі болып табылады. Жиі біліктілікті тексеру провайдерлері тағайындалған мәнді таңдау кезінде бірқатар проблемаларға тап болады. Зертханааралық салыстыру нәтижелерін толық талдау зертхананың құзыреттілігін дәл емес бағалауға әкеледі, бұл қатысушы-зертхананың аккредиттеу аттестациясын қайтарып алуға ықпал етеді.

Бұл мақалада ГОСТ ISO/IEC 17043-2013 ұсынған барлық статистикалық талдаулардың мазмұнымен турдың басынан аяғына дейін зертханааралық салыстыру нәтижелерін толық статистикалық талдауды ұсынуға әрекет жасалды.

Буферлік ерітіндідегі pH өлшемдерінің метрологиялық бақылануын қамтамасыз етуге бағытталған Қазақстанның сынақ зертханаларында жүргізілген зертханааралық салыстырулардың нәтижелері ұсынылған. Буферлік ерітіндінің тірек мәндері мемлекеттік ғылыми метрологиялық орталықта анықталған.

Түйін сөздер: қадағалануы; референттік зертхана; метрология; сынақ зертханасы; зертханааралық салыстыру.

Б.У. Байхожаева, А.К. Жумагали, А.Е. Молдахметова
Евразийский национальный университет им.Л.Н.Гумилева
Нур-Султан, Казахстан

Сличение результатов измерений pH в буферном растворе

Аннотация. Возрастает необходимость изучения выбора приписанного значения при проведении межлабораторных сличений, что становится все более актуальным вопросом, поскольку приписанное значение является опорной точкой при сравнении результатов участников квалификационного теста. Зачастую провайдеры проверки квалификации сталкиваются с рядом проблем при выборе приписанного значения. Неполный анализ результатов межлабораторных сличений приводит к неточной оценке компетентности лаборатории, что способствует аннулированию сертификата аттестации участника-лаборатории.

В данной статье предпринята попытка предоставления полного статистического анализа результатов межлабораторных сличений с начала до завершения тура с содержанием всех статистических анализов, рекомендованных в ГОСТ ISO/IEC 17043-2013.

Представлены результаты межлабораторных сличений, проведенных в испытательных лабораториях Казахстана, которые направлены на обеспечение метрологической прослеживаемости измерений pH в буферном растворе. Эталонные значения буферного раствора определены в государственным научном метрологическом центре.

Ключевые слова: прослеживаемость, референтная лаборатория, метрология, испытательная лаборатория, межлабораторное сличение.

References

1. GOST ISO/IEC 17025-2019 «Obshchie trebovaniya k kompetentnosti ispytatel'nyh i kalibrovochnyh laboratorij» [General requirements for the competence of testing and calibration laboratories]. [Elecronic resource]. Available at: https://docs.cntd.ru/document/1200166732 (Accessed at: 24.11.2020) [in Russian].

2. GOST ISO/IEC 17043-2013 «Ocenka sootvetstviya. Osnovnye trebovaniya k provedeniyu proverki kvalifikacii» [Conformity assessment. Basic requirements for proficiency testing]. [Elecronic resource]. Available at:https://docs.cntd.ru/document/1200108187 (Accessed at: 24.11.2020) [in Russian].

3. Grafik provedeniya mezhlaboratornyh slichenij [Schedule of interlaboratory comparisons]. [Elecronic resource]. Available at: https://kazinmetr.kz/upload/services/10_graph_2020.pdf (Accessed at: 08.12.2020) [in Russian].

4. Attestat akkreditacii proverki kvalifikacii [Certificate of proficiency testing accreditation]Available at: https://kazinmetr.kz/upload/services/%D0%9F%D1%80%D0%BE%D0%B2%D0%B0%D0%B9%D0%B4%D0%B5%D1%80%20%E2%84%96KZ.%D0%A1.01.1512_05.08.2019_%D1%80%D1%83%D1%81.jpg (Accessed at: 08.12.2020) [in Russian].

5. ST RK ISO 13528-2010 «Statisticheskie metody, primenyaemye pri proverke kvalifikacii laboratorij posredstvom mezhlaboratornyh slichenij» [Statistical methods used in the verification of laboratory proficiency through interlaboratory comparisons]. [Elecronic resource]. Available at: https://www.egfntd.kz/rus/tv/343634.html?sw_gr=-1&sw_str=&sw_sec=24 (Accessed at: 25.11.2020) [in Russian].

6. D.A. Palyanichko, V.I. Zgurya, R.G. Papusha Primenenie robastnyh metodov analiza dannyh pri ogranichennom chisel nablyudenij [Papusha Application of robust data analysis methods with a limited number of observations]: Elektricheskie i komp'yuternye sistemy [Electrical and computer systems]. [Elecronic resource]. Available at: https://elibrary.ru/item.asp?id=17782085 (Accessed at: 14.11.2020) [in Russian].

Information about authors:

B.U. Baikhozhayeva - Head of the Department "Standardization, Certification and Metrology", L. N. Gumilyov Eurasian National University, Nur-Sultan, Kazakhstan.

A.K. Zhumagali - The 2nd year Master's student, Department of "Metrology", L. N. Gumilyov Eurasian National University, Nur-Sultan, Kazakhstan.

A.E. Moldakhmetova - Head of the Department of Scientific Projects and Publications, L. N. Gumilyov Eurasian National University, Nur-Sultan, Kazakhstan.

Б.У. Байхожаева - Л.Н. Гумилев атындағы ЕҰУ, "Стандарттау, сертификаттау және метрология" кафедрасының меңгерушісі, Нұр-Сұлтан, Қазақстан.

А.Қ. Жұмағали - «Метрология» кафедрасының 2 курс магистранты, Л.Н. Гумилев атындағы ЕҰУ, Нұр-Сұлтан, Қазақстан.

А.Е. Молдахметова - ғылыми жобалар мен жарияланымдар кафедрасының меңгерушісі, Л.Н. Гумилев атындағы ЕҰУ, Нұр-Сұлтан, Қазақстан.

IRSTI 67.01.37

A. Aniskin[1], A. Tulebekova[2,3*]

[1]University North, Koprivnica, Croatia
[2]CSI Research & Lab, LLP, Nur-Sultan, Kazakhstan
[3]L.N. Gumilyov Eurasian National University, Nur-Sultan, Kazakhstan
Corresponding author: krasavka5@mail.ru

A unified approach for temperature and strength control of concrete

Abstract. The development of theoretical and experimental research in the field of quality control has led to the development of many methods for assessing the strength of concrete. The temperature-strength control (TSCC) method, which is based on the relationship between concrete temperature and curing time, is the most adapted method for quickly determining the strength of the concrete in the formwork during the early phase of curing. The concrete strength tests must be carried out in accordance with the requirements of the standards. The most adapted standards are ASTM C1074 (USA); NEN 5970 (Netherlands); ST-NP SRO SSK-04-2013 (Russia). However, there are no existing approaches to TSCC that consider all the advantages of each method. Using the method of paired comparison, the authors determined the weights of the significance of each criterion of methods and tasks for TSCC. Based on of the obtained results a unified approach to temperature-strength control of concrete has been formed considering the assessment of its applicability. This approach will solve the problem of limitation of the application of most methods, which in its basis have the best methods in solving tasks of control stages. The unified approach to temperature-strength control of concrete will allow to achieving high quality and durability of concrete and reinforced concrete structures.

Keywords: standard; concrete curing temperature; non-destructive testing of concrete; embedded sensor.

DOI: doi.org/10.32523/2616-7263-2021-135-2-71-81

Introduction

The fixing of the concrete hardening temperature enables timely monitoring of the concrete hardening process, its regulation and forecasting during documentation. In addition, as numerous studies have shown [1-4], the temperature factor is fundamental in determining the required concrete properties. When concrete strength is controlled using various measuring systems, the current temperature values are sent to the measuring instrument. The temperatures and measuring times are used to calculate the current strength of the concrete. The standards specify methods of determination of concrete hardness. Each of the existing methods has a specific scope of application and has advantages and disadvantages. However, the possibility of using alternative methods of temperature-strength control of concrete (TSCC) in practice is limited due to the lack of relevant normative and technical documents, regulations, and standards. In this regard, the development of a unified approach to TSCC will serve as an important tool for controlling temperature and strength gain during all stages of concrete curing. The approach should incorporate best practice techniques from around the world, as global experience is an important factor in the choice of techniques and objectives for TSCC.

Analysis of best practices from around the world to TSCC

The software "Snow Leopard" was applied in the study [5], which allows to predict the final strength of concrete and the time of cooling, and in case of negative predictions to choose the heat treatment mode or the required thermal insulation. Another advantage of the program is the possibility to automate the data entry process, obtained from multi-channel recorders, which increases quality,

accuracy, and productivity. Registration of temperature at the enterprise was carried out using device Terem-4.1.When observing the temperature of the concrete at reference points, a temperature-strength control list is drawn up. With the help of "Snow Leopard" program schedules of temperature changes and concrete strength gain were built for each of the control points.

In a study [6] to control the temperature of concrete curing, cube specimens were made of fine-grained concrete of class B25, size 100*100*100 mm using Portland cement of grade M400. The samples were placed in the body of the heated volume of the floor slab structure model. Temperature measurement data were entered in the on-site computer and processed using a program that performs a complete analysis of temperature parameters of concrete with the determination of concrete strength at control points [6].

In April 2019, a construction company specializing in complex projects began experimenting with Giatec SmartRockTM sensors during the construction of a major arch bridge project [7]. To investigate the benefits of using SmartRock technology, the team conducted extensive testing by embedding the sensors at key points on the bridge. By placing the sensors in the center and at the edge of the arch, the strength gain was measured at different locations in the reinforced concrete element. The sensor placed at the edge recorded a lower temperature profile and therefore the lowest strength gain. Whereas sensors placed in the center of the arches measured the point of greatest temperature and strength gain. By monitoring these locations, the actual strength of the concrete element at the critical point was measured. This is only possible with the sensors, as the laboratory samples cannot reproduce the actual curing conditions of the concrete element.

CIBC Square (Ontario, Canada) is a highly visible pair of innovative 3 million square foot office towers in the city center. Exact Technology sensors were used in the construction of the facility. These precision devices provide concrete maturity monitoring at CIBC Square to determine when concrete strength is approaching the 16 MPa threshold [8] that allows self-compacting formwork to be moved, and formwork pressure readings for self-compacting mix loads. Relays, recorders, and probes are in the center of the Exact sensor for maturity and temperature control. The use of the sensors has had a positive effect on construction.

The study [9] recommends the use of three or more marks per gauge to obtain the most accurate maturity and strength. This leads to the conclusion that the maturity of the poured concrete will depend on the lowest slab temperature and not necessarily on the temperature in the middle of the slab.

In the study [10] three concrete mixtures were considered: the first mixture of pure Portland cement, the others included a partial replacement of cement with fly ash and ground granulated blast furnace slag at 30 % respectively. In this work the reference temperature was chosen to be 11°C, which is an average value among those recommended [11]. The concrete specimens in the single cube moulds were covered with polyethylene foil immediately after pouring and cured at room temperature (approx. 20 °C) [12] for one day. They were then removed from the moulds and placed in a water bath set at 20 °C. A computer-controlled programmable water bath was used to simulate the temperature conditions in situ. The test ages of the standard curing concrete specimens were 1, 2, 3, 5, 7, 14, 28, 42, 84, 156, and 365 days, while the temperature cured concrete specimens were tested at 1, 2, 3, 3, 7, 14, and 28 days. According to [13], "equivalent" mortar mixtures can be used to determine the activation energy of concrete mixtures. The Dutch method for determination of maturity and the method for determining the equivalent age depends on the mix and require the determination of a weighted Cn factor and activation energy. A close convergence between the strength data at 20°C and 50°C was not obtained. Thus, the authors note the difficulties encountered in additional investigations with the Dutch method and the Arrhenius equation method for determining maturity.

The authors [14] monitored the hydration temperature continuously after the concrete was poured and temperature sensors provided data to assess the degree of maturity of the concrete as it hardened. The hydration temperature history data was applied to the Nurse-Saul function to predict the maturity index.

Research methods

By analyzing the best practices reviewed, it is possible to identify certain techniques and tasks of the methods used in them (i.e. methods of temperature and strength control of concrete), which have led to the effectiveness of the results obtained in the particular best practices. The list of these techniques and tasks is interpreted and presented in Table 1.

Table 1

List of techniques and tasks of best practice TSCC methods

Methods	Techniques and objectives
Best practice 1 [5]	
ST-NP SRO SSK-04-2013 [15]	The use of the "Snow Leopard" software made it possible to predict the concrete strength, cooling time and achievable final strength of the concrete; statistical processing of the results was carried out.
Best practice 2 [6]	
ST-NP SRO SSK-04-2013 [15]	The use of the program made it possible to determine probabilistic estimates of concrete strength and to advise on continuing heating and curing times for the entire sample of homogeneous structures under the prevailing curing conditions.
Best practice 3[7]	
ASTM C 1074 [13]	Sensor placement was carried out at key locations. By creating a maturity calibration, using and interpreting the SmartRock sensor data, the strength of the concrete was determined. A simple interpretation of the temperature graphs and monitoring of the concrete's strength development saved time.
Best practice 4 [8]	
ASTM C 1074 [13]	Wireless sensors were installed in the concrete formwork, fixed to the reinforcement, before pouring. Temperature data was collected by the sensor and there was no difficulty in using it. The concrete strength was calculated using the Nurse-Saul temperature-time factor.
Best practice 5 [9]	
ASTM C 1074 [13]	Particular attention was paid to the location of the concrete temperature measuring points, which allowed the most accurate determination of maturity, and showed that the maturity of the poured concrete would depend on the lowest slab temperature, and not necessarily on the temperature in the middle of the slab.

Best practice 6[10]	
ASTM C 1074 [13]	It is noted that the mixture calibration method is very simple, having made a minimum of 17 cylinders; 2 were used for temperature monitoring and the remaining samples for determining the compressive strength. By selecting minimum 5 time intervals, 1, 3, 7, 14 and 28 days, for each day the compressive strength of two cylinders was determined, during the intervals data was also obtained from two cylinders which were used for temperature monitoring and the average value of these values was determined. Entering these values into the Nurse-Saul function or the Arrhenius method gave a maturity value. To calculate the Arrhenius method, additional investigations were carried out to determine the activation energy, which was a time consuming process. The Nurse-Saul function does not differentiate the temperature sensitivity of different cement systems, especially for mixtures with different bases (with additives, accelerators).
NEN 5970 [16]	The "weighted maturity" method requires additional research, the determination of a weighted Cn coefficient, but in the study the strength data at 20 and 65 °C did not match.
Best practice 7[14]	
ASTM C 1074 [13]	The resulting Nurse-Saul concrete strength data provided accurate and reliable results. The application of the sensors did not cause any difficulty in use.

The main normative documents governing the requirements for TSCC are ASTM C1074 (USA); NEN 5970 (Netherlands); ST-NP SRO SSK-04-2013 (Russia), which are predominantly reflected in use, therefore, these standards were adopted for the analysis (Figure 1).

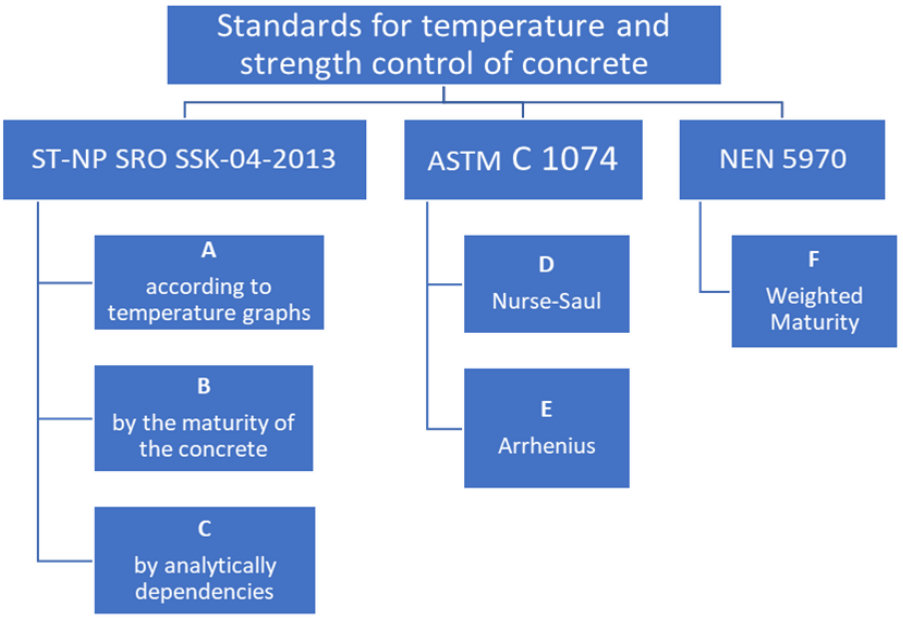

Figure 1. Standards for temperature and strength control of concrete

Three essential types of processes have also been defined: laboratory, field and resultant. Laboratory tests result in the acquisition of strength isotherms for a given type of mixture. Field tests are used to obtain data on concrete temperature, and the resulting calculation of concrete maturity. The sorted and classified science-based techniques and tasks of the TSCC methods are presented in Figure 2.

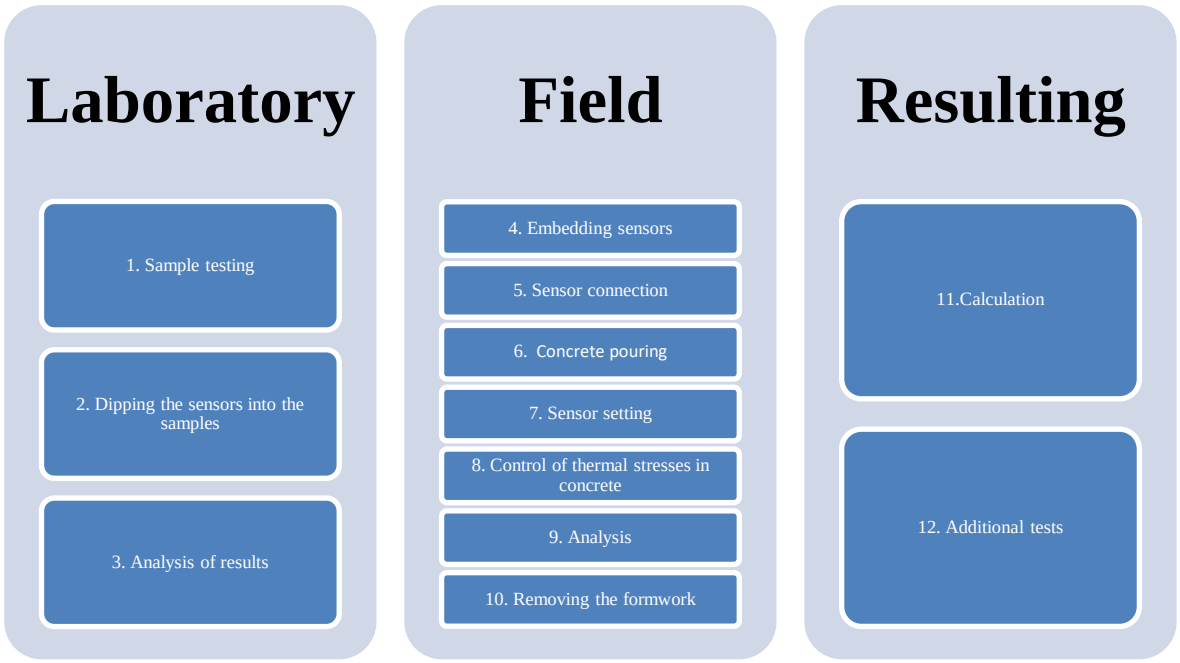

Figure 2. List of sorted and categorized evidence-based techniques and objectives of TSCC method

Based on the classified science-based techniques and tasks of TSCC methods (Figure 2), Table 2 presents a multi-criteria analysis based on the results of best practices, where the evaluation criteria for TSCC processes are: K1 - reliability of the method and availability of normative literature; K2 - possibility of application to various structures (by form, reinforcement, responsibility); K3 - labor input; K4 –the safety of testing; K5 - accuracy of calculations. The indexes are expressed in points from 1 to 10 with a scale of 1. A score of 10 indicates compliance with the quality criteria.

Table 2

Multi-criteria analysis

Process numbering as per Figure 2	Indicator	ST-NP SRO SSK-04-2013			ASTM C 1074		NEN 5970
		A	B	C	D	E	F
1	K1	10	10	10	9	9	9
	K3	10	10	10	8	8	8
	K4	9	9	9	9	9	9
	K5	10	10	10	8	8	8
2	K3	8	9	9	10	10	10
3	K1	6	9	10	8	8	8
	K3	5	10	8	9	6	8
	K5	8	10	9	10	9	10

4	K1	9	10	10	8	8	8
	K2	10	10	10	10	10	10
	K3	9	10	9	9	9	9
5	K3	9.5	9.5	9.5	10	10	10
6	K3	10	10	10	10	10	10
7	K3	9	9	9	10	10	10
8	K1	9	10	9	8	8	7
	K5	8	10	8	6	7	7
9	K1	9	9	10	9	9.5	9
10	K3	8	8	9	9	9	9
11	K1	5	7	6	10	8	8
12	K3	4	7	5	10	7	7

*A,B,C,D,E,F – Methods regarding figure 1

Using the paired comparison method, a criterion analysis was carried out for the TSCC methods, assigning a degree of preference to each pair of criteria, and constructing a matrix of paired comparisons (Table 3). Iterations were defined to determine the weights for each criterion. And the final weights were then found for each criterion: for K1- 0.312179; K2 - 0.129903; K3-0.188206; K4-0.071029; K5-0.298683. Based on the weights obtained for each process, a ranking of the data presented in Table 4 was carried out.

Table 3

Pairwise comparison of criteria

	K1	K2	K3	K4	K5
K1	1	4	0.33	2	4
K2	0.25	1	2	4	0.2
K3	3.03030303	0.5	1	1	0.25
K4	0.5	0.25	1	1	0.2
K5	0.25	5	4	5	1

Table 4

Calculation of the weighted sum

Name of processes	Indicator	A	B	C	D	E	F
1	K1	3.1218	3.1218	3.1218	2.8096	2.8096	2.8096
	K3	1.8821	1.8821	1.8821	1.5056	1.5056	1.5056
	K4	0.6393	0.6393	0.6393	0.6393	0.6393	0.6393
	K5	2.9868	2.9868	2.9868	2.6881	2.3895	2.6881
	Σ	8.6299	8.6299	8.6299	7.6427	7.3440	7.6427
2	K3	1.5056	1.6939	1.6939	1.8821	1.8821	1.8821
	Σ	1.5056	1.6939	1.6939	1.8821	1.8821	1.8821
3	K1	1.8731	2.8096	3.1218	2.4974	2.4974	2.4974
	K3	0.9410	1.8821	1.5056	1.6939	1.1292	1.5056
	K5	2.3895	2.9868	2.6881	2.9868	2.6881	2.9868
	Σ	5.2036	7.6785	7.3156	7.1781	6.3148	6.9899

4	K1	2.8096	3.1218	3.1218	2.4974	2.4974	2.4974
	K2	1.2990	1.2990	1.2990	1.2990	1.2990	1.2990
	K3	1.6939	1.8821	1.6939	1.6939	1.6939	1.5056
	Σ	5.8025	6.3029	6.1147	5.4903	5.4903	5.3021
5	K3	1.8821	1.8821	1.8821	1.8821	1.8821	1.8821
	Σ	1.7880	1.7880	1.7880	1.8821	1.8821	1.8821
6	K3	1.8821	1.8821	1.8821	1.8821	1.8821	1.8821
	Σ	1.8821	1.8821	1.8821	1.8821	1.8821	1.8821
7	K3	1.6939	1.6939	1.6939	1.8821	1.8821	1.8821
	Σ	1.6939	1.6939	1.6939	1.8821	1.8821	1.8821
8	K1	2.8096	3.1218	2.8096	2.4974	2.4974	2.1853
	K5	2.3895	2.9868	2.3895	1.7921	2.0908	2.0908
	Σ	5.1991	6.1086	5.1991	4.2895	4.5882	4.2760
9	K1	2.8096	2.8096	3.1218	2.8096	2.8096	2.8096
	Σ	2.8096	2.8096	3.1218	2.8096	2.8096	2.8096
10	K3	1.5056	1.5056	1.5998	1.6939	1.6939	1.6939
	Σ	1.5056	1.5056	1.5998	1.6939	1.6939	1.6939
11	K1	1.5609	2.1853	1.8731	3.1218	2.4974	2.4974
	Σ	1.5609	2.1853	1.8731	3.1218	2.4974	2.4974
12	K3	0.7528	1.3174	0.9410	1.8821	1.3174	1.3174
	Σ	0.7528	1.3174	0.9410	1.8821	1.3174	1.3174

Results and discussion

The analysis shows that the significant processes that lead to the effectiveness of TSCC are those regulated by regulations:

- The process 1 – ST-NP SRO SSK-04-2013;
- The process 2 – ASTM C 1074;
- The process 3 – ST-NP SRO SSK-04-2013by the maturity of the concrete;
- The process 4 – ST-NP SRO SSK-04-2013by the maturity of the concrete;
- The process 5 – ASTM C 1074 Nurse-Saul;
- The process 6 – ST-NP SRO SSK-04-2013, ASTM C 1074;
- The process 7 – ASTM C 1074;
- The process 8 –ST-NP SRO SSK-04-2013by the maturity of the concrete;
- The process 9 – ST-NP SRO SSK-04-2013by analytically dependencies;
- The process 10 – ASTM C 1074 Nurse-Saul;
- The process 11 – ASTM C 1074 Nurse-Saul;
- The process 12 – ASTM C 1074 Nurse-Saul.

Concrete plays an important role in ensuring the safety, serviceability and durability of concrete and reinforced concrete structures, the quality of which is primarily determined by a combination of formulation and technological factors, and therefore the importance of concrete strength control systems cannot be overestimated.

Conclusion

Based on the research, the processes regulated by the American standard are mostly included in the unified approach to TSCC. In process 1, however, the use of cubic specimens for laboratory tests is singled out for aggregation, and in order not to disturb the consistency of the ASTM C 1074 algorithm, it will be accepted that the use of at least 15 specimens is sufficient. The requirements for processes 3 and 4 are quite clearly described in the ST-NP SRO SSK-04-2013 standard and will be adopted in a uniform approach. The number of temperatures measuring points has been shown to play an important role as best practice. The concrete must gain sufficient strength at some critical points before the project proceeds to the next stage. Critical points may vary depending on the type of structural element being monitored. In single-sided or double-sided slab systems, structurally important zones are in negative and positive design moments. As a rule, the maximum positive moment is in the middle of the span and the maximum negative moment is located at the slab-column junction. The standard ST-NP SRO SSK-04-2013, which gives detailed recommendations and an algorithm of actions, also deals with the control of temperature stresses in concrete in a scrupulous manner. Changing temperature conditions have a great influence on deformations and stresses in concrete. During the construction period, temperature stresses arise during the development and dissipation of exothermic heat, often accompanied by cracking. Measurement of the concrete temperature is therefore mandatory when monitoring concrete stresses. This monitoring is especially important in winter when additional concrete heat treatment may be necessary.

The results of this study are important for builders as they will eliminate existing gaps in the current approaches used in temperature-strength control of the concrete.

Acknowledgments

This research was funded by the Science Committee of the Ministry of Education and Science of the Republic of Kazakhstan (Grant № AP08956209).

References

1. Poorarbabi A., Ghasemi M., Azhdary Moghaddam M. Concrete compressive strength prediction using non-destructive tests through response surface methodology // Ain Shams Eng J. -2020. -Vol.11. -№ 4. -P.939-949.

2. Karahan Ş., Büyüksaraç A., Işık E. The Relationship Between Concrete Strengths Obtained by Destructive and Non-destructive Methods // -Iran J Sci Technol Trans Civ Eng. -2020. -Vol. 44. № 1. -P.91-105.

3. Rasmussen R.O., Cable J.K., Turner D.J., Voigt G.F. Strength prediction by using maturity for Portland cement concrete pavement construction at airfields // Transp. Res. Rec. -2004. -Vol. 1893. -№ 1. -P.18-25.

4. Ebensperger L., Oyarzún J.C., Torres R. Determinación de la temperatura datum para la aplicación de la madurez en climas fríos. // Rev Ing construcción. -2020. -Vol. 35. №1. -P.84-99.

5. Головнев С.Г. и др. Компьютерный контроль и регулирование процессов выдерживания бетона в зимних условиях // Академический вестник УралНИИпроект РААСН. -2010. -№ 2. -Р. 75-78.

6. Гныря А.И., Бояринцев А.П., Коробков С.В. Обоснование метода температурно-прочностного контроля // Вестник ТГАСУ. -2017. -№ 3. –С. 161-170.

7. South African Arch Bridge Project [Electronic resource]. -2019. -URL: https://www.giatecscientific.com/case-study/south-african-arch-bridge-project/ (date of access 04.2019).

8. Sensors capture and relay maturity, temperature, formwork pressure data [Electronic resource]. -2020. -URL: http://concreteproducts.com/equipment/reports/12199-sensors-capture-and-relay-maturity-temperature-formwork-pressure-data.html#.XykFQCgzbIV. (date of access 02.03.2020).

9. Will Hansen, Sunny Surlaker. Embedded Wireless Temperature Monitoring Systems For Concrete Quality Control. -2006. -43 p.

10. Soutsos M., Kanavaris F., Hatzitheodorou A. Critical analysis of strength estimates from maturity functions. // Case Stud Constr Mater. -2018. -Vol. 9. -P. e00183.

11. Han F., Maturity method // in: H.W. Reinhardt, C.U. Grosse (Eds.), Advanced Testing of Cement-Based Materials During Setting and Hardening, RILEM Report 31. -2018. -P. 277–296.

12. Soutsos M., Hatzitheodorou A., Kanavaris F., Kwasny J. Effect of temperature of the strength development of GGBS and fly ash // Mag Concr Res. -2017. -Vol. 69, № 15. -P. 787–801.

13. ASTM C1074–19. Standard Practice for Estimating Concrete Strength by the Maturity Method. -2019. -10 p.

14. Tareen N., Kim J., Rim W., Park S. Comparative Analysis and Strength Estimation of Fresh Concrete Based on Ultrasonic Wave Propagation and Maturity Using Smart Temperature and PZT Sensors // Micromachines. -2019. -Vol. 10, № 9. -P.559.

15. СТ-НП СРО ССК-04-2013. Температурно–прочностной контроль бетона при возведении монолитных конструкций в зимний период. -2013. -25 с.

16. NEN 5970. Determination of strength of fresh concrete with the method of weighted maturity. -2001. -21 p.

А.Анискин[1], А.С.Тулебекова[2,3]

[1]Солтүстік Университеті, Копривница, Хорватия

[2]«CSI Research & Lab» ЖШС, Нұр-Сұлтан, Қазақстан

[3]Л.Н. Гумилев атындағы Еуразия ұлттық университеті, Нұр-Сұлтан, Қазақстан

Бетонның температурасы мен беріктігін бақылаудағы бірыңғай тәсіл

Аңдатпа. Сапаны бақылау саласындағы теориялық және эксперименттік зерттеулердің дамуы бетонның беріктігін бағалаудың көптеген әдістерінің пайда болуына әкелді. Қалыптағы бетонның беріктігін жедел анықтау үшін ерте ұстау сатысында бетонның температурасы мен оны ұстау уақытының өзара байланысына негізделген температуралық–беріктік бақылау (БТББ) тәсілі неғұрлым бейімделген болып табылады. Бетонның беріктігін зерттеу стандарттардың талаптарына сәйкес жүргізілуі керек. Нормативтік құжаттама бойынша неғұрлым бейімделген стандарттар ASTM C1074 (АҚШ) болып табылады); NEN 5970 (Нидерланды); СТ–НП СРО ССК–04–2013 (Ресей). Алайда, БТББ әрбір әдістің барлық артықшылықтарын ескерген БТББ -ға қатысты қазіргі тәсілдері жоқ. Авторлар жұптық салыстыру әдісін қолдана отырып, БТББ әдістері мен міндеттерінің әр критерийі маңыздылығының салмағын анықтады. Алынған нәтижелер негізінде бетонның қолданылуын бағалауды ескере отырып, оның температуралық-беріктік бақылауына бірыңғай тәсіл құрылды. Бұл тәсіл бақылау кезеңдерінің есептерін шешуде ең жақсы әдістерге ие көптеген әдістерді қолдануды шектеу мәселесін шешеді. Бетонның температуралық-беріктік бақылауына біріздендірілген тәсіл бетон және темірбетон конструкцияларының Жоғары сапасы мен ұзақ мерзімділігіне қол жеткізуге мүмкіндік береді.

Түйін сөздер: стандарт, бетонның қатаю температурасы, бетонды бұзбай сынау, ендірілген сенсор.

А. Анискин[1], А.С. Тулебекова[2,3]
[1]University North, Копривница, Хорватия
[2,]ТОО «CSI Research&Lab», Нур-Султан, Казахстан
[3]Евразийский национальный университет имени Л.Н. Гумилева, Нур-Султан, Казахстан

Унифицированный подход к температурно-прочностному контролю бетона

Аннотация. Развитие теоретических и экспериментальных исследований в области контроля качества привело к появлению значительного количества методов оценки прочности бетона. Для оперативного определения прочности бетона, находящегося в опалубке, на ранней стадии выдерживания наиболее адаптированным является способ температурно–прочностного контроля (ТПКБ), базирующегося на взаимосвязи температуры бетона и времени его выдерживания.

Исследования прочности бетона должны выполняться по требованиям стандартов. Наиболее адаптированными по нормативной документации являются стандарты ASTM C1074 (США); NEN 5970 (Нидерланды); СТ–НП СРО ССК–04–2013 (Россия). Однако существующие подходы к ТПКБ, которые учитывали бы все преимущества каждого из методов, отсутствуют. Авторы, используя метод парного сравнения, определили вес значимости каждого критерия методов и задач к ТПКБ. На основании полученных результатов был сформирован унифицированный подход к температурно-прочностному контролю бетона с учетом оценки его применимости. Данный подход позволит решить проблему ограничения применения большинства методов, которые в своей основе имеют лучшие приемы в решении задач этапов контроля. Унифицированный подход к температурно-прочностному контролю бетона позволит достигнуть высокого качества и долговечности бетонных и железобетонных конструкций.

Ключевые слова: стандарт, температура твердения бетона, неразрушающий контроль бетона, встраиваемый датчик.

References

1. Poorarbabi A., Ghasemi M., Azhdary Moghaddam M. Concrete compressive strength prediction using non-destructive tests through response surface methodology. Ain Shams Eng J. 11(4), 939-949 (2020).

2. Karahan Ş., Büyüksaraç A., Işık E. The Relationship Between Concrete Strengths Obtained by Destructive and Non-destructive Methods. Iran J Sci Technol Trans Civ Eng. 44(1),91-105 (2020).

3. Rasmussen R.O., Cale J.K., Turner D.J., Voigt G.F. Strength prediction by using maturity for Portland cement concrete pavement construction at airfields. Transp. Res. Rec. 1893(1), 18-25 (2020).

4. Ebensperger L., Oyarzún J.C., Torres R. Determinación de la temperatura datum para la aplicación de la madurez en climas fríos. Rev Ing construcción. 35(1), 84-99 (2020).

5. Golovnev S.G. i dr. Komp'yuternyj kontrol' i regulirovanie processov vyderzhivaniya betona v zimnih usloviyah [Computer control and regulation of concrete curing processes in winter conditions]. Akademicheskij vestnik UralNIIproekt RAASN [Academic Bulletin Ural Research Institute project RAASN].2, 75-78 (2010) [in Russian].

6. Gnyrya A.I., Boyarincev A.P., Korobkov S.V. Obosnovanie metoda temperaturno-prochnostnogo kontrolya [Substantiation of the method of temperature and strength control]. Vestnik TGASU [Bulletin of TSASU].3, 161-170 (2017) [in Russian].

7. South African Arch Bridge Project [Electronic resource]. 2019. URL: https://www.giatecscientific.com/case-study/south-african-arch-bridge-project/ (date of access 04.2019).

8. Sensors capture and relay maturity, temperature, formwork pressure data [Electronic resource]. 2020. URL: http://concreteproducts.com/equipment/reports/12199-sensors-capture-and-relay-maturity-temperature-formwork-pressure-data.html#.XykFQCgzbIV. (date of access 02.03.2020).

9. Will Hansen, Sunny Surlaker. Embedded Wireless Temperature Monitoring Systems For Concrete Quality Control. 2006. 43 p.

10. Soutsos M., Kanavaris F., Hatzitheodorou A. Critical analysis of strength estimates from maturity functions. Case Stud Constr Mater. 9, e00183 (2018).

11. Han F., Maturity method in: H.W. Reinhardt, C.U. Grosse (Eds.), Advanced Testing of Cement-Based Materials During Setting and Hardening, RILEM Report 31. 2018. P. 277-296.

12. Soutsos M., Hatzitheodorou A., Kanavaris F., Kwasny J. Effect of temperature of the strength development of GGBS and fly ash. Mag Concr Res. 69(15) 787-801 (2017).

13.ASTM C1074-19. Standard Practice for Estimating Concrete Strength by the Maturity Method. 2019. 10 p.

14. Tareen N., Kim J., Rim W., Park S. Comparative Analysis and Strength Estimation of Fresh Concrete Based on Ultrasonic Wave Propagation and Maturity Using Smart Temperature and PZT Sensors. Micromachines. 10(9), 559 (2019).

15. СТ-НПСРОССК-04-2013. Temperaturno–prochnostnoj kontrol' betona pri vozvedenii monolitnyh konstrukcij v zimnij period [Temperature and strength control of concrete during the erection of monolithic structures in winter]. 2013. 25 s. [in Russian].

16. NEN 5970. Determination of strength of fresh concrete with the method of weighted maturity. 2001. 21 p.

Information about authors:

А. Анискин - Ph.D., Солтүстік Университеті, Копривница, Хорватия

А.С. Тулебекова - «Ғимараттар және құрылыстарды жобалау» кафедрасының доценті, Ph.D., Л. Н. Гумилев атындағы Еуразия ұлттық университеті, Нұр-сұлтан, Қазақстан; «CSI Research & Lab» ЖШС–ның аға ғылыми қызметкері.

A. Aniskin - Ph.D., Assistant Professor in Department of Civil Engineering, University North, Koprivnica, Croatia.

A.S. Tulebekova - Ph.D., Associate Professor in Department of Civil Engineering, L.N. Gumilyov Eurasian National University, Nur-Sultan, Kazakhstan; Senior Researcher of CSI Research & Lab, LLP, Nur-Sultan, Kazakhstan.

IRSTI 67.11.29

Bing Wu[1], Hong-Hu Zhu[1,2*], Dingfeng Cao[3]

[1] School of Earth Sciences and Engineering, Nanjing University, Nanjing, China
[2] State Key Laboratory of Frozen Soil Engineering, Lanzhou, China
[3] School of Civil Engineering, Sun Yat-sen University, Guangzhou, China
Corresponding author: zhh@nju.edu.cn

Measuring thermal conductivity of frozen soil using fiber optic sensors

Abstract. The thermal conductivity is crucial for determining heat transfer in frozen soil. However, it is a challenge to obtain accurate measurement values due to the instability of soil properties. Recently, the fiber optic sensing technologies has enabled accurate and distributed in-situ monitoring of a variety of geotechnical parameters. This paper aims to explore the feasibility of actively heated fiber Bragg grating (AH-FBG) method in measuring thermal conductivity of frozen soil. A series of laboratory experiments were performed on frozen soil samples at different initial temperatures from −16 to 5 °C. The theoretical upper and lower limits of thermal conductivity were used to evaluate the AH-FBG measurements. The thermal conductivity recorded by a heat transfer analyzer was used to identify the measurement accuracy. The experimental results that the AH-FBG method can accurately measure the thermal conductivity of frozen soil when the initial temperature is below −6 °C, and the measurement error is within acceptable range of 0.8%. When the soil temperature is between −6 and 0 °C, significant measurement errors were observed due to the disturbance of heating to the frozen soil.

Keywords: frozen soil; fiber optic sensor; fiber Bragg grating (FBG); actively heated fiber optics (AHFO); monitoring; phase change.

DOI: doi.org/10.32523/2616-7263-2021-135-2-82-93

Introduction

Frozen soils have complicated thermal properties governing the heat transfer and freeze-thaw process [1,2]. In heat transfer modeling of frozen soils, thermal conductivity is one of the most important input parameters [3]. It has long been recognized that the thermal conductivity of soil is strongly influenced by its density and compositions (soil particles, water, ice, and air) [4,5]. In particular, the thermal conductivity of frozen soil is hard to determine due to the complex phase change process.

In the last few decades, many studies have been conducted in this research area, and some theoretical and empirical models have been proposed [3,6-8]. Transient and steady-state methods have been used to determine thermal conductivity, but most of them are only applicable to laboratory tests. It is therefore of great importance to develop an effective and reliable in-situ measuring technology of thermal conductivity for frozen soils [4,5,9]. This is a bottleneck problem that seriously hinders the development of fundamental theories and engineering design schemes of frozen soils.

In engineering practices, the heat pulse (HP) method is widely used to measure the soil thermal properties based on the analogies of radial heat flow from a line source [8,10,11]. For frozen soils, this method has been applied to estimate unfrozen water contents or ice contents [12-14], water and heat flux [15], and snow density [16], as well as thermal properties [15,17]. It has the advantages of fast measurement, low cost, and superior portability for field applications [18]. However, some drawbacks are encountered during field monitoring, such as limited measurement ranges and low accuracy. More importantly, only point-type measurement can be achieved, so large-scale and long-distance monitoring can hardly be performed.

Fiber optic sensing technologies, which have the advantages of distributed measurement, anti-interference, and corrosion resistance [19-22], have been dramatically developed and employed in strain and temperature sensing in recent years [22,23]. Based on distributed temperature sensing (DTS), the

actively heated fiber optic (AHFO) method has been developed to overcome the shortcomings of traditional HP methods. For unfrozen soils, it has been widely applied for measuring water and heat flux [24-28]. However, it was rarely used in frozen soils due to the complex phase change process and temperature dependence of thermal properties [18].

In this paper, the actively heated fiber Bragg grating (AH-FBG) has been proposed to perform quasi-distributed monitoring of thermal conductivity of frozen soils. A series of laboratory experiments were carried out at different initial temperatures to explore the feasibility of the proposed method in thermal conductivity measurement and determine its measurement accuracy and range.

Methodology

Figure 1 shows the working principle of an FBG sensor. According to Bragg's law, when a broadband source of light has been injected into the fiber, FBG reflects a narrow spectral part of light at a specific wave length λ_B. For the FBG sensor, this wavelength is sensitive to changes in temperature (T) or strain (ε). To accurately measure the actual temperature, strain relief of the FBG sensor is very important. In this study, the loose FBG sensor is encapsulated in a small corundum tube to avoid strain effects. Thus this sensor is only for temperature measurement, and the temperature can be expressed as [29]

$$\Delta T = \frac{\Delta\lambda_B}{\lambda_B c_{\mathrm{T}}} \tag{1}$$

where c_{T} is the wavelength sensitivity coefficients for temperature, $\Delta\lambda_B$ is the wavelength change, ΔT is the temperature change.

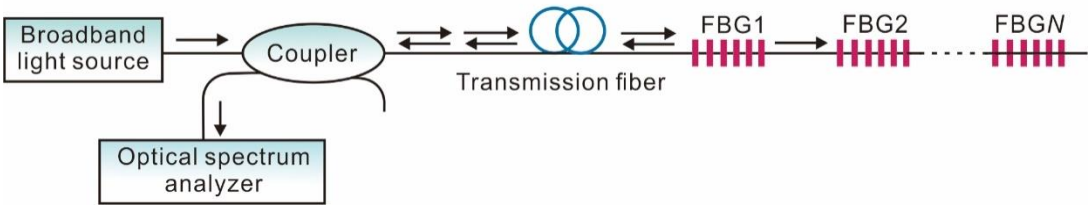

Figure 1. Working principle of the FBG sensing technology

When an AH-FBG sensor is inserted in frozen soil, due to the infinite line heat source model and cylindrical geometry of the single probe dissipation sensors, the temperature (T) of the AH-FBG sensor during heating is related to time (t) according to the theoretical solution for a line heat source [30]:

$$T - T_0 = -\frac{q}{4\pi\lambda}\ln t + B \tag{2}$$

where T_0 is the initial temperature before heating (℃). t and q are the heating time (s) and the heat source strength per unit of length (W/m), respectively. λ is the thermal conductivity (W/(m·℃)) of the frozen soil. B is a constant.

Accounting for the finite dimensions of the heat source and the contact resistance between the heat source and the medium outside it, Eq. (2) is valid for the constant heating strength and sufficient heating time. Linear regression can be used to calculate λ from the slope K of the heating data with Eq. (2)

$$\lambda = \frac{q}{4\pi K} \tag{3}$$

For frozen soils, the thermal parameters are related to several factors such as soil moisture, ice content, soil composition, and density. The thermal conductivity has an upper limit (λ_U) and a lower limit (λ_L), which can be expressed as [6]

$$\lambda_L = \sum \theta_\alpha \lambda_\alpha \tag{4}$$

$$\frac{1}{\lambda_U} = \frac{1}{\sum \frac{\theta_\alpha}{\lambda_\alpha}} \tag{5}$$

where θ_α and λ_α are the volumetric content (m^3/m^3) and thermal conductivity of the phases (unfrozen water, ice, soil particles, and air). The sum of the volumetric contents of all components is 1. Thus, the thermal conductivity can be calculated according to the volume fraction of each substance in the frozen soil, which can be used as the reference value for the thermal conductivity measured by the AH-FBG method.

Material and laboratory test setup

To measure the thermal conductivities of the frozen soil using the AH-FBG method, a series of laboratory experiments have been conducted. Figure 2 shows the structure of the AH-FBG sensor. The AH-FBG sensor includes an aluminum oxide tube with high thermal conductivity, a bare FBG sensor, an electrical resistance wire, and a stainless-steel tip and flange for packaging and protecting. The electrical resistance wire is used for heating, and the FBG sensor is used for temperature sensing. They are installed in parallel in different holes of the corundum tube.

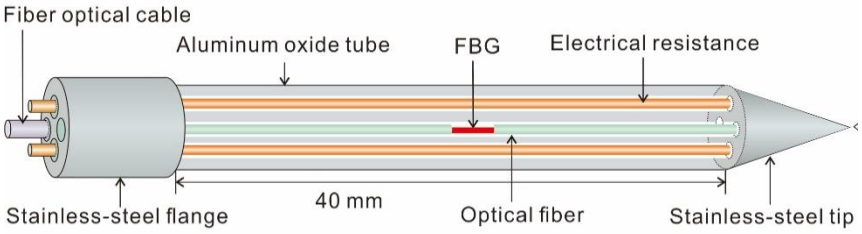

Figure 2. Schematic diagram of AH-FBG sensor

The experiments were carried out in a low-temperature test chamber. Different experimental temperatures were set to control the temperature of the soil samples from -16 to 5°C. The soil samples were collected from Huining, Gansu Province, China. The basic properties of the test soil are given in table 1.

The experiments were carried out in a low-temperature test chamber. Different experimental temperatures were set to control the temperature of the soil samples from -16 to 5°C. The soil samples were collected from Huining, Gansu Province, China. The basic properties of the test soil are given in table 1.

Table 1

Basic physical parameters of the test soil

Soil type	Liquid limit (%)	Plastic limit (%)	Optimum water content (%)	Natural dry density (g·cm^{-3})	Maximum dry density (g·m^{-3})	Specific gravity
Low plasticity clay	34.0	17.3	13.8	1.42	1.53	2.76

As shown in figure 3, the soil samples were compacted and filled in the stainless-steel cutting rings and PVC molds. The dry density was 1.4 g/cm^{3}and the initial moisture contents were set as 16%. The AH-FBG sensors were inserted into the center of the soil samples and connected to an FBG interrogator and a direct current (DC) power supply, respectively. The FBG interrogator was connected to a computer for real-time FBG data collecting. The total heating time was determined to be 300 s, and the heat source strength was set between 6~8 W/m. The FDR sensors and thermistors were installed in the PVC samples to measure the unfrozen water contents and soil temperatures, and both were connected to the data logger. In addition, a heat transfer analyzer was used to obtain the thermal conductivity reference value (λ_c) of the frozen soil sample at the temperature of -16 ℃.

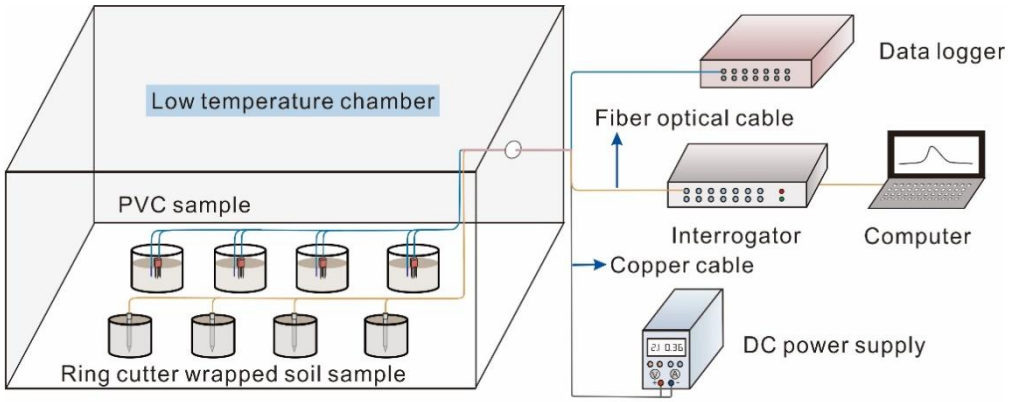

Figure 3. Schematic image of the experimental setup

Results and analysis

The soil temperature data measured by the thermistors and the unfrozen water content data measured by the FDR sensors are shown in figure 4. The results show that the freezing evolution of soil samples can be divided into four stages. In Stage I and Stage IV, the soil samples were completely unfrozen and frozen states, respectively. The compositions of the soil did not change. In Stage II, the soil temperature was between −3.16 and −1.2 ℃ (severe phase transition zone), and the soil temperature curve reached a relatively stable state, as shown in Fig. 4(a). Simultaneously, the unfrozen water content decreased sharply as the temperature decreased in Fig. 4(b). This phenomenon can be explained by the fact that the moisture in the sample underwent a severe phase change and the process of water freezing into ice is exothermic [9]. The heat generated by the phase change offsets part of the heat dissipation of the sample at a lower ambient temperature. It has to be noted that the thermal properties of the frozen soil are very unstable due to the severe phase change in Stage II. While most of the free water freezes, the temperature of the soil sample continued to drop, and the unfrozen water content slowly decreased to a final value, as shown in Stage III. According to the measured unfrozen water content, the initial moisture

content, and dry density of the soil samples, the theoretical limits of the thermal conductivity (λ_L and λ_U) can be calculated using Eqs. (4) and (5).

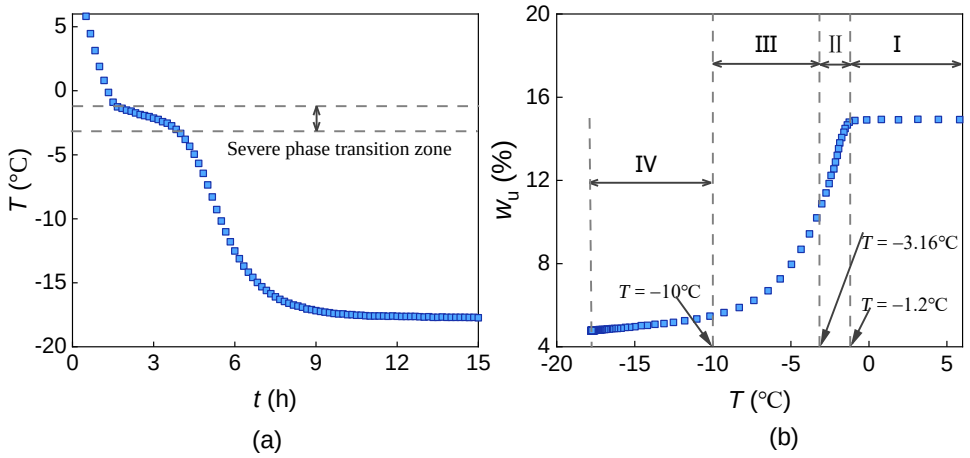

Figure 4. Evolution of (a) soil temperatures (T) obtained by thermistors and (b) unfrozen water contents (w_u) obtained by FDR sensors

Figure 5 shows the temperatures of the AH-FBG sensors during heating with different initial temperatures. It can be seen from figure 5(a) that under the same moisture content and heating power, the temperature rise rates of AH-FBG sensors varied significantly at different temperatures, which means the variant thermal conductivities of the frozen soil.

As described above, when using the linear heat source method to infer the thermal conductivity of the surrounding soil, the heat transfer time in the probe is invalid due to the sensor size and contact thermal resistance [18]. As such, the measurement temperature during this period is also useless and would not be considered. In this study, the sensor temperatures increase rapidly and have a linear relationship with time in the first 40 s of heating due to the heat conduction inner the sensor tube, as shown in figure5(a). After 40 s, the heat starts to transfer in the soil, and the temperature growth slows down. Thus, the valid period for the soil samples is considered 40~300 s, as shown in figure 5(b). The thermal conductivity measured by the AH-FBG method (λ_a) can be calculated after substituting the temperature within the valid period into Eqs. (2) and (3).

Figure 6 shows the comparison between the limit values of thermal conductivity (λ_L and λ_U) calculated by Eqs. (4) and (5), the reference value (λ_c) obtained by the heat transfer analyzer and the measured values (λ_a) obtained by the AH-FBG method. As shown in figure 6, when the initial temperature was less than -6 ℃ and greater than 0℃, λ_a is between the upper limit (λ_U) and the lower limit (λ_L). They all have the same trends with the temperature, which indicates the rationality measurement of λ_a. In addition, at the temperature of -16 ℃, λ_c and λ_a have great consistency, and the error between them is only 0.8%, which shows the high accuracy of λ_a. While the initial temperature is between -6 and 0℃, especially between -3.16 and 0℃, λ_a fluctuates wildly. This can be explained by the fact that the frozen soil with a higher initial temperature undergoes a severe phase change after heating, and its properties are greatly disturbed. So, the accuracy of thermal conductivity measurement is reduced. This result denotes that when the soil is unfrozen, or its temperature is lower than -6 ℃, there would have a higher measurement accuracy of the thermal conductivity using the AH-FBG method. The proposed method is currently not applicable to measure the thermal conductivity

of frozen soils with an initial temperature of $-6 \sim 0$ ℃.

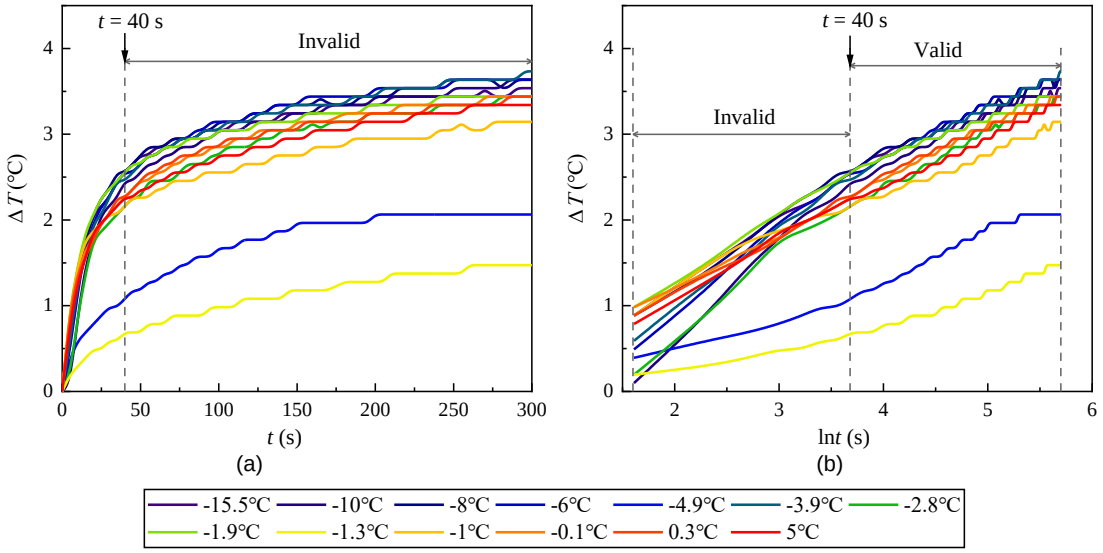

Figure 5. Measured temperature changes (a) as a function of t and (b) as a function of $\ln t$ during heating at different initial temperatures

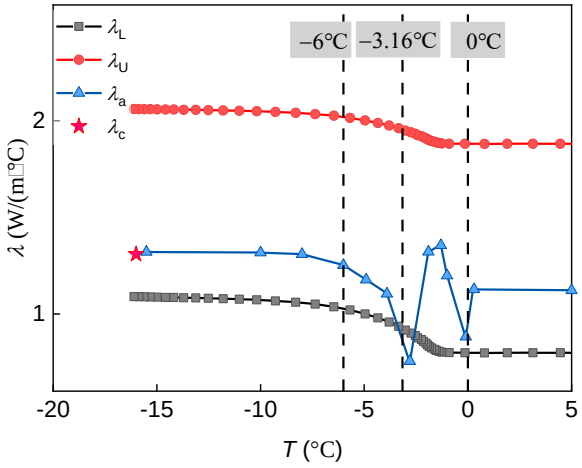

Figure 6. Comparison between the reference values of thermal conductivity (λ_L, λ_U and λ_c) and the measured values of thermal conductivity (λ_a) obtained by the AH-FBG method

Conclusion

The AH-FBG method for measuring the thermal conductivity of frozen soil is proposed and developed. The feasibility of the proposed method was verified by laboratory experiments. Some conclusions are drawn in this study: Due to the unavoidable process of ice-water phase change, the AH-FBG method is only applicable to the soil with the initial temperature below −6 °C and above 0°C. And the measurement error can be within the acceptable range of 0.8%. The disturbance of heating to frozen soil will cause more significant measurement errors when the soil temperature is between −6~0 °C.

More theoretical and experimental studies are needed to solve severe phase change caused by heating and further improve the measuring parameters of the AH-FBG method. Several field observations stations have been established in Hebei, Gansu, and Sichuan Provinces of China. Long-term fiber optic monitoring of in-situ frozen soils is in progress.

References

1. Nusier, O. Abu-Hamdeh, N. Laboratory techniques to evaluate thermal conductivity for some soils// Heat and Mass Transfer. -2003. -Vol.39. №2. -P. 119-123.

2. Hansson, K., Šimůnek, J. Mizoguchi, M., Lundin, L.-C., Van Genuchten, M.T. Water flow and heat transport in frozen soil// Vadose Zone Journal. -2004. -Vol.3. №2. -P. 693-704.

3. Cote, J., Konrad J. Thermal conductivity of base-course materials// Canadian Geotechnical Journal. -2005. -Vol.42. №1. -P. 61-78.

4. Penner, E. Thermal conductivity of frozen soils// Canadian Journal of Earth Sciences. -1970. -Vol.7. №3. -P. 982-987

5. Tarnawski, V.R., Wagner, B. Modeling the thermal conductivity of frozen soils// Cold Regions Science and Technology. -1993. -Vol.22. №1. -P. 19-31.

6. Zhang, N., Wang, Z. Review of soil thermal conductivity and predictive models// International Journal of Thermal Sciences. -2017. -Vol.117. -P. 172-183.

7. Dong, Y., Mccartney, J.S. and Lu, N. Critical review of thermal conductivity models for unsaturated soils// Geotechnical and Geological Engineering. -2015. -Vol.33. №2. -P. 207-221.

8. Mickley, A.S. The Thermal conductivity of moist soil// Transactions of the American Institute of Electrical Engineers. -1951. -Vol.70. №2. -P. 1789-1797.

9. Liu, G., Si, B.C. Soil ice content measurement using a heat pulse probe method// Canadian Journal of Soil Science. -2011. -Vol.91. №2. -P. 235-246.

10. de Vries, D.A. A nonstationary method for determining thermal conductivity of soil in situ// Soil Science. -1952. -Vol.73. №2. -P. 83-90.

11. Van der Held, E.F.M., Van Drunen, F.G. A method of measuring the thermal conductivity of liquids // Physica. -1949. -Vol.15. №10.

12. Kojima, Y., Nakano, Y., Kato, C., Noborio, K., Horton, R. A new thermo-time domain reflectometry approach to quantify soil ice content at temperatures near the freezing point// Cold Regions Science and Technology. -2020. -Vol.174. 103060.

13. Kojima, Y., Heitman, J.L., Flerchinger, G.N., Ren, T., Horton, R. Sensible heat balance estimates of transient Soil ice contents// Vadose Zone Journal. -2016. -Vol.5. №5.

14. Putkonen, J. Determination of frozen soil thermal properties by heated needle probe// Permafrost and Periglacial Processes. -2003. -Vol.14. №4. -P. 343-347.

15. Ochsner, T.E., Baker, J.M. In situ monitoring of soil thermal properties and heat flux during freezing and thawing// Soil Science Society of America Journal. -2008. -Vol.72. №4. -P. 1025-1032.

16. Liu, G., Si, B.C. Dual-probe heat pulse method for snow density and thermal properties measurement// Geophysical Research Letters. -2008. -Vol.35. №16. -P. L16404.

17. He, H., Dyck, M.F., Horton, R., Li, M., Jin, H., Si, B.C. Distributed temperature sensing for soil physical measurements and its similarity to heat pulse method// Advances in Agronomy. -2018. -Vol.148. -P. 173-230.

18. He, H., Dyck, M. F., Horton, R., Ren, T., Bristow, K.L., Lv, J., Si, B,C. Development and application of the heat pulse method for soil physical measurements// Reviews of Geophysics. -2018. -Vol.56. №4. -P. 567-620.

19. Shi, B., Zhang, D., Zhu, H.-H., Zhang, C.-C; Kai, G., Sang, H., Han, H., Sun, M., Liu, J. DFOS applications to geo-engineering monitoring// photonic sensors. -2021. -Vol.11. №2. -P. 158-186.

20. Zhu, H.-H., Wang, Z.Y., Shi, B., Wong, K.W. Feasibility study of strain based stability evaluation of locally loaded slopes: Insights from physical and numerical modeling // Engineering Geology. -2016. -Vol.208. -P. 39-50.

21. Zhu, H.-H., Shi, B., Yan, J.F., Zhang, J., Wang, J. Investigation of the evolutionary process of a reinforced model slope using a fiber-optic monitoring network // Engineering Geology. -2015. -Vol.186. -P. 34-43.

22. Joe, H.-E., Yun, H., Jo, S.-H., Jun, M.B.G., Min, B.-K. A review on optical fiber sensors for environmental monitoring// International Journal of Precision Engineering and Manufacturing-Green Technology. -2018. -Vol.5. №1. -P. 173-191.

23. Zhang, C.-C., Zhu, H.-H., Liu, S.P., Zhang, D. A kinematic method for calculating shear displacements of landslides using distributed fiber optic strain measurements// Engineering Geology. -2018. -Vol.234. -P. 83-96.

24. Cao, D., Shi, B., Zhu, H.-H., Shi, B., Inyang, H.I., Wei, G.-Q., Duan, C.-Z. A soil moisture estimation method using actively heated fiber Bragg grating sensors// Engineering Geology. -2018. -Vol.242. -P. 142-149.

25. Ciocca, F., Lunati, I., Van de Giesen, N., Parlange, M.B. Heated optical fiber for distributed soil-moisture measurements: a lysimeter experiment/ Vadose Zone Journal. -2012. -Vol.11. №4.

26. Sayde, C., Buelga, J.B, Rodriguez-Sinobas, L., El Khoury, L., English, M., van de Giesen, N., Selker, J.S. Mapping variability of soil water content and flux across 1-1000 m scales using the Actively Heated Fiber Optic method// Water Resources Research. -2014. -Vol.50. №9. -P. 7302-7317.

27. Sayde, C., Gregory, C., Gil-Rodriguez, M., Tufillaro, N., Tyler, S., van de Giesen, N., English, M., Cuenca, R., Selker, J.S. Feasibility of soil moisture monitoring with heated fiber optics// Water Resources Research. -2010. -Vol.46. №6.

28. Yan, J.-F., Gregory, C., Gil-Rodriguez, M., Wang, B.-J., Wei, G.-Q., Cao, D.-F. A quantitative monitoring technology for seepage in slopes using DTS// Engineering Geology. -2015. -Vol.186. -P. 100-104.

29. Zhu, H.-H., Liu, L.C., Pei, H.F., Shi, B. Settlement analysis of viscoelastic foundation under vertical line load using a fractional Kelvin-Voigt model// Geomechanics and Engineering. -2012. -Vol.4. №1. -P. 67-78.

30. Wu, R., Martin, V., McKenzie, J., Broda, S., Bussière, B., Aubertin, M., Kurylyk, B.L. Laboratory-scale assessment of a capillary barrier using fibre optic distributed temperature sensing (FO-DTS)// Canadian Geotechnical Journal. -2020. -Vol.57. №1. -P. 115-126.

Бин Ву[1], Хун-Ху Чжу[1,2], Динфэн[3]
[1]Жер туралы ғылымдар және инженерлік мектебі, Нанкин университеті, Нанкин, Қытай
[2]Мұздатылған топырақ құрылысының мемлекеттік кілт зертханасы, Ланьчжоу, Қытай
[3]Құрылыс мектебі, Сунь Ятсен университеті, Гуанчжоу, Қытай

Мұздатылған топырақтың жылу өткізгіштігін талшықты-оптикалық датчиктерді қолдану арқылы өлшеу

Аңдатпа. Жылу өткізгіштігі мұздатылған топырақтағы жылу беруді анықтау үшін өте маңызды, бірақ топырақ қасиеттерінің тұрақсыздығына байланысты дәл өлшеу мәндерін алу қиынға соғады. Жақында талшықты-оптикалық зондтау технологиялары әртүрлі геотехникалық параметрлерді дәл және таралатын орнында бақылауға мүмкіндік берді. Бұл жұмыста мұздатылған топырақтың жылу өткізгіштігін өлшеу кезінде белсенді қыздырылған талшықты Bragg торы (AH-FBG) әдісінің орындылығы зерттеліп, мұздатылған топырақ үлгілері бойынша бастапқы 16-дан 5 С-ге дейінгі әр түрлі бастапқы температураларда бірқатар зертханалық тәжірибелер жасалды. AH-FBG өлшемдерін бағалау үшін жылу өткізгіштіктің теориялық жоғарғы және төменгі шектері қолданылды. Өлшеу дәлдігін анықтау үшін жылу өткізгіштік анализаторы жазған жылу өткізгіштік қолданылды, AH-FBG әдісі мұздатылған топырақтың жылу өткізгіштік коэффициентін бастапқы температура - 6 °C градустан төмен болғанда және өлшеу қателігі дәл болғанда өлшей алады деген тәжірибелік нәтижелер алынды, ал өлшеу қателігі 0,8% деңгейінде қалыптасты. Топырақтың температурасы −6 мен 0 С аралығында болған кезде, мұздатылған топыраққа қызудың бұзылуына байланысты өлшеудің айтарлықтай қателіктері байқалды.

Түйін сөздер: мұздатылған топырақ, талшықты-оптикалық датчиктер, Bragg талшықты торы (FBG), белсенді қыздырылған оптикалық талшықтар (AHFO), жылу өткізгіштік, фазалық өзгеріс.

Бин Ву[1], Хун-Ху Чжу[1,2], Динфэн[3]
[1]Школа наук о Земле и инженерии, Нанкинский университет, Нанкин, Китай
[2]Государственная ключевая лаборатория инженерии мерзлых грунтов, Ланьчжоу, Китай
[3]Школа гражданского строительства, Университет Сунь Ятсена, Гуанчжоу, Китай

Измерение теплопроводности мерзлого грунта с помощью оптоволоконных датчиков

Аннотация. Теплопроводность имеет решающее значение для определения теплопередачи в мерзлом грунте. Однако получить точные значения измерений сложно из-за нестабильности свойств почвы. В последнее время технологии оптоволоконного зондирования сделали возможным точный и распределенный мониторинг на месте различных геотехнических параметров. В данной статье исследуется возможность использования метода активно нагретой волоконной Брэгговской решетки (AH-FBG) для измерения теплопроводности мерзлого грунта. Серия лабораторных экспериментов была проведена на образцах мерзлого грунта при

различных начальных температурах от -16 до 5 °C. Теоретические верхний и нижний пределы теплопроводности использовались для оценки измерений AH-FBG. Для определения точности измерения использовалась теплопроводность, зарегистрированная анализатором теплопередачи. Экспериментальные результаты показывают, что метод AH-FBG может точно измерять теплопроводность мерзлого грунта, когда начальная температура ниже -6 °C, а ошибка измерения находится в пределах допустимого диапазона 0,8%. Когда температура почвы составляет от –6 до 0 °C, наблюдаются значительные ошибки измерения из-за нарушения нагрева мерзлого грунта.

Ключевые слова: мерзлый грунт, оптоволоконные датчики, волоконная Брэгговская решетка (FBG), активно нагреваемая волоконная оптика (AHFO), теплопроводность, изменение фазы.

References

1. Nusier, O. Abu-Hamdeh, N. Laboratory techniques to evaluate thermal conductivity for some soils. Heat and Mass Transfer. 39(2), 119-123 (2003).

2. Hansson, K., Šimůnek, J. Mizoguchi, M., Lundin, L.-C., Van Genuchten, M.T. Water flow and heat transport in frozen soil. Vadose Zone Journal. 3(2), 693-704 (2004).

3. Cote, J., Konrad J. Thermal conductivity of base-course materials. Canadian Geotechnical Journal. 42(1), 61-78 (2005).

4. Penner, E. Thermal conductivity of frozen soils. Canadian Journal of Earth Sciences. 7(3), 982-987 (1970).

5. Tarnawski, V.R., Wagner, B. Modeling the thermal conductivity of frozen soils. Cold Regions Science and Technology. 22(1), 19-31 (1993).

6. Zhang, N., Wang, Z. Review of soil thermal conductivity and predictive models. International Journal of Thermal Sciences. 117, 172-183 (2017).

7. Dong, Y., Mccartney, J.S. and Lu, N. Critical review of thermal conductivity models for unsaturated soils. Geotechnical and Geological Engineering. 33(2), 207-221 (2015).

8. Mickley, A.S. The Thermal conductivity of moist soil. Transactions of the American Institute of Electrical Engineers. 70(2), 1789-1797 (1951).

9. Liu, G., Si, B.C. Soil ice content measurement using a heat pulse probe method. Canadian Journal of Soil Science. 91(2), 235-246 (2011).

10. de Vries, D.A. A nonstationary method for determining thermal conductivity of soil in situ. Soil Science. 73(2), 83-90 (1952).

11. Van der Held, E.F.M., Van Drunen, F.G. A method of measuring the thermal conductivity of liquids. Physica. 15(10), 1949.

12. Kojima, Y., Nakano, Y., Kato, C., Noborio, K., Horton, R. A new thermo-time domain reflectometry approach to quantify soil ice content at temperatures near the freezing point. Cold Regions Science and Technology. 2020. Vol.174. 103060.

13. Kojima, Y., Heitman, J.L., Flerchinger, G.N., Ren, T., Horton, R. Sensible heat balance estimates of transient Soil ice contents. Vadose Zone Journal. 5(5), (2016).

14. Putkonen, J. Determination of frozen soil thermal properties by heated needle probe. Permafrost and Periglacial Processes. 14(4), 343-347 (2003).

15. Ochsner, T.E., Baker, J.M. In situ monitoring of soil thermal properties and heat flux during freezing and thawing. Soil Science Society of America Journal. 72(4), 1025-1032 (2008).

16. Liu, G., Si, B.C. Dual-probe heat pulse method for snow density and thermal properties measurement. Geophysical Research Letters. 35(16), L16404 (2008).

17. He, H., Dyck, M.F., Horton, R., Li, M., Jin, H., Si, B.C. Distributed temperature sensing for soil physical measurements and its similarity to heat pulse method. Advances in Agronomy. 148, 173-230 (2018).

18. He, H., Dyck, M. F., Horton, R., Ren, T., Bristow, K.L., Lv, J., Si, B,C. Development and application of the heat pulse method for soil physical measurements. Reviews of Geophysics. 56(4), 567-620 (2018).

19. Shi, B., Zhang, D., Zhu, H.-H., Zhang, C.-C; Kai, G., Sang, H., Han, H., Sun, M., Liu, J. DFOS applications to geo-engineering monitoring (photonic sensors). 11(2), 158-186 (2021).

20. Zhu, H.-H., Wang, Z.Y., Shi, B., Wong, K.W. Feasibility study of strain based stability evaluation of locally loaded slopes: Insights from physical and numerical modeling. Engineering Geology. 208, 39-50 (2016).

21. Zhu, H.-H., Shi, B., Yan, J.F., Zhang, J., Wang, J. Investigation of the evolutionary process of a reinforced model slope using a fiber-optic monitoring network. Engineering Geology. 186, 34-43 (2015).

22. Joe, H.-E., Yun, H., Jo, S.-H., Jun, M.B.G., Min, B.-K. A review on optical fiber sensors for environmental monitoring. International Journal of Precision Engineering and Manufacturing-Green Technology. 5(1), 173-191 (2018).

23. Zhang, C.-C., Zhu, H.-H., Liu, S.P., Zhang, D. A kinematic method for calculating shear displacements of landslides using distributed fiber optic strain measurements. Engineering Geology. 234, 83-96 (2018).

24. Cao, D., Shi, B., Zhu, H.-H., Shi, B., Inyang, H.I., Wei, G.-Q., Duan, C.-Z. A soil moisture estimation method using actively heated fiber Bragg grating sensors. Engineering Geology. (242), 142-149 (2018).

25. Ciocca, F., Lunati, I., Van de Giesen, N., Parlange, M.B. Heated optical fiber for distributed soil-moisture measurements: a lysimeter experiment. Vadose Zone Journal. 11(4), (2012).

26. Sayde, C., Buelga, J.B, Rodriguez-Sinobas, L., El Khoury, L., English, M., van de Giesen, N., Selker, J.S. Mapping variability of soil water content and flux across 1-1000 m scales using the Actively Heated Fiber Optic method. Water Resources Research. 50(9), 7302-7317 (2014).

27. Sayde, C., Gregory, C., Gil-Rodriguez, M., Tufillaro, N., Tyler, S., van de Giesen, N., English, M., Cuenca, R., Selker, J.S. Feasibility of soil moisture monitoring with heated fiber optics. Water Resources Research. 46(6), (2010).

28. Yan, J.-F., Gregory, C., Gil-Rodriguez, M., Wang, B.-J., Wei, G.-Q., Cao, D.-F. A quantitative monitoring technology for seepage in slopes using DTS. Engineering Geology. 186, 100-104 (2015).

29. Zhu, H.-H., Liu, L.C., Pei, H.F., Shi, B. Settlement analysis of viscoelastic foundation under vertical line load using a fractional Kelvin-Voigt model. Geomechanics and Engineering. 4(1), 67-78 (2012).

30. Wu, R., Martin, V., McKenzie, J., Broda, S., Bussière, B., Aubertin, M., Kurylyk, B.L. Laboratory-scale assessment of a capillary barrier using fibre optic distributed temperature sensing (FO-DTS). Canadian Geotechnical Journal. 57(1), 115-126 (2020).

Information about authors:

Бин Ву- Жер туралы ғылымдар және инженерлік мектебі, Нанкин университеті, Нанкин, Қытай.

Хун-Ху Чжу - Мұздатылған топырақ құрылысының мемлекеттік кілт зертханасы, Ланьчжоу, Қытай.

Динфэн Цао - Құрылыс мектебі, Сунь Ятсен университеті, Гуанчжоу, Қытай.

Bing Wu - School of Earth Sciences and Engineering, Nanjing University, Nanjing, China.

Hong-Hu Zhu - State Key Laboratory of Frozen Soil Engineering, Lanzhou, China.

Dingfeng Cao - School of Civil Engineering, Sun Yat-sen University, Guangzhou, China.

IRSTI 45.41.33, 50.43.17

B. Sarsembayev

Nazarbayev University, Nur-Sultan, Kazakhstan
E-mail: bayandy_enu@mail.ru

Disturbance observer based discrete PI control system with back-calculation anti-windup technique for improvement transient performance of PMSM

Abstract. In this paper discrete-time field-oriented control (FOC) for PMSM speed control has been proposed. The cascade structure of the discrete-time PI-PI control system with tracking back-calculation anti-windup scheme. The novel anti-windup scheme for both loops has been adopted. Windup phenomena in traditional PI controllers have greater negative effects on the transient performance in engineering applications such as PMSM. In the real-time experiments, the proposed control system achieves less speed errors and faster response. The experimental results have proved the feasibility of the proposed control scheme.

Key words: PI controller, field-oriented control (FOC), permanent magnets synchronous motor (PMSM), back-calculation algorithm, discrete-time PI controller, anti-windup technique.

DOI: doi.org/10.32523/2616-7263-2021-135-2-94-105

Introduction

Permanent magnet synchronous motors (PMSMs) have been utilized in the various applications. It is preferable due to its compact structures, high air-gap flux density, high power density, high torque to inertia ratio; higher efficiency than other electric motors [1].

Due to so-called windup phenomena in traditional PI, the controller's performance is not satisfactory for PMSM drives applications. This phenomena is characterized by long periods of overshoot, which results in poor control performance and even makes the overall system unstable. Therefore, modern PI-PI control system for motor drives are typically equipped with various anti-windup (AW) techniques to reduce integral effect on control system performance. The effectiveness of back-calculation based tracking gains AW scheme's performance has been experimentally demonstrated among other anti-windup techniques such as, simple limited integration, limited output with dead zone element, and conditioned integration with following applications such as angular position control of a servo system [2] and for PMSM control [3].

PI speed controller equipped with anti-windup scheme demonstrates good performance in both transient and steady-state times than with conventional forms [3]-[5]. However, PI controllers are sensitive to model uncertainty which is a case in practical applications[6]. In addition, the tuning gains of PI controller is tedious and time-consuming work. The defining of optimal gains for PI-PI control system based on analyzing plant's dynamics with step response method is most common among others [4].

In this paper cascade discrete PI-PI control has been utilized. While, the inner loop controls armature currents/torque whereas outer loop regulates the speed of motors by providing the current/torque reference [6].

Motivated by [3] in this study, PI-PI control scheme with novel anti-windup algorithm has been proposed for the PMSM speed regulation. The tracking back-calculation anti-windup scheme has been adopted and applied for both loops of the control system to compensate windup phenomena with aim of improving transient performance and achieving asymptotic stability of the closed-loop system. The discrete-time PI-PI control system are equipped with discrete-time tracking anti-windup scheme to handle windup phenomena.

Surface mounted pmsm system

A. Electrical subsystem model of pmsm

The electrical model of the machine contains the equations for the stator current, stator flux and electromagnetic torque.

PMSM's stator d-q voltages are:

$$V_d = \frac{d\Psi_d}{dt} - \omega_{el}\Psi_q + R_s i_d \quad (1)$$

$$V_q = \frac{d\Psi_q}{dt} + \omega_{el}\Psi_d + R_s i_q \quad (2)$$

ω_{el} – electrical speed, rad/s

i_q – q-axis current, A

i_d – d –axis current, A

Ψ_d and Ψ_q - d-axis and q-axis magnetic flux linkages

R_s – stator resistance, Ohm

L_s – stator inductance, H

In the equations above it is the cross couplings of the two magnetic flux variables that stand out. Furthermore, the magnetic flux in the d- axis Ψ_d acts positevely on the voltage V_q, and the magnetic flux in the q-axis Ψ_q acts negatively on the voltage V_d.

The magnetic flux linkages are defined as

$$\Psi_d = L_d i_d + \lambda_m \quad (3)$$

$$\Psi_q = L_q i_q \quad (4)$$

λ_m– permanent magnet flux coefficient, Wb

The equation (3) demonstrates that the permanent flux is only aligned with the d-axis.

B. Torque subsystem model of PMSM

The voltages produced by $\omega_{el}\Psi_d$ and $-\omega_{el}\Psi_q$ corresponds to the back-emf in the system.

$$P_{el} = -\omega_{el}\Psi_q i_d + \omega_{el}\Psi_d i_q \quad (5)$$

Where the mechanical rotor shaft speed can be converted to electrical one through the expression

$$\omega_{el} = z_p \omega \quad (6)$$

z_p – number of poles,

Taking into consideration that with $\Psi_d i_q$ and $\Psi_q i_d$ we are dealing with the peak value, it is then possible to compute the mechanical value of the active power using the following equation:

$$P_m = \frac{3}{2} z_p \omega(-\Psi_q i_d + \Psi_d i_q) \quad (7)$$

From definition of torque as related to power, the electromagnetic torque can be derived as

$$T_e = \frac{3}{2} z_p[(L_d - L_q) i_d i_q + \lambda_m i_q] \quad (8)$$

For the torque subsystem the following equations apply. The mechanical or produced torque considers losses due to friction, viscosity, and drag resulting from time-varying flux. The total torque, T is difference between mechanical torque, T_m (minus mechanical losses) and load torque, T_L.

Total torque is

$$T = T_m - T_L \tag{9}$$

T_L – rated load torque, Nm

Mechanical torque is

$$T_m = T_e - T_{friction} - T_{viscous} - T_{d\Psi} \tag{10}$$

The torque losses due to friction is

$$T_{friction} = (C_{hy} + C_f)sign(\omega) \tag{11}$$

C_f – static moment of friction, Nm

C_{hy} – hysteresis losses coefficient, N·m

The torque losses due to viscousity is

$$T_{viscous} = (C_{ed} + d)\omega \tag{12}$$

The torque losses due to time-varying flux in the PMSM is

$$T_{d\Psi} = d_{ed}\frac{\frac{d\Psi_{dq}}{dt}\times\Psi_{dq}}{|\Psi_{dq}|^2} \tag{13}$$

c_{ed} – eddy currents coefficient, Nm/(rad/s)

d_{ed} – damping coefficient due to eddy currents Nm/(rad/s).

d – viscous damping coefficient, Nm/(rad/s)

ω – mechanical speed, rad/s

Ψ_{dq} – d-q frame magnetic flux linkage, Wb.

C. Mechanical subsystem model of PMSM

Using equations (9) - (13) mechanical subsystem can be expressed as

$$T = J\frac{d\omega_m}{dt} \tag{14}$$

J – rotor inertia, kg·cm^2

From this mechanical speed of the rotor shaft of the PMSM system can be expressed as

$$\dot{\omega}_m = \frac{3}{2}\frac{z_p\lambda_m}{J}i_q - \frac{(C_{hy} + C_f)sign(\omega_m)}{J} - \frac{(C_{ed}+d)}{J}\omega_m - \frac{d_{ed}\frac{\frac{d\Psi_{dq}}{dt}\times\Psi_{dq}}{|\Psi_{dq}|^2}}{J} - \frac{T_L}{J}$$
$$y = \omega_m \tag{15}$$

The highly complex PMSM system should be controlled with sophisticated control system. The ordinary PI controller does not satisfy to the performance requirements in terms of overshoot and dynamic response due to so called windup phenomena.

In this control system, the time varying magnetic flux due to eddy currents, friction and hysteresis cause torque losses, which are also considered in the motion equation. The eddy currents are induced when a nonmagnetic, conductive material is moving in a magnetic field [7]–[9]. The eddy currents

circulate in the rotor's conductive material and dissipate causing a repulsive force between the magnet and the conductor. Hence, the mechanical or produced torque considers losses due to static moment of friction, hysteresis, and time-varying flux.

Control system design

B. Discrete-time cascade pi-pi control system

For the speed regulation of the PMSM's parameters are not needed due to model free nature of PI control algorithm. Then PI-PI cascade closed-loop control is sufficient to achieve satisfactory performance for speed regulation (Figure 1). The control objective in this case is to achieve a specified tracking performance by means of the PI controller and facilitate zero errors in finite time.

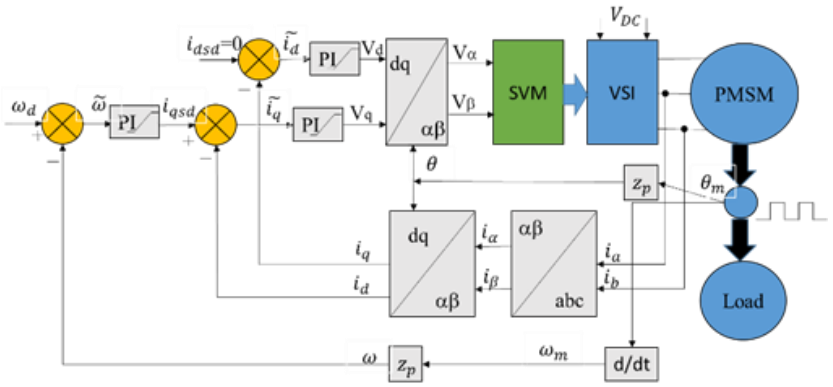

Figure 1. Discrete-time cascade PI-PI control system for PMSM speed regulation

The speed loop controller as well as currents controllers can be formulated with the following formulas based on Figure 2.

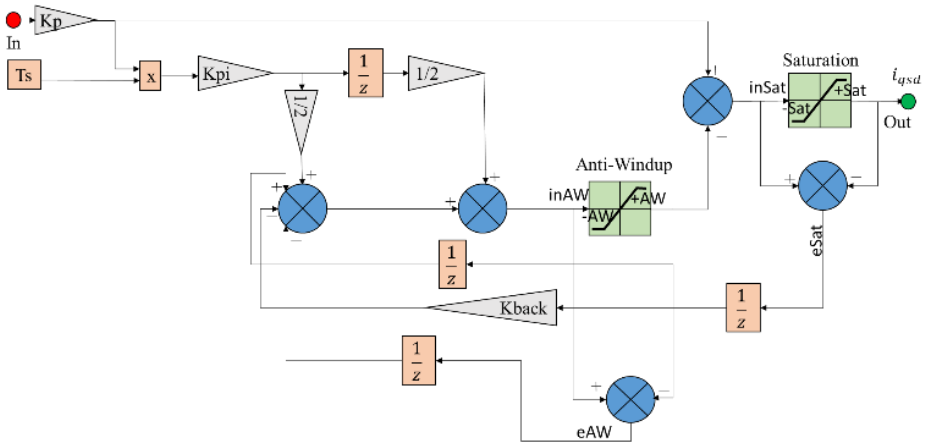

Figure 2. Discrete-time PI controller with tracking anti-windup scheme

$$|\text{inSat} = 0|, \text{ and } |\text{inAW} = 0| \{\text{out} = 0\} \quad (3)$$

$$|\text{inSat} \geq \mp\text{Sat}|, \text{ and } |\text{inAW} \geq \mp\text{AW}| \{\text{out} = \mp\text{Sat}\} \quad (4)$$

$$|\text{inSat} < \mp\text{Sat}| \text{ and } |\text{inAW} \geq \mp\text{AW}|, \\ \{\text{out} = \tilde{\omega}\text{K}_\text{p} - (\mp\text{AW})\} \quad (5)$$

$$|\text{inSat} < \mp\text{Sat}| \text{and } |\text{inAW} < \text{AW}|\ ,$$

$$\left\{\begin{matrix} \text{out} = \tilde{\omega}\text{K}_\text{p} - (\frac{1}{2}\frac{1}{\text{z}}\text{K}_\text{pi}\tilde{\omega}\text{K}_\text{p}\text{T}_\text{s} + (\frac{1}{2}\text{K}_\text{pi}\tilde{\omega}\text{K}_\text{p}\text{T}_\text{s} + \\ \frac{1}{\text{z}}\text{inAW} - \frac{1}{\text{z}}\text{eSatK}_\text{back} - \frac{1}{\text{z}}\text{eAW})) \end{matrix}\right\} \quad (6)$$

where

inSat – input of saturation block
$\mp$Sat – output of saturation block
out – output of PI controller
inAW – input of anti-windup block
$\mp$AW – output of anti-windup block
eSat – error of saturation block
eAW – error of anti-windup block
$\tilde{\omega}$ – speed error, RPM
K_p – proportional gain
K_pi – proportional-integral gain
T_s – sampling time
$\frac{1}{\text{z}}$ – unit delay
K_back – back-calculation gain

Experimental results

For the experimental setup DSP based "Controlled permanent magnet servo drive with MATLAB/Simulink 300W" (manufactured by Lucas-Nuelle gGmbH) was used to test the proposed PI-PI control system with tracking anti-windup scheme. The experimental setup comprises surface mounted type PMSM that coupled with 1024 pulses incremental position encoder and servo-machine operated with ActiveServo software acting as a load. The control algorithm is written in Matlab/Simulink (R2016b) environment then the code generated by Code Composed Studio 5 is sent to servo-converter for real-time experiment control. Note, after loading the code, no modification of gains is allowed. For a new configuration and modification of gains, the code generation has to be performed again. The switching period of the self-commutated converter is set to 125 μs. The control routine frequency for the pulse width modulation technique (PWM) in the inverter is set to 8 kHz. The parameters of the PMSM are listed in Table 1.

To confirm the effectiveness of the proposed control system design, let us consider a prototype of SPMSM with the following nominal parameters given in Table 1.

Table 1

PMSM nominal parameters

Motor parameters	Symbol	Value
Rated speed	n_n (RPM)	6000
Rated torque	M_n (Nm)	0.97
Rated power	P_n (W)	300
Torque constant	K_{tRMS} (Nm/A)	0.41
Voltage constant	K_{eRMS} (Nm/A)	26.1
Permanent magnetic flux coefficient	λ_m (Vs)	0.089

Winding resistance Ph-Ph	R_s (Ohm)	4.74
Winding inductance Ph-Ph	L_s (mH)	8.6
Rotor's moment of inertia	J (kgcm^2)	0.33
Number of poles	z_p	8
Static moment of friction	C_f (Nm)	0.014
Hysteresis losses coefficient	C_{hys} (Nm)	0.08
Viscous damping coefficient	b (N·m/(rad/s))	0.002
Eddy currents coefficient	c_{ed} (Nm/(rad/s))	0.0015
Eddy currents damping coefficient	d_{ed} (Nm/(rad/s))	0.003

A space vector pulse width modulation (SVPWM) technique is used to regulate the phase currents flowing into the PMSM. For evaluation of performance of the proposed control scheme, in this paper, the experimental results of the baseline controller without HODO are compared with the results of the proposed HODO based PI-PI control system with tracking anti-windup scheme utilized. Two cases with speed variation and load torque disturbance have been investigated.

Table 2

Control system's parameters

Controllers and Observers	Parameters and Gains
Speed controller PI gains	$K_p = 0.057, K_I = 0.04$
Current controllers PI gains	$K_p = 17.1, K_I = 0.0018$

Case 1: Speed Transient Response with nominal parameters
1) The desired speed (ω_d): 300 RPM $\rightarrow$ 600 RPM.
2) Constant load torque $T_L = 0.5$ Nm.
3) No load torque disturbance.
Case 2: Load Torque Transient Response
1) The desired speed $\omega_d = 500$ RPM.
2) Load torque disturbance $T_L = 0.3$ Nm $\rightarrow$ 0.5 Nm.

The round or trapezoidal shaped reference speed has been chosen for PMSM, as it is more effective against wear of mechanical coupling of the prototype PMSM like in the industrial applications [10]. However, the load torque disturbance has been applied as step-wise.

Traditional discrete-time PI controller has been equipped with tracking back-calculation anti-windup scheme to improve transient performance PMSM system. The speed response and the references currents have been plotted for graphical evaluation purposes.

Figs. 3-8 show the experimental results of the proposed control method under two operational cases to assess its performance . The currents and the voltages have been measured and converted to d-q frame ($i_{qs}, i_{ds}, V_{qs}, V_{ds}$). The mechanical speed of PMSM (ω) as well as its tracking error ($\tilde{\omega}$) have been shown and compared with their reference values. Figures 3, 4, and 5 are results under conditions in *Case 1*, while Figures 6, 7, and 8 are results obtained under operation conditions in *Case 2*. The detailed performance of the proposed control design is summarized in Table 3. The experimental results shown below are assessed by the maximum angular shaft speed errors, settling time and absolute mean mechanical speed error. The maximum angular shaft speed errors are 42 and 17 RPM for *Case 1* and *Case 2* respectively. While the settling time 0.3 and 0.17 seconds, the absolute mean mechanical speed errors are 1.4838% and 0.172% respectively. The control inputs V_{qs} and V_{ds} under operational conditions in *Case 1* and *Case 2* have been demonstrated in Figures 5 and 8.

Table 3

Performance of the proposed discrete-time PI-PI with tracking back-calculation anti-windup control scheme for both loops

Criteria and cases		PI with anti-windup
Maximum angular shaft speed error, RPM	Case 1	42
	Case 2	17
Settling time, s	Case 1	0.3
	Case 2	0.17
Absolute mean of the mechanical speed error,%	Case 1	1.4838%
	Case 2	0.172%

In the PMSM system, the pulsating torques can be seen in the d-q currents plots as well as they are reflected in PMSM angular shaft speed response. The origin of these ripples may come from cogging torques associated with the shape of th rotor of the machine, but also high-frequency electromagnetic noise associated with switching time periods in the power converter. The minimizing the current ripples in the PMSM prototyping kit will be sought in future research.

a)

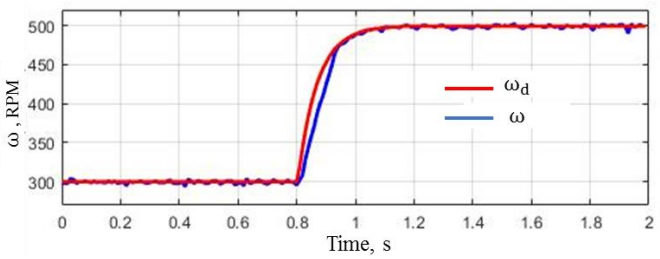

b)

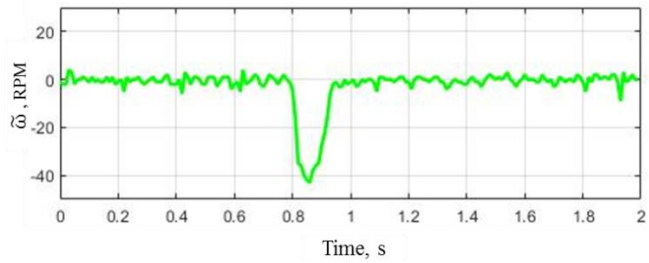

Figure 3. Experimental results of the proposed control for Case 1. (a) Mechanical speed response of PMSM; (b) Mechanical speed errors.

a)

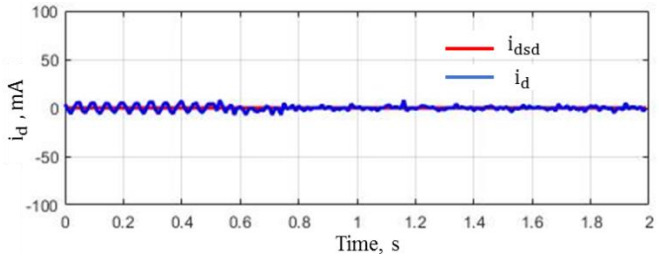

b)

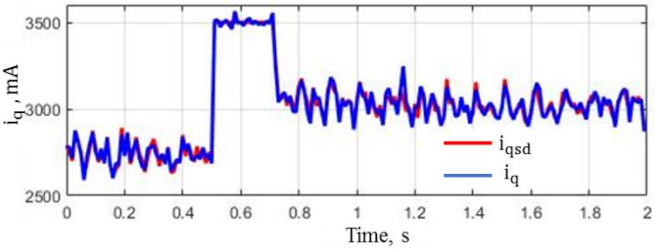

Figure 4. dq-axis currents of the proposed control for case 1. (a) i_{ds} and its desired value i_{dsd}; (b) i_{qs} and its desired value i_{qsd}.

a)

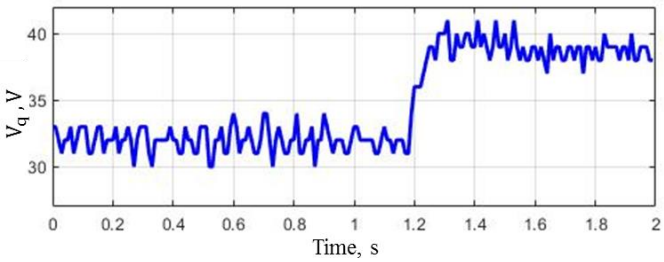

b)

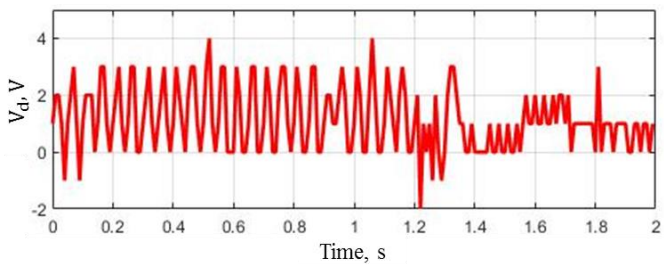

Figure 5. dq-axis voltages of the proposed control for Case 1. (a) control input on q-axis V_{qs}; (b) control input on d-axis V_{ds}.

a)

b)

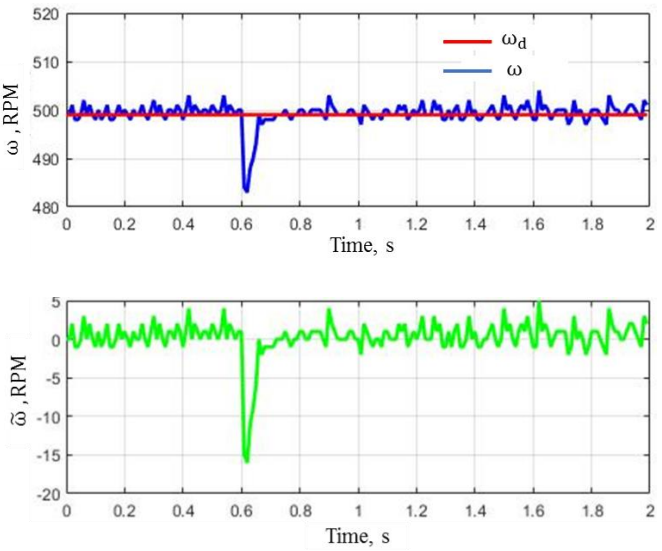

Figure 6. Experimental results of the proposed control for Case 2. (a) Mechanical speed response of PMSM; (b) Mechanical speed error.

a)

b)

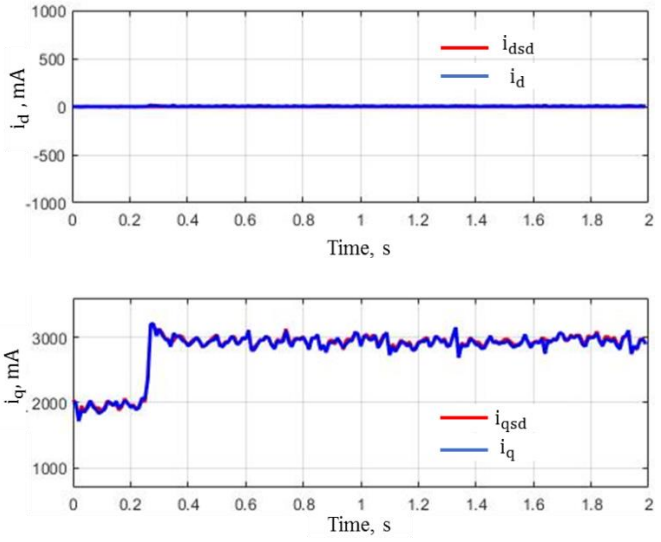

Figure 7. dq- axis currents of the proposed control for Case 2. (a) i_{ds} and its desired value i_{dsd}; (b) i_{qs} and its desired value i_{qsd}.

a)

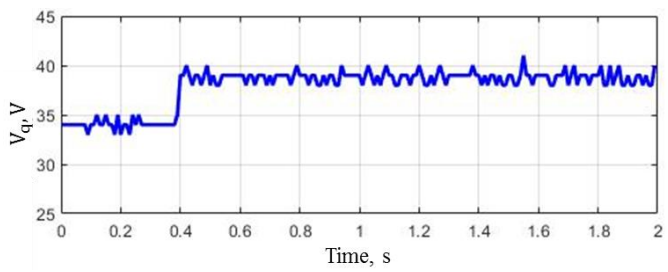

b)

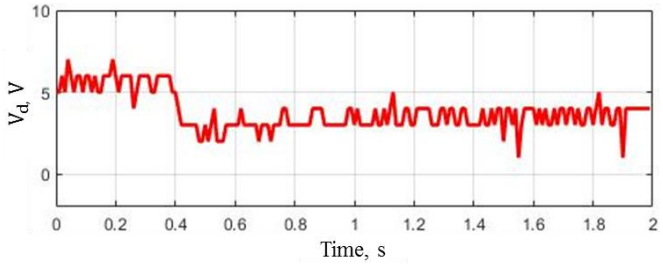

Figure 8. dq- axis voltages of the prposed control for Case 2. (a) control input on q-axis V_{qs}; (b) control input on d-axis V_{ds}.

Conclusion

In this paper, field-oriented control based discrete-time PI-PI with tracking back-calculation anti-windup scheme is proposed. The cascade discrete-time PI-PI control structure with novel anti-windup scheme has been adopted for both loops. Unlike traditional PI controllers, the proposed controller can significantly improve the performance of PMSM system under speed and load torque variations. As the currents ripples are unavoidable, their reduction will be considered in future works.

References

1. T.D. Do, H.H. Choi, and J.-W. Jung, "Nonlinear Optimal DTC Design and Stability Analysis for Interior Permanent Magnet Synchronous Motor Drives," *IEEE/ASME Trans. Mechatronics*, -2015. -vol. 20, no. 6. -pp. 2716-2725.

2. R.E. Precup, R. C. David, E. M. Petriu, M. B. Radac, and S. Preitl, "Adaptive GSA-based optimal tuning of PI controlled servo systems with reduced process parametric sensitivity, robust stability and controller robustness," *IEEE Trans. Cybern.* -2014. -vol. 44, no. 11. -pp. 2168-2267.

3. J. Espina, A. Arias, J. Balcells, C. Ortega, and S. Galceran, "Speed anti-windup PI strategies review for field oriented control of permanent magnet synchronous machines servo drives with matrix converters," in *13th European Conference on Power Electronics and Applications*, Barcelona, Spain, -2009. -pp. 279-285.

4. K.J. Astrom and T. Hagglung, *Advanced PID Control*. NC, USA: ISA, -2006.

5. Y. Zhetpissov, A. Kaibaldiyev, and T. D. Do, "PI anti-windup speed control of permanent magnet synchronous motor based on feedforward compensation," 2018 ELEKTRO, Mikulov, Czech Rep., -2018, -pp. 1-8, doi: 10.1109/ELEKTRO.2018.8398275.

6. R. Errouissi, A. Al-Durra, and S. M. Muyeen, "Experimental Validation of a Novel PI Speed Controller for AC Motor Drives with Improved Transient Performances," IEEE Trans. Control Syst. Technol. -2018. -vol. 26, no. 4. -pp. 1414-1421.

7. J. Bae, J. Hwang, J. Park, and D. Kwag, "Modeling and experiments on eddy current damping caused by a permanent magnet in a conductive tube," *J. Mech. Sci. Technol.* -2009. -vol. 23. -pp. 3024-3035.

8. H.A. Sodano and J. Bae, "Eddy Current Damping in Structures," *Shock Vib. Dig.* -2004. -vol. 36, no. 6. -pp. 469–478.

9. Abdullah, J.-H. Ahn, and H.-Y. Kim, "Effect of Electromagnetic Damping on System

Performance of Voice-Coil Actuator Applied to Balancing-Type Scale," Actuators. -2020. -vol. 9, no. 8. -pp. 1-23.

10. S. Li, J. Yang, W.-H. Chen, and C. Xisong, *Disturbance observer-based control: methods and applications*. Boca Raton-London-New York: CRC Press, -2014.

Б. Сарсембаев
Назарбаев Университеті, Нұр-Сұлтан, Қазақстан

ТМСЭҚ-нің өнімділігін жақсарту үшін контроллердің ауытқуға қарсы кері есептеу алгоритмі қолданған кедергілерді бақылаушыға негізделген дискретті PI басқару жүйесі

Аңдатпа. Бұл жұмыста тұрақты магнитті синхронды электр қозғалтқыш (ТМСЭҚ) жылдамдығын басқаруға арналған дискретті уақыттық өрістік бағдарлау басқарудың (ӨББ) негізінде ұсынылды. Қайта есептелетін ауытқуға қарсы схемасы бар дискретті уақытты ПИ-ПИ басқару жүйесінің каскадты құрылымы қолданды. Екі шенбер үшін де ауытқуға қарсы жаңа схема қабылданды. Дәстүрлі ПИ контроллерлеріндегі өтпелі құбылыстары ТМСЭҚ сияқты инженерлік шешімдерде өтпелі жұмысына үлкен теріс әсер етеді. Нақты уақыттағы эксперименттерде ұсынылған басқару жүйесі аз қателікке және жылдам жауап беруге қол жеткізеді. Тәжірибе нәтижелері ұсынылған бақылау схемасының орындылығын дәлелдеді.

Түйін сөздер: тұрақты магниттер синхронды электр қозғалтқыш (ТМСЭҚ), кері есептеу алгоритмі, PI дискретті контроллер.

Б. Сарсембаев
Назарбаев Университет, Нур-Султан, Казахстан

Дискретная система ПИ-регулирования с техникой обратного вычисления на основе наблюдателя возмущений для улучшения переходных характеристик в СЭПМ

Аннотация. В этой статье было предложено управление с дискретным временем, ориентированное на поле (УОП) для управления скоростью СЭПМ. Каскадная структура системы управления PI-PI с дискретным временем и схемой анти-вихревание с отслеживанием обратных вычислений. Была принята новая схема предотвращения закручивания для обоих контуров. Явление закрутки в традиционных контроллерах PI имеет большее отрицательное влияние на переходные характеристики в инженерных приложениях, таких как СЭПМ. В экспериментах в режиме реального времени предлагаемая система управления обеспечивает меньшее количество ошибок скорости и более быструю реакцию. Результаты экспериментов подтвердили реализуемость предложенной схемы управления.

Ключевые слова: синхронный электродвигатель с постоянными магнитами (СЭПМ), алгоритм обратного вычисления, дискретный ПИ-регулятор.

References

1. T. D. Do, H. H. Choi, and J.-W. Jung, "Nonlinear Optimal DTC Design and Stability Analysis for Interior Permanent Magnet Synchronous Motor Drives," *IEEE/ASME Trans. Mechatronics*, vol. 20, no. 6, pp. 2716–2725, 2015.

2. R. E. Precup, R. C. David, E. M. Petriu, M. B. Radac, and S. Preitl, "Adaptive GSA-based optimal tuning of PI controlled servo systems with reduced process parametric sensitivity, robust stability and controller robustness," *IEEE Trans. Cybern.*, vol. 44, no. 11, pp. 2168-2267, 2014.

3. J. Espina, A. Arias, J. Balcells, C. Ortega, and S. Galceran, "Speed anti-windup PI strategies review for field oriented control of permanent magnet synchronous machines servo drives with matrix converters," in *13th European Conference on Power Electronics and Applications*, Barcelona, Spain, 2009, pp. 279–285.

4. K. J. Astrom and T. Hagglung, *Advanced PID Control*. NC, USA: ISA, 2006.

5. Y. Zhetpissov, A. Kaibaldiyev, and T. D. Do, "PI anti-windup speed control of permanent magnet synchronous motor based on feedforward compensation," 2018 ELEKTRO, Mikulov, Czech Rep., 2018, pp. 1-8, doi: 10.1109/ELEKTRO.2018.8398275.

6. R. Errouissi, A. Al-Durra, and S. M. Muyeen, "Experimental Validation of a Novel PI Speed Controller for AC Motor Drives with Improved Transient Performances," *IEEE Trans. Control Syst. Technol.*, vol. 26, no. 4, pp. 1414–1421, 2018.

7. Bae, J. Hwang, J. Park, and D. Kwag, "Modeling and experiments on eddy current damping caused by a permanent magnet in a conductive tube," *J. Mech. Sci. Technol.*, vol. 23, pp. 3024–3035, 2009.

8. H. A. Sodano and J. Bae, "Eddy Current Damping in Structures," *Shock Vib. Dig.*, vol. 36, no. 6, pp. 469-478, 2004.

9. Abdullah, J.-H. Ahn, and H.-Y. Kim, "Effect of Electromagnetic Damping on System Performance of Voice-Coil Actuator Applied to Balancing-Type Scale," *Actuators*, vol. 9, no. 8, pp. 1-23, 2020.

10. S. Li, J. Yang, W.-H. Chen, and C. Xisong, *Disturbance observer-based control: methods and applications*. Boca Raton-London-New York: CRC Press, 2014.

Information about authors:

B. Sarsembayev - Department of Robotics, School of Engineering and Digital Sciences (SEDS), Nazarbayev University, Nur-Sultan Z05H0P9, Kazakhstan

Б. Сарсембаев - Робототехника бөлімі, Инженерлік және цифрлық ғылымдар мектебі (SEDS), Назарбаев Университеті, Нұр-Сұлтан Z05H0P9, Қазақстан.

IRSTI 44.41.35

A.S. Nikiforov[1], A.E. Karmanov[1], E.V. Prikhod'ko[1], A.K. Kinzhibekova[1*], M.G. Zhumagulov[2]

[1]Toraighyrov university, Pavlodar, Kazakhstan
[2]LN Gumiliyov Eurasian National University, Nur-Sultan, Kazakhstan
Corresponding author: john1380@mail.ru

Research of heating the lining of high-temperature units in order to increase their residual resource

Abstract. The article contains an analysis of the initial stage of the heating process of high-temperature units. The heating modes used at the enterprises lead to various difficulties: a delay in the heating process or heating at a high speed at which mechanical stresses arise and exceed the permissible values. The proposed graphical dependencies for heating allow us to heat up at the highest possible speeds, taking into account the time spent on drying. In this case, the ultimate strength of refractory materials is not exceeded, which leads to a significant reduction in the time for the heating process.

Key words: refractory materials, drying, heating rate, lining, high-temperature unit, heating schedule.

DOI: doi.org/10.32523/2616-7263-2021-135-2-106-112

Introduction

Currently, enterprises that operate high-temperature units have an important task - to determine the residual working time of the equipment (units). This allows as avoiding emergencies situations related to the safety of the operating personnel so predicting the time and amount of resources consumed.

Technological processes in high-temperature heat-technological installations are distinguished by a great variety and are determined by the following [1]:

- intensity of heat supply to the surface of the processed material (intensity of external heat transfer) and heat transfer inside the processed material;
- the intensity of mass supply from the outside to the reacting surface of the processed material (intensity of external mass transfer) and the intensity of molecular mass transfer inside the processed material;
- intensity of mixing of phases (solid, liquid) in the zone of their heat treatment;
- the speed of the actual chemical reaction and separation of target and related products;
- a combination of two or more of the listed factors.

This classification makes it possible to consider and analyze entire classes of technological processes from a single point of view and uniform methods. The approach facilitates the borrowing of the research results of some types of technological processes for the organization of others, using physical and mathematical analogies.

Research methods

Thermal stresses in the lining are a decisive condition in assessing the residual time, since a decrease in the thickness of the lining due to the action of temperature stresses is the most common reason for the withdrawal of high-temperature units for repair.

Let's consider three methods of heating high-temperature units that use fireclay bricks as lining.

Heating up of high-temperature units should be carried out with the avoidance of thermal stresses in the lining of the unit exceeding the permissible limit. The technique developed by the authors

makes it possible to select the temperatures at which this condition is met. The analysis of various heating modes was carried out for the material under study (chamotte) to a temperature of 110 °C (the temperature of the drying process beginning) using the developed program. The drying process and further heating to operating temperature were also investigated. Three heat up options were considered:

- uniform heating up to operating temperature;
- initial heating at minimum speeds and further heating at maximum speeds;
- the maximum possible rising of temperature from the initial stage.

The maximum heating rate was limited by the arising temperature stresses, and the choice of the optimal heating method was determined by its minimum time. Let's consider different ways of heating the unit intensity.

The way No 1. The intensity of heating should be as follows: The first four steps have a speed of 10 °C/min (the time step was 10 minutes), then nine minutes with 1 °C/min, then - 2 °C/min until the temperature of 110 ° C is reached. Exposure at this temperature is 37 minutes.

The way No 2 has a heating rate of 2 °C/min until the temperature of 110 °C is reached. Temperature holding in this case takes 44 minutes and then heating occurs to the operating temperature.

The way No 3. The first six minutes have a heating rate of 2 °C/min, the next five minutes at 10 °C/min, and the remaining nine minutes at 1 °C/min, which takes 38 minutes.

Thus, the most optimal heating mode in terms of time is obtained at a temperature holding of 37 minutes, when the arising thermal stresses (compression, expansion) does not exceed the limit values.

There are factory lining heating methods. In many cases, they do not take into account the initial stage of drying up to 110 °C, the so-called temperature holding (horizontal section on the temperature graph). In the case when they even take into account the time to reach this temperature, the resulting limiting stresses are ignored [2]. Studies of drying samples have shown that the rate of evaporation of capillary moisture falls within the temperature range from 55-65 °C to 100-110 °C.

The values of many parameters are taken for calculations as constant, i.e., independent of temperature when developing thermal regimes for heating high-temperature units. For example, the values of the specific volumetric heat capacity c, thermal conductivity coefficient λ and ultimate strength σ are taken constant for calculations.

Meanwhile, the value of such a parameter as the ultimate compressive strength of a material is highly dependent on temperature.

Research results

The initial stage in the development of rational heating schedules for high-temperature units is the construction of existing heating schedules and their analysis from the standpoint of the arising temperature stresses. The program developed by the authors has the ability to calculate temperature fields and stresses by temperature at one point - on the inner surface of the lining for analyzing heating graphs. That is, if the temperature is measured during heating at one point, then the desired values of temperature stresses can be obtained over the entire section of the lining.

Such work was carried out on 25-ton steel-pouring ladles in the process of heating them up after overhaul. The operation of these ladles according to the appropriate technology assumes a major overhaul after 40 heats on average. Complete replacement of the lining, including the reinforcing layer, takes place during the overhaul. After that, the ladles are heated to operating temperature on special benches by burning a propane-butane mixture in a burner.

Periclase-carbon refractories are widely used for lining steel-pouring ladles. Let's take a look at the drying and heating schedule for a 25-ton steel ladle lining with a 135 mm working layer of periclase carbon. The heat up time to an operating temperature of 938 ° C is 24 hours (Figure 1).

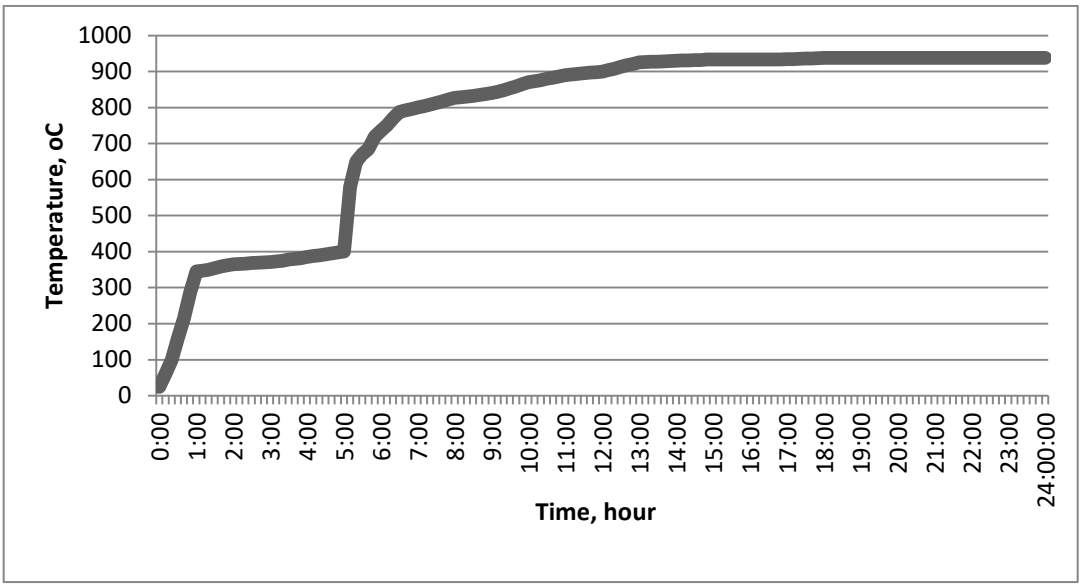

Figure 1. Drying and heating of steel ladle lining

The first stage (0-1:20 hours) has an interval of 20-350 °C and is carried out at an average speed of 37.2 °C/hour. At the same time, heating proceeds quickly, but evenly, without holding at a temperature of 100-110 °C to remove moisture. Further, from 1:20 to 5:00, the heating rate decreases to an average rate of 2-3 °C/hour, forming a horizontal section in the figure. Based on the figure, this horizontal section is necessary for relaxation of temperature stresses, after which the temperature rises from 400 °C to 650 °C in 20 minutes with an average heating rate of 75 °C/hour. Further, heating goes from 650 °C to 800 °C in 1:40 hours at an average rate of 13.6 °C/hour. Then a long period of temperature rise follows up to 900 °C in 5 hours. After that, slow heating takes 3 hours at a rate of 2 °C/hour to the holding temperature at 933 °C (horizontal section in the figure) for relaxation of temperature stresses. The lining temperature has been maintained at 938 °C for the last six hours instead of heating up. Thus, the average heating rate of the lining of a steel-pouring ladle from 20 °C to 938 °C is 40 °C/hour.

Analysis of this figure shows that thermal stresses arise in the lining when it is heated (Figure 2), which leads to the appearance of cracks and further to its destruction (Figure 3).

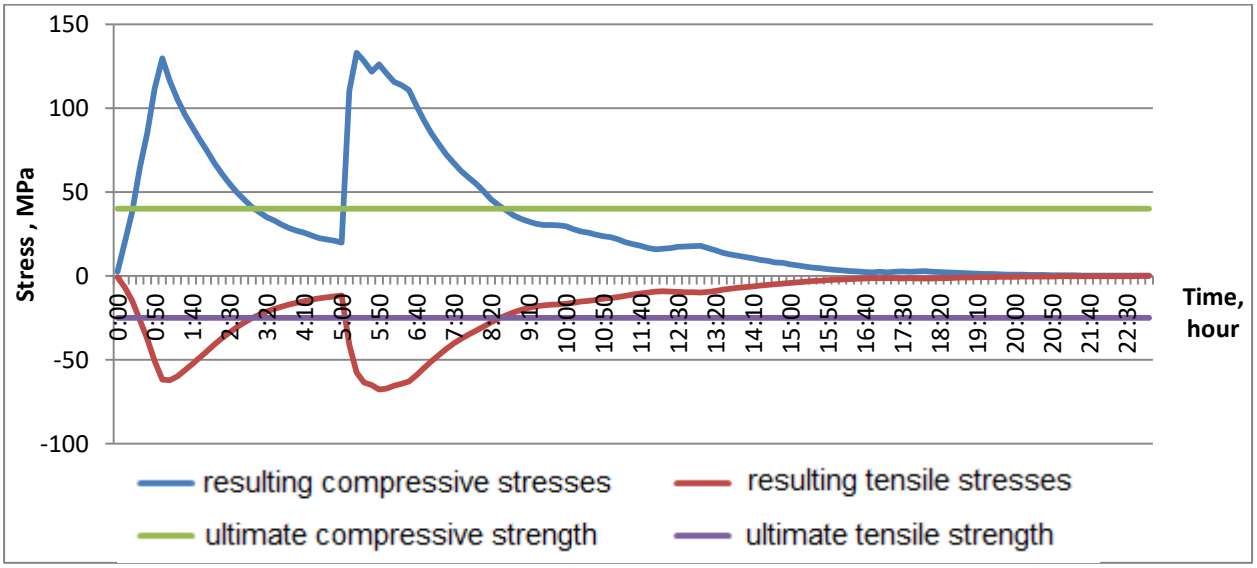

Figure 2. The resulting temperature stresses

The figure shows that the resulting thermal compressive stresses are twice the ultimate strength specified by the manufacturer for periclase-carbon refractories (40 MPa in compression and 25 MPa in tension).

Lining cracking is the result of heating at a high rate. The nature of the destruction is shown in Figure 3 for the lining of a 25 ton steel-pouring ladle after 22 melting cycles [3].

Figure 3. Cracks in the lining of a steel ladle

As a result, it can be concluded that the permissible heating rates are exceeded at the corresponding points in time. In addition, the ladle is heated up within 24 hours, and from the graph (Figure 4, curve 2) it can be seen that the inner surface of the lining reaches its maximum temperature after 16 hours of heating. Thus, the maximum lining temperature is maintained during the last 8 hours instead of heating up.

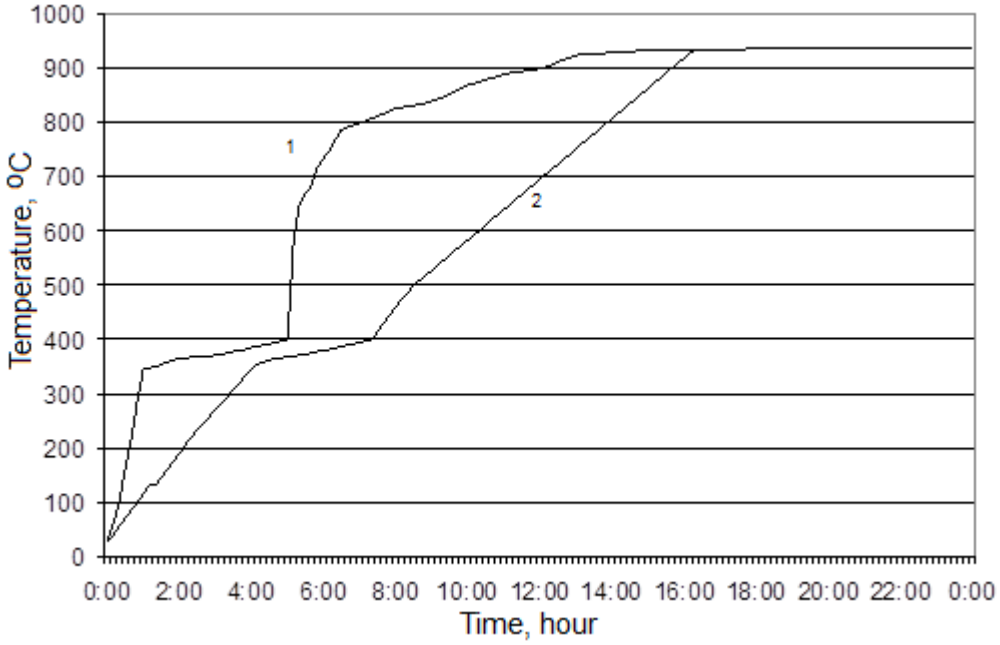

1 - factory warm-up schedule; 2- the author's warm-up schedule.

Figure 4. Steel ladle heating schedules

The rates of temperature rise were selected individually for each section of the curve. The average rate of temperature increase in areas from 18 to 500 °C (not containing drying areas) was approximately 90 °C/h. The total heat-up time to a temperature of 938 ° C is 16 hours and 20 minutes.

Conclusion

The research shows that the durability of the lining in high-temperature units is more dependent on temperature differences than on the chemical effect of the process material, etc. Thus, the main reason that determines the residual working time of high-temperature units is the wear of the lining during operation, associated with irrational processes drying and heating. Reducing the temperature stresses that arise during the heating process, taking into account the drying process, to normalized values, allows us to increase the residual working time of the high-temperature unit lining.

The heating schedules obtained by the authors allow the heating process to be carried out at the highest possible rates and to control it without exceeding the ultimate strength of refractory materials. In this case, a significant reduction in the time for the heating process occurs.

This research is funded by the Science Committee of the Ministry of Education and Science of the Republic of Kazakhstan (Grant No. AP09561854).

References

1. Chaouki S., Iz – Eddine E. A., Abderrahman A. Recent advances in silica - alumina refractory: A review, Journal of Asian Ceramic Societies. -2014. -No 2(83). -P. 96-99. DOI: http://dx.doi.org/l0.l0l6/j.jascer.20l4.03.001.

2. Suat Y. (2003) Thermomechanical Modelling for Refractory Lining of a Steel Ladle Lifted by Crane, Steel research. -2003. -No 7 (74). -P. 483-488.

3. Nikiforov, A.S., Prikhod'ko, E.V., Kinzhibekova, A.K., Karmanov, A.E. (2020) Investigation of the Dependence of Refractory Thermal Conductivity on Impregnation with a Corrosive Medium, Refractories and Industrial Ceramics. -2020. -No 60(5). -P. 463-467. DOI: 10.1007/s11148-020-00386-3.

А.С.Никифоров[1], А.Е.Карманов[1], Е.В. Приходько[1], А.К. Кинжибекова[1], М.Г. Жумагулов[2]

[1]Торайғыров университеті, Павлодар, Қазахстан

[2]Л.Н.Гумилев атындағы Еуразия ұлттық университеті, Нұр-Сұлтан, Қазахстан

Жоғары температуралы қондырғылардың қалдық ресурсын арттыру мақсатында жылыту процесін зерттеу

Аңдатпа. Мақалада жоғары температуралы қондырғыларды жылыту процесінің бастапқы кезеңіне талдау жасалған. Кәсіпорындарда қолданылатын жылыту режимдері әртүрлі қиындықтарға әкеледі: қыздыру процесінің кешігуі немесе жылдамдықта қыздыру. Нәтижесінде кернеулер рұқсат етілгендерден асып түседі. Кептіруге кететін уақытты ескере отырып, жылытуға арналған дамыған графикалық тәуелділіктер, отқа төзімді материалдардың шекті беріктігінен аспастан, мүмкін болатын ең жоғары жылдамдықпен қыздыруға мүмкіндік береді, бұл жылыту процесінің уақыты айтарлықтай қысқарады.

Түйін сөздер: отқа төзімді материалдар, кептіру, қыздыру жылдамдығы, футеровка, жоғары температуралы қондырғы, жылыту графигі.

А.С. Никифоров[1], А.Е. Карманов[1], Е.В. Приходько[1], А.К. Кинжибекова[1], М.Г. Жумагулов[2]
[1]Торайгыров университет, Павлодар, Казахстан
[2]Евразийский национальный университет имени Л.Н.Гумилева, Нур-Султан, Казахстан

Исследование процесса разогрева футеровок высокотемпературных агрегатов с целью повышения их остаточного ресурса

Аннотация. Статья содержит анализ начального этапа процесса разогрева высокотемпературных агрегатов. Применяемые на предприятиях режимы разогрева приводят к различным трудностям: затягиванию процесса разогрева или разогрев со скоростями, возникающие напряжения при которых превышают допустимые. Разработанные графические зависимости для разогрева, с учётом затрат времени на сушку, позволяют производить разогрев с максимально возможными скоростями, не превышая предел прочности огнеупорных материалов, что приводит к значительному снижению времени на процесс разогрева.

Ключевые слова: огнеупорные материалы, сушка, скорость разогрева, футеровка, высокотемпературный агрегат, график разогрева.

References

1. Chaouki S., Iz – Eddine E. A., Abderrahman A. Recent advances in silica - alumina refractory: A review, Journal of Asian Ceramic Societies. 2(83), 96-99 (2014). DOI: http://dx.doi.org/l0.l0l6/j.jascer.20l4.03.001.

2. Suat Y. (2003) Thermomechanical Modelling for Refractory Lining of a Steel Ladle Lifted by Crane, Steel research. 7(74), 483-488 (2003).

3. Nikiforov, A.S., Prikhod'ko, E.V., Kinzhibekova, A.K., Karmanov, A.E. (2020) Investigation of the Dependence of Refractory Thermal Conductivity on Impregnation with a Corrosive Medium, Refractories and Industrial Ceramics. 60(5), 463-467 (2020). DOI: 10.1007/s11148-020-00386-3.

Information about authors:

А.С. Никифоров - техника ғылымдарының докторы, «Жылуэнергетика» кафедрасының профессоры, Торайғыров университеті, Павлодар, Қазақстан.

А.Е. Карманов - PhD, «Жылуэнергетика» кафедрасының доцент м.а., Торайғыров университеті, Павлодар, Қазақстан.

Е.В. Приходько - техника ғылымдарының кандидаты, «Жылуэнергетика» кафедрасының профессоры, Торайғыров университеті, Павлодар, Қазақстан.

А.К. Кинжибекова - техника ғылымдарының кандидаты, «Жылуэнергетика» кафедрасының профессор м.а., Торайғыров университеті, Павлодар, Қазақстан.

М.Г. Жумагулов - PhD, «Жылуэнергетика» кафедрасының доценті, Л.Н.Гумилев ат. Еуразия ұлттық университеті, Нұр-Сұлтан, Қазахстан.

A.S. Nikiforov - doctor of technical sciences, professor of the Thermal Power Engineering Department, Toraihyrov University, Pavlodar, Kazakhstan. Office address: 140008, Kazakhstan, Pavlodar, Lomov str., 64.

A.E. Karmanov - PhD, associate professor of the Thermal Power Engineering Dept., Toraihyrov University, Pavlodar, Kazakhstan. Office address: 140008, Kazakhstan, Pavlodar, Lomov str., 64.

E.V. Prikhod'ko - Candidate of Technical sciences, professor of the Thermal Power Engineering Department, Toraihyrov University, Pavlodar, Kazakhstan. Office address: 140008, Kazakhstan, Pavlodar, Lomov str., 64.

A.K. Kinzhibekova - Candidate of Technical sciences, professor of the Thermal Power Engineering Department, Toraihyrov University, Pavlodar, Kazakhstan.

M.G. Zhumagulov - PhD, associate professor of the Thermal Power Engineering Department, LN Gumiliyev Eurasian national university, Nur-Sultan, Kazakhstan.

Бас редакторы: **Г.Т. Мерзадинова**

Авторларға арналған нұсқаулықтар,
жарияланым этикасы журнал сайтында берілген: http://bultech.enu.kz

Л.Н. Гумилев атындағы Еуразия ұлттық университетінің
Хабаршысы. Техникалық ғылымдар және технологиялар
сериясы.
- 2(135)/2021 - Нұр-Сұлтан: ЕҰУ. - 113 б.
Шартты б.т. - 6,68. Таралымы - 8 дана.
Басуға қол қойылды: 29.06.2021 ж.
Ашық қолданыстағы электронды нұсқа: http://bultech.enu.kz

Мазмұнына тирпография жауап бермейді

Редакция мекен-жайы: 010008, Қазақстан Республикасы Нұр-Сұлтан қ.,
Сәтбаев көшесі, 2.
Л.Н. Гумилев атындағы Еуразия ұлттық университеті
Тел.: +7(71-72) 70-95-00(ішкі 31-428)
Л.Н. Гумилев атындағы Еуразия ұлттық университетінің баспасында басылды